Axonal homeostasis of VGLUT1 synaptic vesicles in mice

Xiaomin Zhang

THÈSE PRÉSENTÉE

POUR OBTENIR LE GRADE DE

DOCTEUR
DE
L'UNIVERSITÉ DE BORDEAUX

ÉCOLE DOCTORALE

SCIENCES DE LA VIE ET DE LA SANTE

Neurosciences

Par ZHANG Xiaomin

Axonal homeostasis of VGLUT1 synaptic vesicles in mice

Sous la direction de : Dr. HERZOG Etienne
Co-directeur : Prof. Dr. BROSE Nils

Soutenue le Mardi 14 Décembre, 2016

Membres du jury:

Mme. SANS Nathalie	DR-INSERM Bordeaux	Président
M. OHEIM Martin	DR-CNRS Paris	Rapporteur
M. MARTY Serge	CR1-CNRS Paris	Rapporteur
Mme. DANGLOT Lydia	CR1-INSERM Paris	Examinateur
M. PERRAIS David	DR-CNRS Bordeaux	Examinateur
M. HERZOG Etienne	CR1-CNRS Bordeaux	Directeur de thèse

Titre : Homéostasie axonale des vésicules synaptiques des neurones excitateurs VGLUT1 chez la souris

Résumé :

Les vésicules synaptiques (VS), compartiment de stockage du neurotransmetteur, sont essentielles pour la transmission synaptique chimique entre les neurones. Lorsque le potentiel d'action traverse une terminaison pré-synaptique, l'afflux de Ca^{2+} peut déclencher l'exocytose de VS qui sont ancrées et éventuellement amorcées à la zones active (ZA), et libérer leur contenu en neurotransmetteurs dans la fente synaptique. Ensuite, les molécules neurotransmetteurs se lient aux récepteurs situés dans la membrane post-synaptique et induisent des changements de conformation permettant la transduction du signal (échanges ioniques, voies de signalisation). Il existe de nombreuses études sur les mécanismes moléculaires en jeux lors de la neurotransmission. Concernant la partie pré-synaptique de ce processus, des études supplémentaires sont nécessaires pour mieux comprendre la dynamique de remplissage des VS en neurotransmetteurs, la distribution et la mobilité des VS dans l'axone.

Les neurotransmetteurs classiques sont concentrés dans les VS par l'action de transporteurs vésiculaires de neurotransmetteurs (VNT) contre un gradient électrochimique de protons généré par l'ATPase vacuolaire (v-ATPase). Le glutamate, neurotransmetteur excitateur principal, est transporté dans la VS par un transporteur vésiculaire du glutamate (VGLUT). Il existe 3 isoformes de VGLUT qui définissent 3 systèmes glutamatergiques anatomiques distincts dans le cerveau. Les neurones corticaux expriment fortement VGLUT1 qui représente ainsi le meilleur marqueur pour les VS dans ces neurones. Notre laboratoire a généré une souris gain de fonction $VGLUT1^{venus}$ qui permet de suivre VGLUT1 et les VS le portant par épi-fluorescence.

Dans un modèle ancien, les VS ont été considérées comme assignées à une seule terminaison et dans ce modèle chaque terminaison fonctionnait comme une unité autonome en relation directe et exclusive avec le corps cellulaire pour la synthèse et la dégradation de ses composants. Les VS accumulées dans le bouton synaptique étaient reparties selon trois contingents morphologiquement centrifuges à la ZA : le contingent immédiatement libérable, le contingent recyclant et le contingent de réserve. Mais les données obtenues récemment, nous indiquent que les VS ne sont pas organisées de façon laminaire dans le bouton et sont dynamiquement échangées entre plusieurs

boutons pré-synaptiques formés en passant le long des axones. Ce phénomène a conduit à la dénomination d'un contingent additionnel nommé le super contingent de VS («super-pool»). Notre laboratoire a participé à la caractérisation du super contingent vésiculaire in vitro et in vivo grace à l'utilisation des souris VGLUT1^{venus}.

Finalement, la caractérisation des souris perte de fonction pour VGLUT1 (*vglut1*$^{-/-}$) nous a indiqué que la taille du super pool vésiculaire est augmentée alors que le nombre de vésicule à la synapse est diminué. Cela suggère que VGLUT1 joue un rôle dans la régulation de la taille du super contingent vésiculaire en plus de son rôle de transporteur vésiculaire du glutamate.

Mon travail de thèse s'est focalisé sur la mobilité des VS dans les axons, la caractérisation des mécanismes de régulation du super contingent impliquant VGLUT1 et l'élaboration de nouveaux outils pour caractériser le super contingent de VS.

Tout d'abord, j'ai engagé une étude des relations entre la structure de VGLUT1 et ses fonctions. J'ai mesuré l'échange vésiculaire entre le bouton pré-synaptique et le super contingent en utilisant la technique de FRAP pour récupération de fluorescence après photo-blanchiment (Fluorescence Recovery After Photobleaching). J'ai également analysé le mouvement des vésicules synaptiques du super contingent le long des axons par imagerie en temps réel. Les résultats montrent que les taux d'échanges vésiculaires sont dépendants du niveau d'expression de VGLUT1. Dans les cultures cellulaires VGLUT1$^{-/-}$ le taux d'échange des VS est plus important que dans les cultures cellulaires VGLUT1$^{+/+}$. Il y a moins d'échange vésiculaire quand VGLUT1 est surexprimé. Par conséquent, VGLUT1 semble participer à la régulation du stock de VS dans le bouton pré-synaptique.

Pour identifier les structures de VGLUT1 impliquées dans la régulation de la mobilité vésiculaire, nous avons généré un mutant dit "silencieux" de VGLUT1 (sVGLUT1). Ce mutant ne charge plus les VS en glutamate mais est exprimé normalement sur les VS. sVGLUT1 m'a permis d'identifier que la structure de VGLUT1 et non l'état de chargement du glutamate, est essentielle pour la régulation de la mobilité vésiculaire.

Les 3 transporteurs VGLUTs présentent un cœur constitué des domaines transmembranaires très fortement identiques, mais ils sont très divergeant dans leurs parties N et C-terminal. Le motif SYGAT en position 540 s'avère être extrêmement conservé dans la partie C-terminal de toutes les isoformes de VGLUT. S540 est un site potentiel de phosphorylation. VGLUT1, à la différence des deux autres formes, semble

être spécialisé chez les mammifères par le gain de 2 motifs poly-proline spécifiques (PP1, PP2). Les motifs poly-proline contiennent une séquence consensus de liaison des protéines SH3. Des études antérieures ont montré que VGLUT1 peut interagir avec le domaine SH3 de l'endophilin A1. Cette interaction serait impliquée dans le processus de recyclage des vésicules synaptiques ou dans la réduction de la probabilité de libération des vésiculaires synaptiques.

Les cultures neuronales VGLUT1$^{-/-}$ ont été transduites avec des mutants VGLUT1 et le niveau d'expression de chaque mutant est contrôlé par l'expression de VGLUT1 endogène. De façon surprenante, VGLUT1 est une protéine phosphorylée mais S540 n'est pas un site phosphorylé. L'absence de PP2 augmente l'échange des VS avec le super contingent axonal.

Dans un second temps, j'ai généré une lignée de souris gain de fonction VGLUT1^{mEos2} afin d'augmenter notre capacité à étudier le trafic vésiculaire et de caractériser le super contingent de VS. mEos2 est une protéine fluorescente verte photo-convertible en rouge par une illumination aux UV. Grâce à cette lignée, nous pouvons suivre des vésicules synaptiques individuellement avec des techniques de microscopie à super-résolution et faire face aux limites rencontrées lors du traçage des vésicules synaptiques VGLUT1^{venus}.

Chez les animaux KI VGLUT1 mEos2, la protéine VGLUT1mEos2 remplace de façon précise VGLUT1. Mais un effet knock down a été retrouvé dans cette lignée. Comparé aux animaux possédant les allèles VGLUT1$^{+/+}$, l'expression de VGLUT1 n'est que de 20-30% chez les animaux VGLUT1$^{Eo/Eo}$. Cela indique une faible efficacité de la synthèse protéique ou une dégradation de la protéine altérée. Cependant VGLUT1^{mEos2} est fonctionnel pour la neurotransmission. Contrairement au souriceaux VGLUT1$^{-/-}$ qui meurt 3 semaines après leur naissance, les souris VGLUT1$^{Eo/Eo}$ ne montrent aucun déficit majeur comparés aux autres souris VGLUT1$^{Eo/+}$ et VGLUT1$^{+/+}$. Cela indique que le la perte d'expression sévère de VGLUT1 n'a pas un impact majeur et permet de maintenir une activité glutamatergique de base chez la souris.

Avec VGLUT1^{mEos2}, nous pouvons à la fois étendre la caractérisation du super-pool par le traçage des VS sur de longues périodes au niveau d'un seul axone, mais aussi suivre des milliers de molécule de VGLUT1 individuellement par sptPALM (photoactivation localization microscopy). De plus, l'expression réduite de VGLUT1 dans cette lignée de souris peut être aussi un avantage pour étudier la relation entre l'expression de VGLUT1, la mobilité vésiculaire, et la neurotransmission.

En général, mon travail de thèse contribue à la connaissance de VGLUT1 dans la régulation de la mobilité des vésicules synaptiques et fournit de nouveaux outils pour l'investigation de la physiologie du super contingent vésiculaire. Cependant, des questions annexes restent à étudier. Il semble important d'arriver à comprendre le mécanisme d'action par lequel la partie c-terminale de VGLUT1 régule la taille du super contingent vésiculaire. Par ailleurs, le rôle du super contingent de VS sur l'activité neuronale et à fortiori sur le comportement reste inconnu. En utilisant ces nouveaux outils générés pendant ma thèse, il sera possible d'étudier la contribution du super-pool dans l'activité neuronale d'un comportement donné par le biais d'approche d'imagerie in vivo.

Mots clés : mobilité des vésicules synaptiques, VGLUT1, super-pool, imagerie en temps réel, analyse structure-fonction.

Title : Axonal homeostasis of VGLUT1 synaptic vesicles in mice

Abstract :

Synaptic vesicles (SVs) are essential for neurotransmission, and more efforts are needed for better understanding their neurotransmitter content, release kinetics, distribution and mobility. SVs are not only clustered in presynaptic boutons, but also dynamically shared among multiple *en passant* presynaptic boutons, a phenomenon named SV super-pool. Previous work from our laboratory suggested that the Vesicular GLUtamate Transporter 1 (VGLUT1) may play a role in regulating SV super-pool size beyond loading glutamate into SV.

My Ph.D project is focused on SVs mobility in axons. Firstly, I generated a VGLUT1^{mEos2} knock-in (KI) mouse line, which provides extended possibilities to study the SV trafficking and characterize SV super-pool. Secondly, I engaged in a thorough VGLUT1 structure-function analysis. I identified that VGLUT1 tends to cluster SVs in the presynaptic boutons and reduce SVs exchange with the super-pool via the second poly-proline motif of its C-terminus.

Overall, my Ph.D work contributes to the knowledge of the role of VGLUT1 in regulating SVs mobility and provides new tools for the further investigations on SV super-pool physiology.

Keywords : synaptic vesicle mobility, VGLUT1, super-pool, live imaging, structure-function analyses.

Team Synapse in Cognition

Interdisciplinary Institute for NeuroScience

Université de Bordeaux

146 rue Léo – Saignat – 33077 Bordeaux Cedex

Acknowledgment

First and foremost, I would like to give my sincere thanks to Etienne Herzog for his great supervision and guidance throughout the past four years. With all the time and energy he invested on teaching, I benefited greatly both on scientific research and self-confidence. I also would like to thank Nils Brose for his support and guidance, especially during my stay in Max Planck Institute of Experimental Medicine, Göttingen. He tried to solve all the problems and made my project smoothly ongoing.

I am very grateful to Martin Oheim, Serge Marty, Lydia Danglot, Nathalie Sans and David Perrais for accepting to be part of my Ph.D thesis jury and taking the time to evaluate and discuss this work.

Moreover, I would like to thank Dr. Yann Humeau for his support and useful suggestions to my project. In addition, he spent a lot of time to teach me the electrophysiological knowledge and techniques. As a great team leader, he organizes a relaxed lab atmosphere that I enjoyed the time that I worked in the lab.

I would like to thank all the members who are in or used to be in the team "Synapse in Cognition". All of them helped and supported my work in the past 4 years. Maria Florencia Angelo, Christelle Martin, Marilyn Lepleux, Elisa Luquet, Chun-Lei Zhang, Hajer EI Oussini, Mattia Amie and Marianne Aincy, thank you all for the help on my work and the administrative issues. I really like the lovely moments we spent together with them in the past four years.

I would like to thank all the team members in Department of Molecular Neurobiology, MPI-EM, Göttingen. Especially, Noa Lipstein, thanks for her great teaching and help on generating the new mouse lines. Birgit Glaeser, Fritz Benseler, Sally Wenger, Dilja Krueger, Benjamin Cooper, Cordelia Imig, they helped me on the administrative issues and experimental techniques. And all the other team members in the department, I have a very nice memory of Göttingen with them.

Special thanks to Clémence Peyrot and Maria Victoria Fernandez Busch, for their 6 months internships and their great contributions on this project.

Many thanks to the PIV members, especially Elisabeth Normand and Méllissa Deshors, for taking care of the mouse lines, and Pierre Costet for the breeding of VGLUT1^{mEos2} mouse line. In addition, I would like to thank the technicians in the animal facility in Göttingen for their excellent work. Without them, there won't be VGLUT1^{mEos2} knock-in mouse line.

Thanks to all the members in Bordeaux Imaging Center. Christel Poujol, Fabrice Cordelières, Sébastien Marais and Patrice Mascalchi, for their help and technical assistance during my imaging experiments.

I would like to thank Rémi Galland, Corey Butler, Jean-Baptiste Sibarita, Pierre Bon and Baudouin Denis de Senneville for the pleasant collaboration with the ongoing work.

Delphine Bouchet, Béatrice Tessier and Angibaud Julie and many other colleagues in the institute, thank you all for your help on my experiments or the technical issues.

And all the friends in Bordeaux and Göttingen, thank you all for the encouragement and comfort when I was depressed or stressed. Especailly to Blanka Kellermayer, Azra Elia Zamri, Jennifer Day, Hung-en Hsia and Trayana Stankova for sharing the complains, dinners, trips and board games.

Last but not least, I would like to thank my parents for their understanding and support of my work. And many thanks to my best friend Dan Li, she is always available whenever I need her. And also thanks to my husband, for his excellent company.

Table of contents

Introduction

Neurotransmission in CNS

Cell organization in the central nervous system

In vertebrates and some invertebrates, brain is the main organ of the central nervous system (CNS). An adult human brain contains around 93 billion neurons and 112 billion glial cells (Herculano-Houzel, 2009). Neurons are highly polarized cells that mainly transmit information at axon varicosities/terminals and receive signals at dendrites; whereas, glial cells play important roles mainly in metabolic support, insulation, and guidance of development but may also impact the neurotransmission more directly (Zahs, 1998; Hatten, 1999; Auld and Robitaille, 2003). These cells form an extremely sophisticated, yet accurate and efficient network, which can produce a variety of complex responses to stimuli.

Neurons are polarized cells with a basal compartment consisting of the soma and dendrites, and an apical axonal compartment (Dotti and Banker, 1987). Dendrites usually extend for hundreds of micrometers and branch multiple times, whereas the axonal projection may travels for centimeters to meters for neurotransmission. Neurons are excitable cells that connect to each other to form networks and transmit electrical or chemical signals to other neurons at synapses.

Synapse and neurotransmission

Morphology

There are two types of synapses in the CNS: electrical synapses and chemical synapses. A minority of electrical synapses are composed of specialized cell-to-cell contacts known as nexuses or gap junctions which mediate the direct transfer of ions and small molecules between adjacent cytosols (Margiotta and Walcott, 1983). Voltage changes in the presynaptic cell can induce the same voltage changes in the postsynaptic cell. Unlike electrical synapse, chemical synapses leave a small gap between the presynaptic and postsynaptic compartments (Fig. 1). This gap, named “synaptic cleft”, is approximately 20 nm wide (Palay, 1956; Gray, 1959; Zuber et al., 2005). Chemical synapses convert the action potentials into chemical signals by releasing neurotransmitter into the

presynaptic cleft at the level of presynaptic boutons. Neurotransmitter molecules bind to receptors located in the plasma membrane of the postsynaptic dendrites (but also on other cells; Fig. 1) to induce an electrical response or achieve a secondary messenger pathway in the postsynaptic neuron (López-Muñoz and Alamo, 2009).

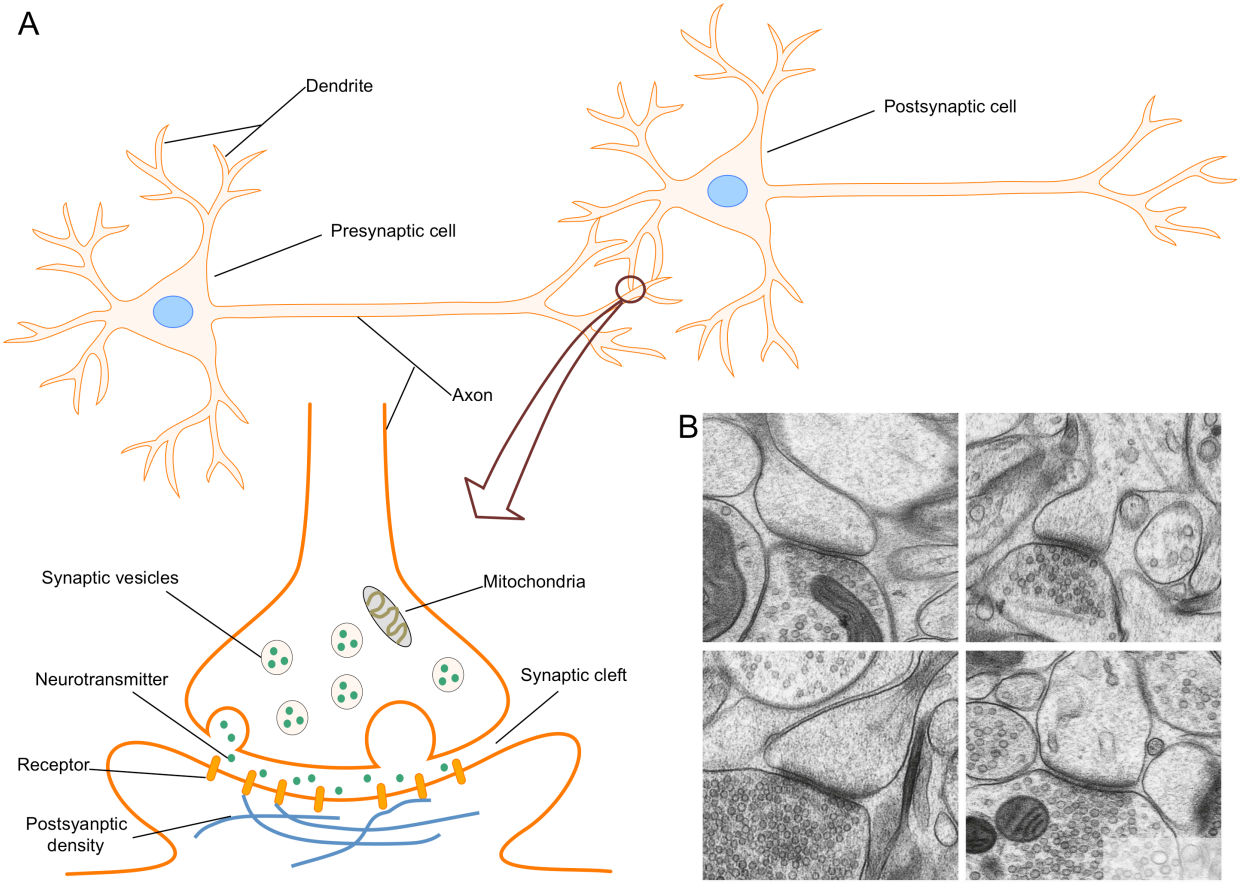

Fig 1. **Chemical synapses.** (A) Neurons contact target neurons at synapses for signal transmission. Chemical synapses (here the example of an excitatory synapse) comprise a presynaptic compartment with synaptic vesicles and mitochondria, and a postsynaptic element with receptors at the surface that are regulated by a wealth of scaffolding molecules assembled at the post-synaptic density. SVs fuse at active zone and release neurotransmitter in the synaptic cleft. Neurotransmitters bind with the receptors and induce and electrical response. (B) Ultrastructure of synapses in cryo-fixed neuropil (Korogod et al., 2015).

Chemical synapses consist of a presynaptic component that is formed by axonal varicosities/terminals, and a postsynaptic part, which mainly locates at dendritic shafts and spines (Fig 1). Using electron microscopy (EM), Gray identified two main categories of synapses: type I or asymmetric, which were later shown as glutamatergic and excitatory; and type II or symmetric, later shown to be GABAergic and inhibitory (Gray, 1959; Uchizono, 1965). The excitatory synapses are the majority and mainly contact spines on dendrites. They have a prominent postsynaptic density as seen by EM, in

contrast with inhibitory synapses, which have less dense postsynaptic specialization and are usually found on the cell body or proximal dendritic shaft (Colonnier, 1968). Through chemical fixation, synaptic vesicles (SVs) in the excitatory synapse appear in round shape and with a clear center under EM, whereas they are flattened and pleomorphic at inhibitory synapse (Uchizono, 1965; Colonnier, 1968; Korogod et al., 2015).

Molecular organization

At the molecular level, both sides of the synapse are highly specialized through a genetic program expressed by either cell and adjusted through trans-synaptic signaling (Brose, 2009). The presynaptic element is packed with macromolecular scaffolds, SVs and mitochondria (Palay, 1956; Gray, 1959; Perkins et al., 2015). SVs dock and fuse at the active zone (AZ) to release neurotransmitters following stimulations. The AZ is a strip of electron-dense material at the presynaptic plasma membrane (Fig. 1B), which provides both a structural and molecular organization for synaptic activity (Heuser et al., 1974; Südhof, 2012). The AZ is formed by a compact protein cytomatrix, which includes Piccolo/Aczonin, Bassoon, Rab3 interacting molecules (RIMs), Unc-13, RIM binding protein (RBP), Liprin-α, and CAST/ELKS/ERC among others (Südhof, 2012).

Dendritic spines are actin-enriched protrusions and are normally the postsynaptic targets of axon terminals releasing glutamate (glutamatergic). In the spine head (Fig. 1), a postsynaptic density (PSD), which comprises neurotransmitter receptors, signaling proteins and cytoskeletal proteins, is precisely apposed to the presynaptic AZ. The plasma membrane of PSD are enriched with 2 types of ionotropic glutamate receptors (AMPA: α-amino-3-hydroxy-5-methyl-4-isoxazolepropionic acid; NMDA: N-methyl-D-aspartic acid and kainic acid) (Sheng and Hoogenraad, 2007; Harris and Weinberg, 2012).

In addition to the pre and postsynaptic compartments, in the cleft, there is a packed electron-dense material (Fig. 1B) that may participate to the maintenance of synapses such as cell adhesion molecules. These cell adhesion molecules include the neuroligins, SynCAMs/Necls, EphBs/ephrinBs, LRRTMs and netrin G ligands (NGLs/LRRC4s) (Sheng and Hoogenraad, 2007; Brose, 2009; Harris and Weinberg, 2012).

Vesicular GLUtamate Transporter (VGLUT)

Vesicular neurotransmitter transporters

Neurotransmitter molecules are packed into synaptic vesicles by the vesicular neurotransmitter transporter (VNT) with the driving force supplied by a vacuolar-type H^+-ATPase (V-ATPase). V-ATPases are located at SVs membrane and generate an electrochemical proton gradient ($\Delta\mu H^+$) across the membrane (fig. 2A). Thus the vesicle lumen is acidified to a pH value of ~5.5 (Moriyama et al., 1992; Edwards, 2007). $\Delta\mu H^+$ consists of two components, the membrane potential ($\Delta\Psi$) and the pH gradient (ΔpH). According to the human genome nomenclature, vesicular transporters belong to three solute carrier (SLC) families. Vesicular monoamine transporters (VMAT) and vesicular acetylcholine transporter (VAChT) are SLC18 transporters. The vesicular monoamine and Ach transport depends more on ΔpH than $\Delta\Psi$ (EIDEN et al., 2004). Glutamate and the putative ATP transporter belong to SCL17 family and rely more on $\Delta\Psi$ than ΔpH (Reimer and Edwards, 2004). The SLC32 family comprises the vesicular inhibitory amino acid transporter (VIAAT, or VGAT for vesicular GABA transporter) (Gasnier, 2004). GABA transport with no net charge involves the movement of equal number of H^+ and charge, making VGAT equally dependent on both ΔpH and $\Delta\Psi$ (Edwards, 2007; Anne and Gasnier, 2014).

The lingering history of VGLUT cloning and characterization

Glutamate is transported into SVs by vesicular glutamate transporters (Fig. 2A). Molecularly, VGLUT1 (Fig. 2B) was first cloned by similarity to the kidney Na^+ dependent phosphate co-transporter. Expression of VGLUT1 mRNA in *Xenopus* oocytes resulted in a Na^+ dependent transport of inorganic phosphate (PI). Then, VGLUT1 was formed to be highly expressed in brain and thereby confoundedly named BNPI for Brain specific Na+/PI cotransporter (Ni et al., 1994). Some years later, the group of Robert Edwards could show that BNPI mostly locates at SVs of excitatory synapses instead of plasma membrane where Na^+ dependent transporters are normally found (Bellocchio et al., 1998). Later on, BNPI was shown to uptake glutamate in SVs and renamed as VGLUT1 (Bellocchio et al., 2000; Takamori et al., 2000). Soon after, a highly homologous protein named differentiation-associated Na+/PI cotransporter (DNPI) was discovered and identified as VGLUT2 (Fremeau et al., 2001; Herzog et al., 2001; Takamori et al., 2001). In 2002, the third isoform was identified by homology cloning in a rat

hippocampal cDNA library. Upon vesicular glutamate uptake confirmation, it was named VGLUT3 (Gras 2002; Takamori 2002). VGLUT3 differs from the other two isoforms, as it acts proeminently at neurons previously known to release another neurotransmitter (GABA, acetycholine, serotonin) (Gras et al., 2002; Herzog et al., 2004a).

To date, the Pi transport function of VGLUTs remains as an open question. Though, it was shown that Pi transport by VGLUT2 is resistant to inhibitors and mutations that could alter glutamate uptake (Juge et al., 2006), no other work identified this transport activity and could assign a physiological function to it.

How do VGLUTs uptake glutamate?

Glutamate is the main excitatory neurotransmitter in CNS. Together with other amino-acid neurotransmitters, glutamate was originally considered to be released directly from the cytoplasm of nerve terminals (De Belleroche and Bradford, 1977). But later on, with highly purified SVs, it was demonstrated that glutamate is uploaded into SVs and released through exocytosis (Naito and Ueda, 1983). In addition, SV glutamate transporter does not recognize aspartate or glutamine, and has a marked preference for L-glutamate over D-glutamate (Naito and Ueda, 1983; Maycox et al., 1988).

As described before, V-ATPase builds up a proton electrochemical gradient ($\Delta\mu H^+$) across the vesicle membrane for transporting neurotransmitters (Moriyama et al., 1992; Forgac, 1999). Unlike other vesicular neurotransmitter transport, glutamate uptake depends predominantly on $\Delta\Psi$ rather than ΔpH (Maycox et al., 1988; Edwards, 2007). Wether VGLUTs use intraluminal protons in an antiport mechanism to load glutamate against its concentration gradient inside the SV lumen remains an open question as well as the stoechiometry of glutamate transport (Fig 2A). Chloride (Cl^-) provides charge compensation for the electrogenic H^+-ATPase, enabling the acidification of synaptic vesicles (Maycox et al., 1988).

VGLUT activity has a biphasic dependence on extra vesicular Cl^- (Naito and Ueda, 1985). It reaches maximal transport activity when Cl^- is 2-4 mM, but declines with rising Cl^- concentration from 10-100 mM and very low in the absence of external Cl^- (Naito and Ueda, 1983; Bellocchio et al., 2000). At low concentrations, Cl^- appears to act allosterically (Hartinger and Jahn, 1993). Whereas, at high concentrations, it inhibits glutamate uptake, presumably by dissipating the driving force $\Delta\Psi$. The intracellular Cl^- channel, ClC-3, was considered contributing to Cl^- dependent acidification of SVs. Indeed,

Clcn3$^{-/-}$ mice, display an reduced SV acidification in the presence of ATP (Stobrawa et al., 2001). But later on, a study showed that VGLUT1 knock out abolishes nearly completely the Cl^- dependent acidification of SVs (Schenck et al., 2009). These authors also demonstrated that Cl^- transport was conducted by VGLUT itself and high luminal Cl^- concentration activates the uptake of glutamate (Schenck et al., 2009). The result, is consistant with other studies that support the presence of an allosteric binding site of Cl^- on VGLUTs (Hartinger and Jahn, 1993; Preobraschenski et al., 2014; Eriksen et al., 2016; Farsi et al., 2016)

V-ATPases activity builds up ΔpH, which in turn limits H^+ pump activity and glutamate uptake. The cation/H^+ exchange could dissipate ΔpH while maintaining ΔΨ, and thereby facilitate glutamate accumulation in vesicles. Indeed, manipulating presynaptic K^+ at the calyx of Held influenced vesicle quantal size, demonstrating that, K^+/H^+ exchange regulates glutamate release(Goh et al., 2011). Later on, it was identified that K^+/H^+ exchange may be carried by VGLUTs (Preobraschenski et al., 2014). One hypothesis is that, there are three binding sites in VGLUTs: one cationic and two anionic sites (Preobraschenski et al., 2014). But the exact locations of these binding sites are still unknown. Recently, Eriksen and colleagues generated plasma membrane targeted VGLUT1, -2 and -3 expressed in *Xenopus* Oocytes. The resulting "inside-out" vesicles configuration with VGLUT luminal side facing the extracellular space, enabled electrophysiological recording of VGLUTs associated currents. They show that VGLUTs exhibit a Cl^- conductance allosterically activated by luminal H^+ as well as Cl^-. In addition, luminal H^+ and Cl^- activate glutamate transport (Eriksen et al., 2016).

The multiple transport modes of VGLUTs ensure that the transporters have high degree of flexibility to adapt with the changing ionic environment during SV cycle and glutamate loading states (Preobraschenski et al., 2014). Based on the investigations up to now, the Cl^- conductance by VGLUTs is readily accepted. More investigations need to focus on confirming whether VGLUTs indeed mediate multiple transport activities with distinct driving forces and exploring the exact mechanisms (Takamori, 2016).

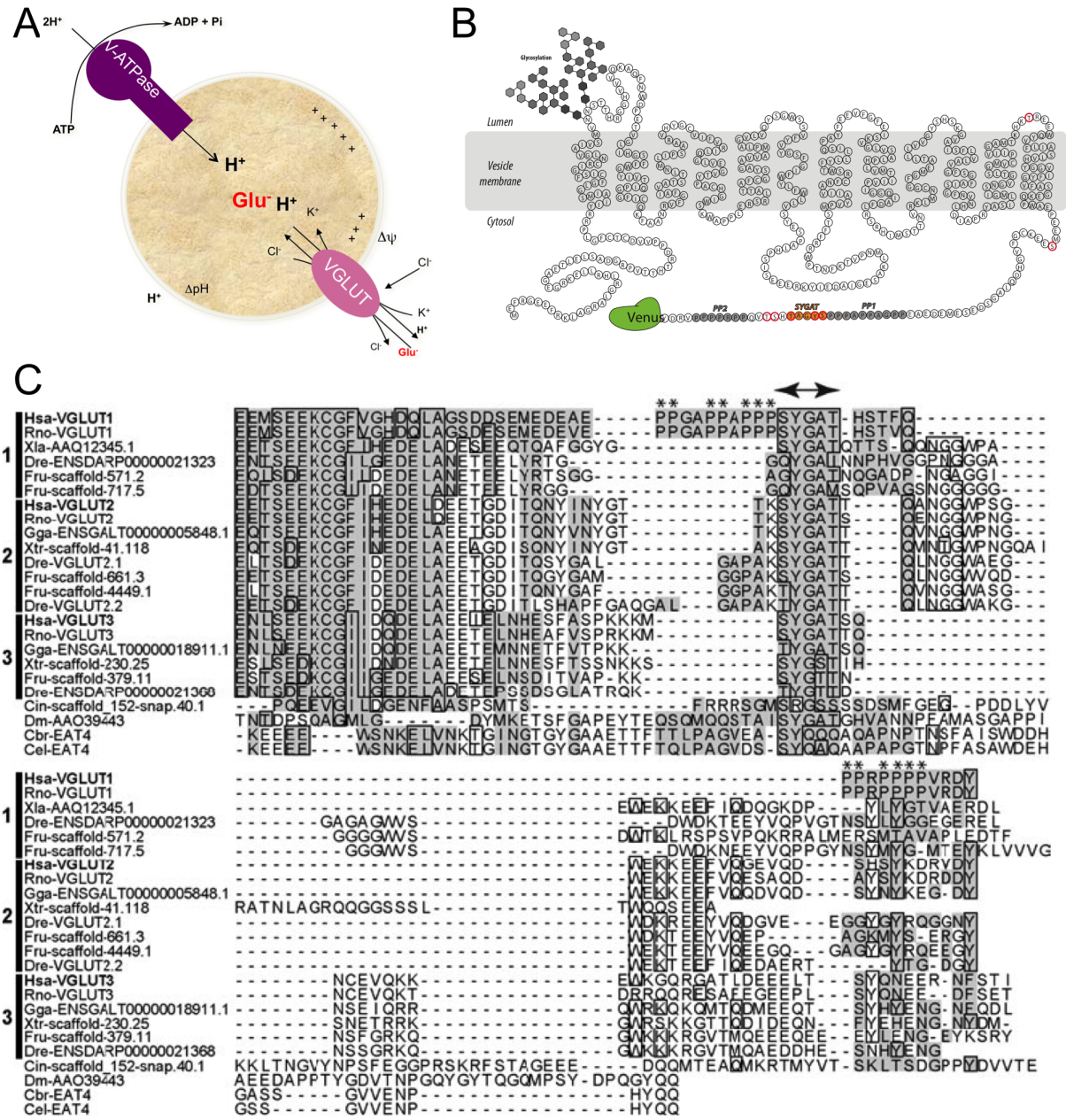

Fig. 2 **Vesicular glutamate transport.** (A) VGLUT locates at synaptic vesicle and mediates glutamate loading into vesicles. A V-ATPase generates an electrochemical gradient by transporting protons into the vesicle in an ATP dependent fashion. Glutamate transport mainly depends on ΔΨ rather than ΔpH. Cl^- and K^+ also seem to contributes to glutamate loading but this is still debated. (B) Schematic transmembrane profile of VGLUT1. VGLUT1 contains 12 transmembrane domains. N- and C- termini are exposed to the cytoplasmic side. (C) Alignment of VGLUT C-terminal sequences in various species. A highly conserved SYGAT motif (double arrow) exists in all VGLUT homologues and two poly proline domains (asterisks) are specific to mammalian VGLUT1 proteins (Vinatier et al., 2006).

Complementary distribution patterns of VGLUTs

In mammals, there are three isoforms of VGLUT: VGLUT1 (SLC17A7), VGLUT2 (SLC17A6) and VGLUT3 (SLC17A8); these VGLUTs share the same glutamate transport mechanisms, but distinct regional distributions (Fig. 3).

VGLUT1 and VGLUT2 are largely expressed to distinct populations of excitatory neurons in a complementary pattern (Herzog et al., 2001; Kaneko and Fujiyama, 2002; Takamori, 2006). In situ hybridization shows that VGLUT1 mRNA is mainly located in olfactory bulb, neo-cortex, cerebellar cortex, medial habenula, pontine nucleus and hippocampus (including subiculum); and lower expression in lateral septum and thalamic nuclei (Fremeau et al., 2001; Herzog et al., 2001; Varoqui et al., 2002; Boulland et al., 2004). Whereas, VGLUT2 mRNA is detected in all thalamic nuclei (except reticular nucleus typically GABAergic), hypothalamus, inferior and superior colliculi, deep cerebellar nuclei and many neurons from the brainstem. Besides, low levels of VGLUT2 were also detected in hippocampus, some cortical areas and amygdala, (Fremeau et al., 2001; Herzog et al., 2001; Boulland et al., 2004). It was soon observed that VGLUT1 is present at synapse known to exhibit low release probability, whereas VGLUT2 is present at those that are known to exhibit high release probability (Fremeau et al., 2001; Varoqui et al., 2002). Immunofluorescence studies suggested a seggregation of synaptic proteins selectively at VGLUT1-positive synapse and not at VGLUT2-positive contacts (Shank PSD scaffold proteins, (Heise et al., 2016); Endophilin1A (Vinatier et al., 2006)). This further suggests that the molecular organization of VGLUT1 and VGLUT2 synapses may differ and support different modalities of glutamatergic transmission.

Unlike VGLUT1 and VGLUT2, which are mainly expressed in asymmetric synapses, VGLUT3 is expressed at symmetric synapse. VGLUT3 mRNA is found in sparse populations of neurons at regions or in patterns not typically associated to glutamatergic transmission (Gras et al., 2002; Takamori, 2006). VGLUT3 was shown at serotoninergic neurons of raphe nuclei, Cholinergic neurons of the striatum, and subclasses of GABA interneurons (cerebral cortex and hippocampus) (Gras et al., 2002; Herzog et al., 2004a; Gras et al., 2005; Mestikawy et al., 2011). Moreover, VGLUT3 is found in subgroups of primarily glutamatergic neurons in the raphe, habenula, hypothalamus, olfactory tubercles and inner hair cells of the cochlea (Gras et al., 2002; Herzog et al., 2004a; Ruel et al., 2008; Seal et al., 2008). More recently, VGLUT1 and VGLUT2 were also described in some Ach and GABA neurons in CNS (Herzog et al.,

2004b; Zander et al., 2010; Fattorini et al., 2015; Granger et al., 2016). VGLUT2 is even suspected to be expressed in some noradrenaline, adrenaline or dopamine neurons (Stornetta et al., 2002; Kawano et al., 2006; Dal Bo et al., 2008; Mestikawy et al., 2011).

The role of VGLUT co-localization with other classical VNT in the same synapse is under debate. It may serve as an enhancer to uptake and release of both neurotransmitters at synapses (Gras et al., 2008), and/or provide glutamate as a co-transmitter with distinct target or function (Mestikawy et al., 2011).

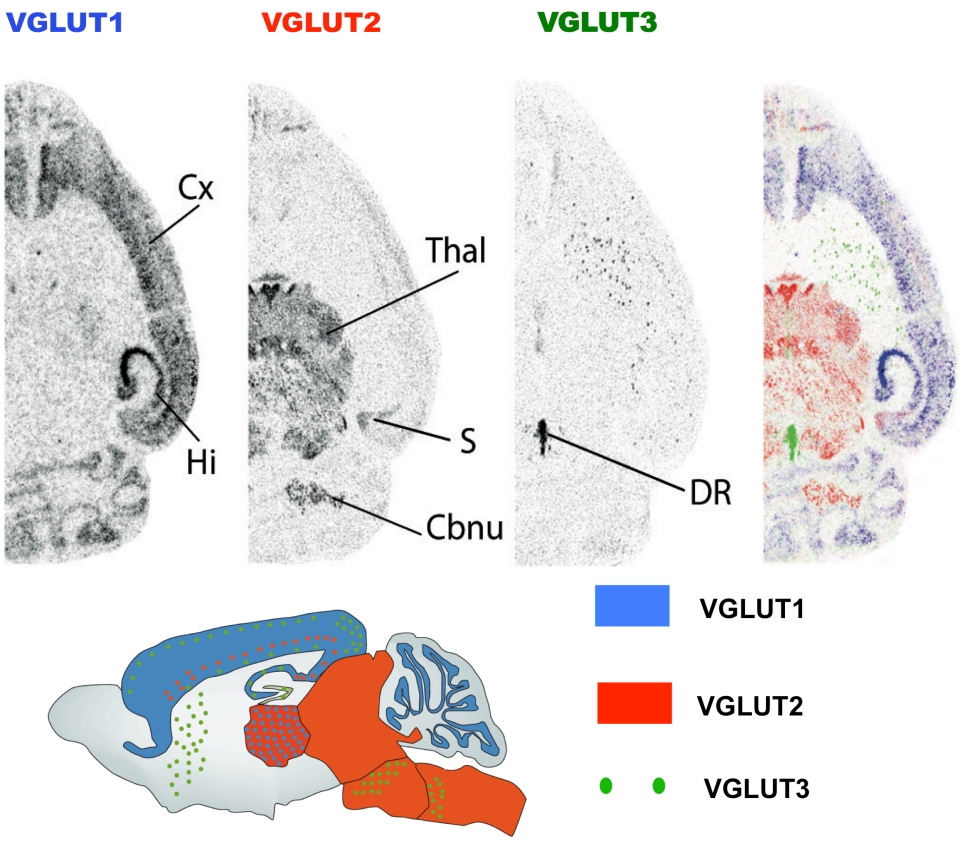

Fig. 3 **Distribution patterns of the Three VGLUTs.** In situ hybridization shows mRNA distribution of VGLUT1, VGLUT2 and VGLUT3 (image from Salah EI Mestikawy). VGLUT1 mainly labels cerebral and cerebellar cortex, while VGLUT2 mainly labels subcortical regions. VGLUT3 is depicting sparse populations of noncanonical glutamatergic neurons.

VGLUTs expression in development

The functional difference between VGLUTs is further enforced by the fact that the three transporters have different regulations during development.

VGLUT2 is expressed at high levels from early prenatal developmental stages and increases slightly to reach a plateau at P21 (Gras et al., 2005). VGLUT2 transcripts are transiently observed in the future VGLUT1 territory before fading away between P7 and P21 (Miyazaki et al., 2003; Fremeau et al., 2004; Gras et al., 2005). Very low levels of

VGLUT1 are detected from E15 to E18 in rat brain. After birth, it massively increases its expression level and replaces most VGLUT2 expression in cortex and hippocampus (Boulland et al., 2004; Miyawaki, 2005). While, VGLUT3 expression at birth is around 60% of adult level, it peaks transiently between P5 and P10 due to transient expression at Purkinjee cells of the cerebellum, and raises again steadily from P15 to adulthood (Boulland et al., 2004; Gras et al., 2005). The transient expression demonstrates that the transmitters release is changed during the development, and the glutamate release plays a role in the refinement of synaptic connection (Gillespie et al., 2005; Gras et al., 2005).

Molecular structure of VGLUTs

Each isoform of the VGLUT polypeptides comprises of 12 transmembrane domains (TMDs, Fig. 2B) with cytosolic N and C termini. The core segment of the transporters share a high degree of amino-acid identity. Correspondingly, they share nearly identical glutamate transport kinetics as discussed here above. The 3D structure of VGLUTs remains unknown. However, VGLUT1 and VGLUT2 are already constructed by homology modeling based on the cytosol-open crystallographic structure of *E. Coli* glycerol-3-phosphate transporter (GlpT) (Juge et al., 2006; Almqvist et al., 2007). These studies show that the residues H128 in TMD2, R184 and E191 in TMD4 of VGLUT2(Juge et al., 2006), and equivalent residence of H120, R176 and E183 in VGLUT1(Almqvist et al., 2007) are essential for L-glutamate transport. Moreover, there are two docking substrates in VGLUT1 structure: R80 and R314 as the central binding site, and R176 and H120 as the upper binding site. These two docking substrates need similar energy for L-glutamate binding. But when Pi is docked, all docked molecules are completely clustered around R314 (Almqvist et al., 2007). Herman *et. al* mutated VGLUT2 successively R88A, R184A, and R322A, only the triple mutant failed to rescue the glutamate transport and release (Herman et al., 2014).

The N-terminal and C-terminal sequences of VGLUTs are highly divergent (Fig. 2C), which may contribute to functional difference by interacting with different proteins of the cytosolic compartment (Takamori, 2006). There is a highly conserved motif 540-SYGAT (Fig. 2C) in the C-terminal end of all VGLUT isoforms and it is shared by most species (Vinatier et al., 2006). The S540 is a predicted GSK-3 substrate, fitting the consensus sequence S/T-X-X-X-S/T(P); it may participate in proteins interaction or SVs trafficking (Santos et al., 2014). Several dileucine-like motifs exist only in VGLUT1,

which are involved in VGLUT1 endocytosis at SVs. Foss et. al showed that the 504-SEEKCGFV motif at C-terminal acts largely via assembly protein complex 2 (AP-2) and N-terminal motif use AP-1 in trafficking regulation, but VGLUT2 mostly depends on the C-terminal motif (Foss et al., 2013). VGLUT1 C-terminal also contains two poly-proline motifs (PP1, PP2), which are not present in the other isoforms. PP1 and PP2 contain the consensus site for SH3 protein interaction domains (PXXP). Several studies showed VGLUT1 could interact with endophilin A1 SH3 domain at PP2/P554 (De Gois et al., 2006; Vinatier et al., 2006; Voglmaier et al., 2006). VGLUT1 might recruit endophilin, which is an essential component of clathrin-mediated endocytosis, to speed up the endocytosis of SVs through AP2 pathway (Voglmaier et al., 2006). Later on, Weston and colleagues reported that VGLUT1/endophilin A1 interaction reduces SVs release probability, yet the detailed mechanism for this phenomenon remains unknown (Weston et al., 2011).

VGLUT genetically modified models

To better understand VGLUTs function and properties, various genetically modified models were generated. We will now discuss the achievements obtained from these models on VGLUTs function at multiscale levels.

VGLUT1

In 2004, Fremeau et al. and Wojcik et al. first revealed the VGLUT1 contributions to CNS with VGLUT1 knockout (KO) mice (Fremeau et al., 2004; Wojcik et al., 2004). Due to the VGLUT2 dominant expression during post-natal development, VGLUT1 KO pups don't show a significant deficit before the end of the second week of life, but start to have a poor food intake afterwards and eventually die at around three weeks after birth. With special food intake care, VGLUT1 KO pups survive for a long time (Fremeau et al., 2004; Wojcik et al., 2004). The synapse number and global morphology in VGLUT1 KO mice and culture is similar to that of WT by ultrastructural analysis, but SVs number in the presynaptic terminal and SVs tonicity are significantly reduced (Fremeau et al., 2004; Siksou et al., 2013). As expected, neurotransmission is impaired when VGLUT1 is lacking: the frequency and amplitude of miniature excitatory synaptic current (mEPSC) are reduced in VGLUT1 KO neuronal culture. The remaining signal may be attributed to VGLUT2 expression (Wojcik et al., 2004). In contrast, *Drosophila* DVGLUT knock-down mutants one unit of VGLUT seemed already enough to fill completely SVs (Daniels et al.,

2006). Meanwhile, overexpression of VGLUT1/DVGLUT resulted in increased quantal content of glutamate (Daniels et al., 2004), but normal mEPSC frequency. In addition, the absence of VGLUT1 doesn't alter the expression of the other two isoforms of VGLUT or most other synaptic proteins (Wojcik et al., 2004; Siksou et al., 2013).

Half expression of VGLUT1 in mice (*vglut1*$^{+/-}$) exhibits no apparent phenotypic abnormalities during development and adulthood (Tordera et al., 2007). Yet, detailed analysis of reduced VGLUT1 expression was shown to cause increased anxiety, impair reversal learning and working memory (Tordera et al., 2007; Inta et al., 2012; Granseth et al., 2015). The LTP induction is significantly decreased in the CA1 region of *vglut1*$^{+/-}$ slices, this is accompanied by a deficit in spatial reversal learning (Balschun et al., 2010). After exposure to chronic mild stress, *vglut1*$^{+/-}$ mice surprisingly show an up regulation of VGLUT2 and an hyperlocomotion (Garcia-Garcia et al., 2009).

VGLUT1 is a specific maker for glutamatergic SVs in CNS. Our laboratory generated a VGLUT1^{Venus} knock-in (KI) mouse line. With this KI mouse line, our laboratory contributed to the characterization of SV sharing among presynaptic boutons along the same axon both in vitro and in vivo (Herzog et al., 2011). This new pool of SVs transiting in the axons was named "super-pool" (Staras et al., 2010). In line with this work, *vglut1*$^{-/-}$ phenotypes were revisited to unravel that SV super pool size is increased while SV cluster is reduced (Siksou et al., 2013). Recently, with VGLUT1^{Venus} mice, a study showed that SVs in mossy fiber terminals have a high mobility and the diffusion limits vesicle reloading during sustained high frequency stimulations (Rothman et al., 2016).

VGLUT2

VGLUT2 deletion in mice results in perinatal lethality, which is due to the respiratory failure (Moechars et al., 2006; Wallén-Mackenzie et al., 2006). Further investigations show that, the neural circuits in the location of the pre-Bötzinger (PBC) inspiratory rhythm generator fail to become active (Wallén-Mackenzie et al., 2006). Similar to VGLUT1 KO condition, the mEPSC amplitude and frequency in *vglut2*$^{-/-}$ are reduced significantly (Moechars et al., 2006; Wallén-Mackenzie et al., 2006). In addition, VGLUT2 absence also seem to cause reduced SVs number and abnormal elongated shape in the terminal (Wallén-Mackenzie et al., 2006).

Behavioral analysis of *vglut2*$^{+/-}$ mice showed unchanged motor function, learning and memory and inflammatory pain, but impairements in the development and maintenance of neuropathic pain (Moechars et al., 2006). VGLUT2 conditional KO mice provides

possibilities to reveal the function of specific VGLUT2 circuits and related behavior (Wallén-Mackenzie et al., 2006; 2009). Selective deletion of VGLUT2 expression in the cortex, hippocampus, and amygdala of preadolescent mice, resulted in increased locomotor activity, altered social dominance and risk assessment, decreased sensorimotor gating and impaired long-term spatial memory. Further investigation identified the existence of a neurocircuitry that connects changes in VGLUT2-mediated neurotransmission to alterations in the dopaminergic system with behavioral deficits reminiscent of some symptoms of schizophrenia (Wallén-Mackenzie et al., 2009).

With *VGLUT2*^{egfp} transgenic mice, VGLUT2 ventral tegmental area (VTA) neurons were shown project to the nucleus accumbens (NAc), lateral habenula, ventral pallidum (VP), and amygdala (Hnasko et al., 2012). In addition, evidence was pointed for the expression of VGLUT2 in domapinergic neurons (DA). The precise contribution of VGLUT2 to dopaminergic neurons still remains debated (Mestikawy et al., 2011).

VGLUT3

Unlike the deletion of VGLUT1 or VGLUT2 that are lethal at some post-natal stages, the phenotype of VGLUT3 KO mice is not as severe (Gras et al., 2008; Ruel et al., 2008; Seal et al., 2008). In the *vglut3*$^{-/-}$ mice, brain architecture as well as the number and morphology of VGLUT3 neurons show no obvious alteration from WT littermates (Gras et al., 2008; Ruel et al., 2008; Seal et al., 2008). Ultrastructure analysis by Seal and colleagues reported abnormally thin, elongated ribbons of inner hair cells in *vglut3*$^{-/-}$ (Seal et al., 2008), whereas, Ruel *et al.* showed no difference compared to WT (Ruel et al., 2008).

The *vglut3*$^{-/-}$ mice are deaf and lack auditory-nerve responses to acoustic stimuli, which is due to the absence of glutamate release from inner hair cells at the first synapse in the auditory pathway (Ruel et al., 2008; Seal et al., 2008). In addition, *VGLUT3* gene was identified to be the responsible gene for DNFA25, which is an autosomal-dominant form of progressive, high-frequency nonsyndromic deafness (Ruel et al., 2008). Finaly, VGLUT3 deletion was shown to impair allodynia (the mechanical hypersensitivity to light stimuli following pain) which is mediated by low threshold mechanoreceptors (C-LTMRs) in dorsal root ganglion (DRG) neurons (Seal et al., 2009).

At the cellular level, several studies report that VGLUT3 supports “vesicular synergy”, a bioenergetic mechanism through which SV loading with serotonin or acetylcholine is enhanced by the presence of glutamate transport on the same organelle (Amilhon and

Mestikawy, 2008; Mestikawy et al., 2011). Deletion of VGLUT3 resulted in decreased acetylcholine release in striatum (Gras et al., 2008), serotonin neurotransmission in raphe nuclei (Amilhon et al., 2010). But the exact mechanism mediating vesicular synergy remains unknown and needs more investigations.

Synaptic vesicles cycle and trafficking

The synaptic vesicle cycle

Neurotransmission is triggered by an action potential that evokes a "quantal release reaction" (Katz, 1971). When an action potential reaches a presynaptic terminal, it induces the opening of voltage dependent Ca^{2+} channels. The influx of Ca^{2+} modifies protein conformations at SVs that are docked or primed at AZs plasma membrane, resulting in exocytosis. To prevent expansion of the presynaptic plasma membrane and a corresponding loss of lateral membrane tension, SV exocytosis is followed by endocytic membrane retrieval (Fig. 4). Then SVs recycle and refill with neurotransmitters for a new around of exocytosis (Heuser and Reese, 1973; Südhof, 2004).

Exocytosis

SVs docking, priming, and fusion at AZs are orchestrated by a complex molecular machinery (Fig. 4). Soluble N-ethylmaleimide-sensitive factor activating protein receptor (SNARE) are generally involved in all cellular membrane fusion processes. These proteins are characterized by a homologous 70-residue sequence called the SNARE motif, which includes four classes: R, Qa, Qb, and Qc motif. The proteins form a stable four-α-helical SNARE complex, whose assembly is though to provide the energy required for membrane fusion (Südhof, 2004; Jahn and Fasshauer, 2012). The core complex is formed by the R-SNARE motif from synaptobrevin/VAMP2, the Qa-SNARE motif from syntaxin1, and the Qb- and Qc-SNARE motifs from SNAP-25 (Südhof, 2004). Besides the SNARE-complex assembly, Sec1/Munc18-like (SM) proteins are also associated with fusion reaction through the binding with syntaxin1 (Hata et al., 1993; Verhage et al., 2000; Dulubova et al., 2007). Munc18-1 initially binds to the closed conformation of sytaxin-1. Sytaxin-1 opens to trigger the preparation of fusion and SNARE complexes form. After the triggering of fusion, Munc18-1 remains attached to syntaxin-1 in the assembling SNARE complex (Dulubova et al., 2007). With the SNARE

complex, the vesicle is pulled close to the plasma membrane, where it is ready to fuse in response to the Ca^{2+} influx. SNARE/SM complex assembly is maintained by chaperones (Burré et al., 2010), and the disassembly is mediated by a specialized ATPase (NSF) and its adaptors (SNAPs) (Söllner et al., 1993).

AZ provides the platform for rapid fusion of SVs after Ca^{2+} influx. Ca^{2+}-channels need to be localized adjacent to docked and primed vesicles (Fig. 4) for fast coupling of an action potential that triggers exocytosis. The mean distances from the edge of Ca^{2+}-channel clusters to vesicles range from 30 to 100 nm (Neher, 2015). The cytoplasmic matrix of the AZ (CAZ) components include the giant proteins bassoon and piccolo, Rab6 interacting proteins (ELKS), liprin and GIT family proteins, RIMs and the SNARE regulator Munc13 (Südhof, 2012). Moreover, RIM, RIM-BP and Munc13 form a protein complex that mediates the docking and priming of SVs at the AZs and recruit Ca^{2+}-channels to the docked and primed vesicles (Kaeser et al., 2011). RIM interacts with small Rab3 and Rab27 GTP-binding proteins on SVs (Gracheva et al., 2008; Kaeser et al., 2011), meanwhile, it also binds and activates Munc13. Munc13 may promote SNARE-complex assembly by catalyzing the conformational switch of syntaxin-1 from closed to open (Brose et al., 1995; Deng et al., 2011; Südhof, 2013). Neurotransmitter release is completely blocked at *munc13-1*$^{-/-}$ synapses (Augustin et al., 1999).

Upon the Ca^{2+} influx, synaptotagmins and complexin are involved and promote the calcium-triggered exocytosis (Jahn and Fasshauer, 2012; Trimbuch and Rosenmund, 2016). Synaptotagmins are Ca^{2+} sensors that are anchored to SVs (Brose et al., 1992). The synaptotagmin C2 domains bind to syntaxin-containing SNARE complexes (Söllner et al., 1993; Li et al., 1995). Complexins are small cytoplasmic proteins that bind to the surface of the SNARE complex. Without Ca^{2+}, complexin stabilizes the SNARE complex by increasing the energy needed for fusion, whereas, Ca^{2+} influx results in a dramatical reduction of energy required for fusion (Xue et al., 2010; Yang et al., 2010; Trimbuch and Rosenmund, 2016). Recently, ultrastructural studies showed that vesicles docking requires Munc13/CAPS priming proteins and all three SNAREs, but not synaptotagmin1 or complexins (Siksou et al., 2009; Imig et al., 2014).

The whole process of exocytosis proceeds in less than a millisecond, and this ultra fast process makes it extremely difficult to establish its molecular mechanism. One model which is supported by abundant evidences proposed that, SNAREs complex are partially assembled to elevate SVs into a pre-fusion state (Jahn and Fasshauer, 2012; Südhof,

2013). SVs membrane fusion with the plasma membrane is the final step of exocytosis, but the detailed mechanisms also remain unclear. It is proposed that SNARE proteins force membranes into close proximity, but the transmembrane region may not directly form a fusion pore and serve as membrane anchors (Südhof, 2013). And SM proteins, riding on top of assembling SNARE complexes, may enable lipid mixing between the fusing membranes (Südhof, 2013). Once SV fuses, neurotransmitters diffuse into the cleft and bind with postsynaptic receptors to induce the signaling cascades.

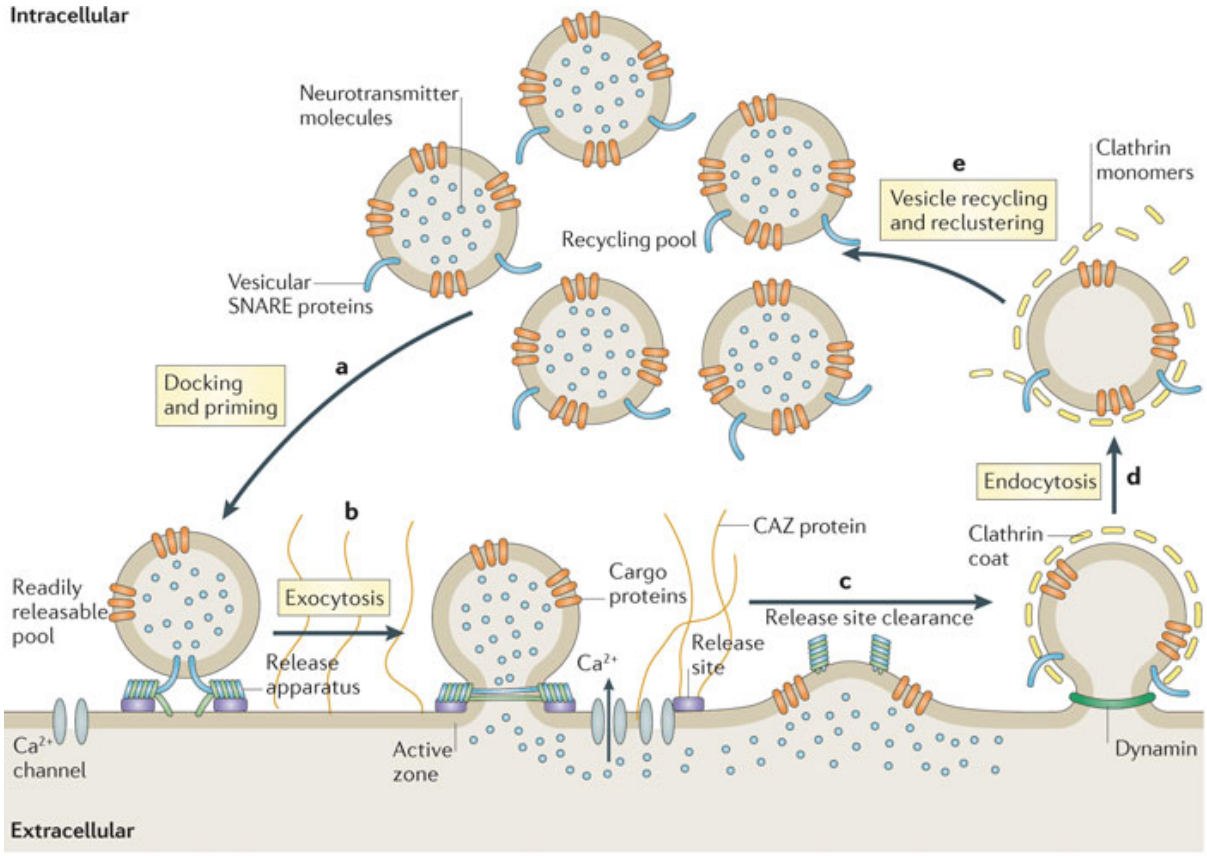

Fig 4. **The synaptic vesicle cycle.** (a) SVs docking and priming at the active zone constitute the readily releasable pool. (b) Ca^{2+} influx induces SVs exocytosis and release neurotransmitter in to the synaptic cleft. (c) After the SV membrane fusion, release site has to undergo clearance. (d) Endocytosis of SV molecules through a clathrin- and dynamin-dependent pathway. (e) After clathrin uncoating and neurotransmitter uptake, SVs return to the recycling pool (Haucke et al., 2011).

Endocytosis

After exocytotic release of neurotransmitter from SVs, to sustain neurotransmission, SV membranes need to be retrieved, and SVs have to be reformed locally (Fig. 4) within presynaptic nerve terminals (Heuser and Reese, 1973; Haucke et al., 2011). In addition, SV recycling involves both retrieval of SV components from the plasma membrane, and

the regeneration of functional SVs of proper composition. There are several SV membrane retrieval modes: (a) an ever debated clathrin-independent rapid mode of SV recycling by kiss-and-run exocytosis/endocytosis at AZs involving a transient fusion pore; (b) a membrane endocytosis by clathrin-mediated endocytosis (CME); (c) an activity-dependent bulk endocytosis upon strong stimulation; (d) a clathrin-independent ultrafast endocytosis recently observed by EM paired with optogenetic stimulation (Südhof, 2004; Rizzoli and Betz, 2005; Soykan et al., 2016).

Kiss-and-run is a fast from of membrane retrieval and was first suggested by Ceccarelli and colleagues in 1970s. In this mode, after closure of the pore, vesicles detach from the plasma membrane and are directly reused through a fast mechanism (Ceccarelli et al., 1973; Saheki and De Camilli, 2012). Kiss-and-run in neurons is still controversial and it may only occur in endocrine cells (Kononenko and Haucke, 2015).

In CME mode, SV components are subsequently retrieved directly from the cell surface though the formation of a clathrin-coated vesicle, in a process lasting tens of seconds (Kononenko and Haucke, 2015). Clathrin-coated intermediates locate at the presynaptic membranes were observed (Heuser and Reese, 1973). Live imaging of CME sequence of events allows to have a clearer view of the complex sequence of molecular interventions at play (Merrifield et al., 2005; Taylor et al., 2011). Clathrin triskelia comprise three ~190 kDa heavy chains and ~25 kDa light chains into a polyhedral lattice (Brodsky et al., 2001; Kononenko and Haucke, 2015). The clathrin coat is composed of two layers: an inner layer of adaptors and an outer clathrin layer (Saheki and De Camilli, 2012). AP-2 as the most abundant endocytic adaptor, targets to the dileucine-like motif of several SV proteins including VGLUT1 and concentrates them in the emerging clathrin-coated pit (CCP) (Voglmaier et al., 2006; Foss et al., 2013; Kononenko and Haucke, 2015). Stonin 2 binds to and sorts synaptogamin 1, and clathrin assembly lymphoid myeloid leukemia (CALM) and AP180 sorts synaptobrevin2/VAMP2 by direct interaction of the ANTH domain (Koo et al., 2011; Saheki and De Camilli, 2012; Gauthier-Kemper et al., 2015). The GTPase dynamin catalyzes membrane scission at late stages of Ω-shaped CCPs (Raimondi et al., 2011; Saheki and De Camilli, 2012), and may be recruited to membranes by bin-amphiphysin-rvs (BAR) domain proteins, such as endophilin, amphiphysin, and SNX9/18 (Di Paolo et al., 2002; Bai et al., 2010; Milosevic et al., 2011; Meinecke et al., 2013). After fission, PI(4,5)P_2-phosphatase synaptojanin, together with Hsc70 and auxilin, remove the coat from the vesicles and disassemble clathrins

(Kononenko and Haucke, 2015). Depletion of clathrin or conditional KO of AP-2 result in defects in SV reformation and and an accumulation of endosome-like vacuoles generated by clathrin-independent endocytosis via dynamin 1/3 and endophilin (Kononenko et al., 2014).

Bulk endocytosis is thought to be driven by strong stimulation, when a large number of synaptic vesicles fuse with the plasma membrane within a short time interval and induce the infolding of plasma membrane distal to the AZ (Heuser and Reese, 1973; Saheki and De Camilli, 2012; Kononenko and Haucke, 2015). Consequently, intracellular vacuoles are generated by a non-selective mechanism of membrane uptake (Heuser and Reese, 1973; Saheki and De Camilli, 2012). In later stages, CME may be one of the pathways for resolving bulk endosomes into SVs (Kononenko and Haucke, 2015).

Recently, a new endocytosis pathway named ultrafast endocytosis was reported, which occurs within 50 to 100 ms after SV fusion at sites flanking the active zone and not compatible with kiss-and-run mode (Watanabe et al., 2013; Kononenko and Haucke, 2015). The molecular mechanism still needs to be explored. An ultrastructure study shows that clathrin is not required for ultrafast endocytosis (Watanabe et al., 2014). Moreover, the invagination is blocked by inhibition of actin polymerization, and scission is blocked by inhibiting dynamin (Watanabe et al., 2013). But dynamin requires seconds or even tens of seconds to complete membrane fission, which doesn't match the time course for ultrafast membrane. Additional factors like actin, BAR donmain proteins such as endophilin or membrane lipids may also be involved in the ultrafast membrane retrieval (Kononenko et al., 2014). In addition, the vesicles after endocytosis may fuse and form endosome like intermediates. The synaptic endosome is resolved into synaptic vesicles by clathrin-mediated budding (Watanabe et al., 2014). Whether ultrafast endocytosis is a general mechanism or a specialization for synapses with high turnover will require further study (Watanabe et al., 2014).

SVs are regenerated with the homogenous size and function after the membrane retrieval (Fig. 4). In the kiss-and-run mode, SVs can be reused directly. CME and endosomal pathways of vesicle budding needs tens of seconds to reforms to functional SVs (Kononenko and Haucke, 2015). But how the endosome-like vacuoles eventually convert to new vesicles is still unknown. The most likely is that the vacuoles may back fuse with the plasma membrane and via clathrin/AP-2 mediated budding (Saheki and De Camilli, 2012; Watanabe et al., 2014; Kononenko and Haucke, 2015). Another possibility

might be AP-3 and AP-1, the heterotetrameric complexes similar to AP-2, are potential candidates for assembling coats that differ from endocytic clathrin coats (Nakatsu et al., 2004; Glyvuk et al., 2010). Newly endocytosed SVs are recycled to the SVs cluster with the guidance of actin, linked to SV-associated actin binding protein, synapsin (Haucke et al., 2011).

Synaptic vesicle pools

At presynaptic terminals, neurotransmitter-filled SVs are organized in a cluster adjacent to the active zone (AZ, Fig. 5). These SVs have an homogeneous appearance under EM and no significant biochemical distinctions was shown to our knowledge. SVs are 40-50 nm in diameter (Landis et al., 1988; Siksou et al., 2013; Imig et al., 2014; Bruckner et al., 2015), and it is reported that the diameters increased by 3-6 nm in Munc13-1/2 DKO, SNAP-25 KO and Synaptobrevin-2 KO slices (Imig et al., 2014). Each SV is linked to one or two neighboring vesicles by short filaments (30-40 nm in length), and longer filaments (50-60 nm in length) connect the SV network to the AZ membrane (Landis et al., 1988; Siksou et al., 2007). Synapsins are thought to be part of the connector (Landis et al., 1988). Yet, synapsin triple KO mice showed less SVs per hippocampal bouton with some connectors still presented (Siksou et al., 2007). This indicates that more partners are involved in the regulation of SV organization.

SVs are classified into different functional pools. Classically, the SVs are assigned into three pools (Fig. 5): the reserve pool, the recycling pool and the readily releasable pool (Südhof, 2004; Rizzoli and Betz, 2005). The readily releasable pool consists of SVs ready to release upon minimal Ca^{2+} elevation or osmotic changes. The recycling pool is defined as the vesicles that maintain release on moderate stimulation and it contains around 5-20% of all vesicles. The reserve pool occupies most of the vesicle clusters (typically ~80-90%) and only recycles upon plasticity induced by a strong stimulation (Rizzoli and Betz, 2005; Denker and Rizzoli, 2010; Verstegen et al., 2014). For many years, it was thought that SVs recycle inside a single terminal and that single terminals function as isolated units distantly operated from the cell soma. In the past decade, SVs were observed in dynamic sharing along the axon among multiple en passant presynaptic boutons. This axonal SV population was designated as “super-pool” (Denker and Rizzoli, 2010; Fowler and Staras, 2015). This super-pool was observed not only in vitro, but also

in vivo thanks to our VGLUT1^{venus} mouse line (Darcy et al., 2006; Staras et al., 2010; Herzog et al., 2011).

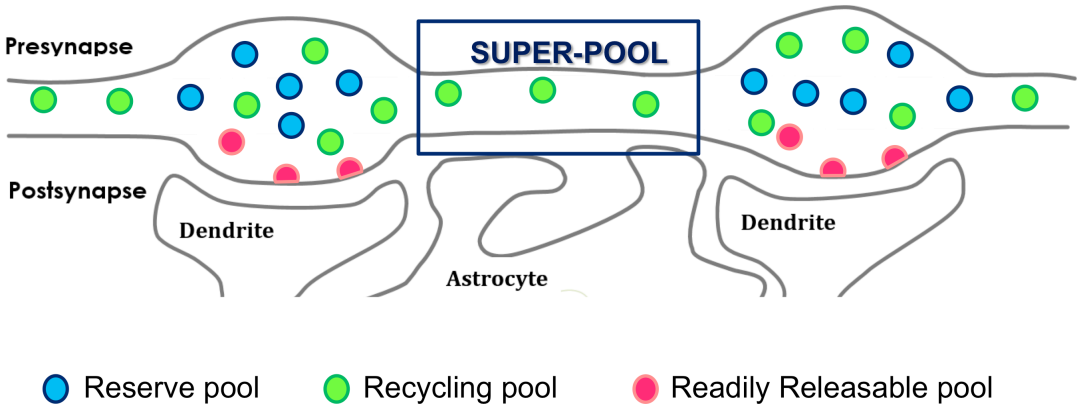

Fig 5. **Synaptic vesicle pools.** The classical model of synaptic vesicle (SV) pools consists of 3 pools: the reserve pool, the recycling pool, and the readily releasable pool. A newly defined "super-pool" comprises SVs that share among en passant presynaptic boutons along the axon.

The mechanism for sorting SVs to distinct pools remains unclear. Some proteins present in SVs at high levels, such as synaptobrevin, synaptotagmin or synaptophysin, are unlikely to be pool tags (Takamori et al., 2006; Denker and Rizzoli, 2010). Yet SV molecular heterogeneity is thought to be a determinant of SV pools segregation. Another possibility is that SV pools refer in part to mobility stages of SVs related to transient association with clustering proteins like synapsin. Indeed, synapsins bind and may immobilize SVs in reserve pool, while the triple KO of synapsins was shown to increases vesicles mobility and expand the super-pool (Denker and Rizzoli, 2010; Vasileva et al., 2012; Verstegen et al., 2014). Yet, a clear model for functional SV pools formation and segregation remains to be established.

Axonal trafficking

Axons, as the output domain of neurons, are particularly long filaments that connect cells that are located far from one another. However, this long distance that axons spanned, makes the delivering of synaptic materials to the developing synapse and subsequently maintenance to be challenging.

Cytoskeleton of axon

Axons are composed with microtubules (MTs), actin filaments and neurofilaments (Fig. 6). Neurofilaments are abundant in axons and control the axonal diameter and

conductance, but metabolic stability of the cytoskeletal structures limits their contribution to axonal plasticity (Yuan et al., 2012; Song and Brady, 2014). Whereas MTs and actins are dynamic structures that continuously grow and shrink to facilitate the remodeling of the cytoskeleton (Kevenaar and Hoogenraad, 2015).

MTs are cylindrical polymers built up from α- and β- tubulin heterodimers, and form an unipolar organization, where all MTs are oriented with their plus-end towards the axon tip, whereas in dendrites their orientation is mixed (Baas et al., 1988; Stone et al., 2008). MTs function as "roads" for long distance movement, which is carried by molecular transport motors named kinesins and dyneins (Brady, 1991; Hirokawa et al., 2010; Kapitein and Hoogenraad, 2011). MTs dynamics are regulated by different factors, such as microtubule-associated proteins (MAPs). MAPs are considered to stabilize microtubules. In addition, the unique MAPs of dendrites (MAP2) and axons (tau) were suggested to provide specialization of microtubules in these compartments (Dehmelt and Halpain, 2004; Song and Brady, 2014).

Actin filaments (F-actin) are polarized polymers, which are built up from monomer globular actin (G-actin). While these monomers are weakly connected, actin filaments rapidly shift between polymerization and depolymerization states (Kevenaar and Hoogenraad, 2015). Actin filaments are enriched in the synaptic regions and form a major cytoskeletal architecture at presynaptic terminals and postsynaptic spines (Hirokawa et al., 2010). With electron microscopy technique and super-resolution microscopy techniques, actins are also found locating along the axons or forming lattice rings around the axons (Xu et al., 2013; Lukinavičius et al., 2014). There might be two populations of axonal actins: the stable actins filaments along axons and actins rings that provide mechanical support, whereas the dynamic inta-axonal actin filaments provide flexibility needed for maintaining axonal and synaptic plasticity (Ganguly et al., 2015). In the presynaptic part, actin filaments have opposed roles that either facilitating docking vesicles or acting as a barrier to prevents the fusion of these vesicles, and these actions may depend on the synaptic activity (Kneussel and Wagner, 2013). Actin-based transport is conveyed by myosins and is important for short-range trafficking and local delivery of cargos to synapse and growth cones (Maeder et al., 2014).

Mechanism and Regulation of axonal transport

To maintain the axon and presynaptic boutons structure and function, related proteins are synthesized in cell body and are transported to the corresponding destinations by molecular motors. The presynaptic components, including AZ proteins piccolo-basson transport vesicles (PTVs) and synaptic vesicle precursors (SVPs), are transported to destinations as cargos. PTVs are dense-core 80 nm vesicles with a coat of electron dense material that contains active zone proteins, such as bassoon, piccolo and ELKS; whereas other AZ proteins are transported by other types of vesicles (Goldstein et al., 2008; Kevenaar and Hoogenraad, 2015). SVPs contain synaptic vesicle proteins such as synaptophysin, synaptogmin, and Rab3A (Hirokawa et al., 2010).

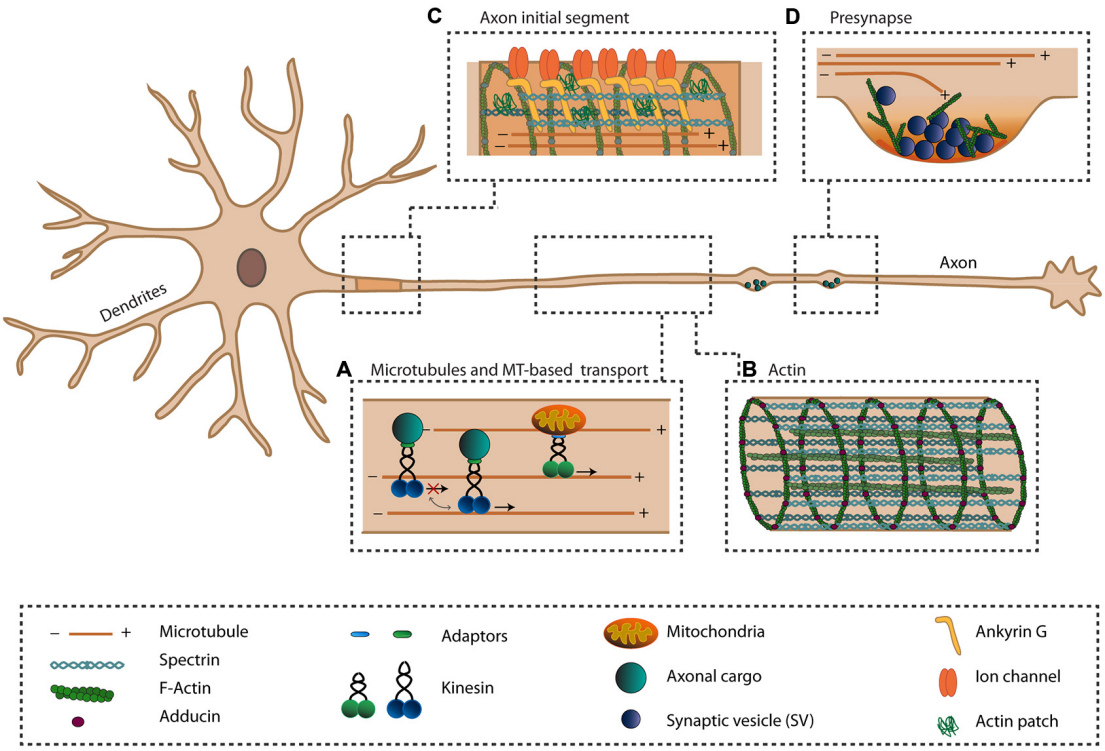

Fig 6. **The axonal cytoskeleton and axonal trafficking.** The axons are extremely long filaments that connect with other cells. Microtubles (MTs), actins and neurofilaments are the main components of axonal cytoskeleton. (A) MTs are unipolar orientated and provide routes for anterograde transports of various cargos via kinesins. (B) Actin filaments distribute underneath the plasma membrane and form lattice rings organized by spectrin and adducing. (C) The axon initial segment (AIS) is important for the initiation of action potentials and maintainance of neuronal polarization by acting as a transport filter. (D) Synaptic vesicles (SVs) are transported and rest in the presynaptic terminals. Actins are enriched at synaptic sites (Kevenaar and Hoogenraad, 2015).

In axons and dendrites, transport occurs bidirectionally, from the cell body to the periphery (anterograde transport) and from the periphery to the cell body (retrograde transport). As mentioned above, both MTs and actins are organized polarized along axons that are responsible for the orientation of trafficking motors movement (Hirokawa et al., 2010; Kapitein and Hoogenraad, 2011).

Energy supply of axonal transport

There are three molecular motor families that mainly convey the axonal transport: kinesins, dyneins and myosins. All motors contain a highly conserved motor domain, which is associated with the cytoskeleton and binds ATP for energy supply for movement (Brady, 1991; Hirokawa et al., 2010).

The molecular motors hydrolyze ATP to carry out the work of stepping along microtubules. Consuming one molecule of ATP, the conventional kinesin-1 motor moves one step, which is 8 nm. Whereas, the step size of the dynein motor ranges from 8 to 32 nm (Maday et al., 2014). A possible mechanism of energy supply for axonal transport is based on the glycolytic enzymes (GAPDH) that are bound to the surface of vesicles moving along the axon. The inhibition of ATP production from mitochondria did not affect vesicles motility, pharmacological or genetic inhibition of the GAPDH reduced transport in culture neurons and in *Drosophila* larvae. This energy source may allow cargos to transit without gaps in ATP supply while dispersed mitochondria may generate uneven ATP gradients along the axon (Zala et al., 2013). Glia supply neurons with lactate under conditions of glucose shortage, bypassing glycolysis in the axon. In addition, there are several forms of axonal transport not associated with vesicular membranes. Without efficient and broadly distributed ATP supply, these transport processes would experience regions of slow to no motility (Maday et al., 2014).

Long distance transport

Kinesins and dyneins convey long distance transport along microtubules toward plus-end or minus-end respectively. And the actin-based transport by myosin is important for short range trafficking and local delivery of cargos to synapse and growth cones (Brady, 1991; Maeder et al., 2014). These motor proteins have a more diverse tail region, which associates with the cargo and contains several elements for regulation. The diversity of the tail domain allows the ability of different motors to bind specific cargoes, together

with adaptor proteins, establishes correct cargo-motor protein association (Hirokawa et al., 2010; Kevenaar and Hoogenraad, 2015).

Kinesin motors are grouped into 14 subfamilies that share structure and functional similarities. Motors from the kinesin-1, kinesin-2, and kinesin-3 families all contribute to axonal transport dynamics (Maday et al., 2014).

Kinesin-1 family drive the transport of a wide range of cargos along the axons, including cargos, organelles, proteins, and RNA particles (Hirokawa et al., 2010). KIF5A and KIF5B are required to move specific vesicles along MTs via binding to distinct adaptor proteins. KIF 5 may transport APP via c-Jun NH_2-terminal kinase-interaction protein 1 (JIP1) (Muresan and Muresan, 2005). In addition, another adaptor protein, syntabulin could mediate KIF5 binding to syntaxin PTVs transport. The syntaxin-syntabulin-KIF5 complex is the motor-adaptor transport machinery critical for assembling presynaptic boutons in developing hippocampal neurons (Cai et al., 2007).

Kinesin-3 family member, KIF1A and KIF1Bβ are considered to convey SVPs and dense core vesicles (DCVs) transport from cell body to axons in vertebrates (Pack-Chung et al., 2007). The PH domain of the motor has affinity with PI(4,5)P(2) on the vesicle surface that is important for SVP binding (Klopfenstein and Vale, 2004; Goldstein et al., 2008). An adaptor protein DENN/MADD is required for SVP transport and specifically binds to the stalk region of KIF1A and KIF1B. In *Denn/Madd* knockout mice, the number and size of SVs are reduced (Tanaka et al., 2001; Hirokawa et al., 2010). Liprin-α is another adaptor that binds directly to KIF1A and enhances the cluster formation (Miller et al., 2005).

Dyneins have only two heavy chain family members, cytoplasmic dynein heavy chain 1 (Dync1h1) and cytoplasmic dynein heavy chain 2 (Dync2h1). But only Dync1h1 is involved in retrograde transport in axon and dendritic shafts. In the axon, dynein transport TrkA (tropomyosin-related kinase A) and TrkB vesicles, brain-derived neurotrophic factor (BDNF) vesicles, the piccolo/bassoon complex and myosin V retrogradely (Hirokawa et al., 2010). Dynein subunits form a cargo-binding-domain, which binds to specific cargo molecules. The diverse subunits of dynein complex can either coassemble or alternatively assemble into distinct complex with specific functions (Maday et al., 2014).

Short distance transport

Myosin family motors are important for short distance transport and the motors travel along actin that beneath the plasma membrane and synaptic regions. As described before, actin filaments are abundant near synapses and polarized with a barbed plus end. Among the myosin family motors, myosin II, V and VI have specific pre- and postsynaptic roles that are required for synapse function (Kneussel and Wagner, 2013).

Myosin II plays an important role in migrating neurons and their growth cones. Moreover, myosin II is located in the presynaptic terminals and is involved in transmitter release by facilitating delivery of SVs to AZs or their subsequent exocytosis (Hirokawa et al., 2010).

Myosin V, and myosin VI are also involved in transport in the synaptic regions. Myosin Va is present on synaptic vesicles and promotes retrograde long-range movements of vesicles containing synaptic vesicle protein 2 (SV2) in superior cervical ganglion neuron (SCGN) axons (Bridgman, 1999; Takamori et al., 2006). However, myosin Va is not generally required for synaptic transmission because the disruption of its function does not impair neurotransmitter release (Schnell and Nicoll, 2001; Takagishi et al., 2005; Kneussel and Wagner, 2013).

Myosin VI acts at several stages of membrane trafficking. Myosin VI is involved in clathrin-mediated endocytosis and becomes recruited to endocytic sites through its adaptor disabled homologue 2 (DAB2) (Morris et al., 2002; Spudich et al., 2007). It is associated with uncoated endocytic vesicles (UEVs) through GIPC1 and is important for the motility of these vesicles (Aschenbrenner et al., 2003; Naccache et al., 2006). In addition, myosin VI, and GIPC1, are essential for the BDNF-TrkB signaling-dependent facilitation of LTP by promoting SV recycling (Hirokawa et al., 2010).

Regulation of vesicles trafficking

The trafficking of presynaptic components from the soma therefore needs to be regulated in a way to assure uniform distribution of all cargos among the presynaptic *en passant* boutons. For instance, DCVs contain neuropeptides and active zone components, which are essential for neurotransmission. An elegant study of DCVs trafficking in *Drosophila* proposed a model that vesicle distribution to terminals would be mediated by sporadic capture of DCVs circulating in both anterograde and retrograde directions (Wong et al., 2012). Vesicles would initially bypass most proximal boutons with a

capture rate of about 10% at an individual bouton and accumulate in the most distal bouton. Then DCVs undergo retrograde transport back through proximal boutons with a similar capture rate. Interestingly, before re-entering the soma, the uncaptured vesicles would reverse for another round of anterograde-retrograde axonal transport. This long-range transport and inefficient bidirectional capture would lead to even distribution of vesicles throughout the release sites (Wong et al., 2012).

The exact mechanism to support SVs mobility in axons still remains unclear. A study in *C.elegans* showed that SV and AZ proteins exhibit extensive cotransport. In this cotransport, the small G protein ARL-8 inhibits assembly by promoting dissociation, while a JNK kinase pathway and AZ assembly proteins inhibit dissociation (Wu et al., 2013). Previous studies showed that SVs traffic along the axon, sharing and exchanging among the *en passant* boutons (Darcy et al., 2006; Staras et al., 2010; Herzog et al., 2011), which behaves in a bidirectional trafficking manner. In addition, our lab previous work showed that the super-pool size is increased in the VGLUT1 KO culture (Siksou et al., 2013). This indicates that, beyond packaging glutamate, VGLUT1 may be also involved in regulating SVs mobility.

Scope of the thesis

As detailed above, synaptic vesicles are central for neurotransmission. Thus, efforts to investigate SV properties, such as neurotransmitter content, release kinetics, distribution and mobility, are instrumental for a good understanding of neurotransmission and synaptic plasticity. In addition to the three functional pools classically investigated at presynapses, SV super-pool was defined mostly based on morphological investigations, and its function in neurotransmission is still poorly understood. A previous study from our lab indicated that beyond glutamate uptake, VGLUT1 might also participate in the regulation or SV super-pool size.

During my Ph.D training, I focused on the study of SVs mobility in axons, trying to characterize super-pool regulation by VGLUT1 and establishing new tools to address SV super-pool characterization. I studied VGLUT1 structure to investigate how VGLUT1 interferes with SVs mobility, and I went to the Department for molecular neuroboilogy of the Max Planck Institute for Experimental Medicine to generate a VGLUT1^{mEos2} KI mouse line. mEos2 is a green to red photo-convertible fluorescent protein (McKinney et

al., 2009). VGLUT1^{mEos2} mice provide the possibility to enhance the characterization of SV super-pool with live imaging approach.

Current Results are gathered in 2 articles in preparation.

Methodologies used for SV tracing

The ability to visualize, track, and quantify molecules and events in living cells with high spatial and temporal resolution is essential for the understanding of biological systems. Through the labeling of SV proteins (fusion with a fluorescent protein) or the endocytosed SV membranes (with styryl dyes), it is possible to visualize the mobility of SVs at real time. During my PhD training, I mostly monitored SV trafficking by tagging VGLUT1/Synaptobrevin2 with fluorescent proteins. I optimized the experiments to mimic WT condition and reduce possible artifacts. Here I wish to expose the main approaches I used and the advantages and disadvantages of them.

Molecular replacement by viral vectors transduction

The transfection of nucleic acids into cells is crucial for the study of many aspects of neuronal cell biology. The various approaches have their own advantages and drawbacks concerning transfection efficiency, expression levels, cell survival, and viability. Manipulating mammalian neurons has more limitations, because these cells are very sensitive to physical stress, alterations in temperature, pH shifts, or changes in osmolarity (Karra and Dahm, 2010). I will briefly introduce the common methods used for importing exogenous nucleic acids to cells and explain the reason that I chose viral transduction for my study.

Transfection

Transfection is the one of the most popular approaches to express exogenous proteins in cells. Genetic material can be introduced into cells either by electrical or chemical transfection methods.

In the calcium phosphate/DNA coprecipitation method, DNA forms crystals with the Ca^{2+} ions in the phosphate buffer, then precipitate onto the cells and are presumably taken up via endocytosis. Lipofection is another chemical transfection method. The cell surface is positively charged by liposomes and attracts negative charged DNA. And the newer generations of lipofection reagents, use nonliposomal lipids to form a complex with nucleic acids. This complex is believed to be endocytosed and released into the cytosol (Washbourne and McAllister, 2002; Karra and Dahm, 2010). These two methods

are cost effective and easy to establish, but the transfection efficiencies in postmitotic neurons are consistently low, rarely reach 30% (Karra and Dahm, 2010).

With the electrical transfection methods, the charged DNA or RNA enters the cytoplasm when the cells are exposed to a voltage pulse, whereas the transfection efficiency is relatively low (Washbourne and McAllister, 2002). A modified electroporation, which named nucleofection, uses a series of high voltage pulses that enable plasmids to directly enter the nucleus and result in high transfection efficiencies (an average of 60-80% and up to 95% for neurons) (Zeitelhofer et al., 2007). This method is more expensive compare to chemical transfection. Moreover, nucleofection can be applied only to cells in suspension (Zeitelhofer et al., 2007).

Viral transduction

Viral vectors are powerful tools for gene delivery *in vitro* and *in vivo*. In general, virus transduction has extremely high efficiency (up to 95% of neurons). Meanwhile, there are also limitations of viral vectors. Firstly, it is a time-comsuming and costly process to achieve a viral product. In addition, although most of recombinant viral vectors now are replication incompetent and comparatively safe to use, it still requires biosafety level 2 facilities for virus application (Karra and Dahm, 2010).

Different viruses have distinct modes of action. For instance, adenoviruses (AdVs) and herpes simplex viruses (HSV) do not integrate DNA into the host genome, thus there is no risk of insertional mutagenesis and they are suitable for transient expression of interest genes. The RNA viruses, Sindbis and Semliki Forest virus (SFV) potentially shut off host protein synthesis within a certain period after infection, and cause cell toxicity. Meanwhile, adeno-associated viruses (AAVs) and lentiviruses transduction would integrate gene into the genome and have stable expression and low toxicity to cells (Washbourne and McAllister, 2002; Karra and Dahm, 2010).

Quantitative control of protein expression

For my project, I needed to express tagged proteins in neurons to trace their subcellular localization and mobility. In order to avoid overexpression bias, I had to tightly control the expression level to stay in the range of WT levels. I also needed to express the transgene in most cells with low variability of expression level between cells of the culture.

Thus, I used viral vectors (lentivectors or AAV) that contain tagged VGLUT1 or Syb2 to transduce dissociated neuronal culture. By titrating the amount VGLUT1 expression with different doses of virus, I could manage to reach VGLUT1 expression near endogenous WT levels with each lentivirus/AAV vector. In addition, I used *VGLUT1*$^{-/-}$ neurons (Wojcik et al., 2004) to perform rescue experiments and avoid interactions between transgenic VGLUT1 and WT endogenous protein.

Live imaging with spinning disk confocal microscope

Spinning disk confocal microscope

Spinning disk confocal microscope is a good choice for live imaging, because of the fast speed and low phototoxic effects on samples. Unlike the laser scanning confocal microscopes that use a single excitation laser beam to scan the specimen, spinning disk confocal microscopes use a rapidly rotating disk with thousands of pinholes to create thousands of points of light to scan the specimen simultaneously. Thus, the rate of frame acquisition is high, theoretically, it can reach up to 2000 frames/s (Stehbens et al., 2012). At the same time, benefit from the high intensity laser light sources and the high sensitive camera, spinning disk confocal microscopes could obtain a sufficiently bright signal of the specimen (Stehbens et al., 2012). However, some out-of-focus emission light will be transmitted to the camera through adjacent pinholes, and reduce the confocality. In addition, the excitation wavelengths in spinning disk confocal are limited to a relatively small number of available laser lines (Ettinger and Wittmann, 2014).

Live imaging to detect synaptic vesicles mobility

I used Fluorescence recovery after photobleaching (FRAP) method to check the exchange rate of SVs in the presynaptic boutons and the super-pool (Darcy et al., 2006; Staras et al., 2010; Herzog et al., 2011). Together with spinning disk confocal microscope, no obvious photo-bleaching effect caused by the acquisition is detected during the whole FRAP process. FRAP is a method to monitor targeted molecules mobility (Axelrod et al., 1976; Lippincott-Schwartz and Patterson, 2003). A selected area is photo-bleached with a high-intensity laser pulse and the unbleached molecules from neighboring areas move into the bleached area. By analyzing the fluorescent intensity recovery curve of the bleached region, the mobile kinetics of targeted protein may be

extracted. The advantage of FRAP is that, protein mobility is observed by alternating the fluorescent state of molecules, without disturbing protein pathway or creating protein degradation (Lippincott-Schwartz and Patterson, 2003).

To analyze the SVs movement along the axons, I used stream acquisition. Stream acquisition provides high frame rates to observe dynamic processes without interval time between frames. But the continuously laser exposure brings a photo bleaching effect. To obtain high quality imaging sequences for analyzing, the expression level of fluorescent molecules might limit the timescale of acquisition. In my case, the tagged VGLUT1 express at the endogenous expression level, which is only available for a 30 seconds acquisition with high quality of images. But based on the SVs trafficking speed, this time scale is already sufficient for the data collection.

Imaging analyze description

Generating VGLUT1^{mEos2} knock-in mouse line

Gene targeting in embryonic stem (ES) cells has been extensively used as a powerful tool to study gene function in the mouse, as a mammalian model organism. Recently, the development of gene editing techniques have simplified the process and provided more possibilities to generate mutant models.

Gene targeting by homologous recombination

The knock-in techniques use homologous recombination to drive targeted gene replacement (Thomas et al., 1986). The key strategy in a KI experiment is to place the expression of an exogenous gene or a modification of the endogenous gene under the transcriptional control of cis-acting elements belonging to the endogenous gene (Roebroek et al., 2003). For a KI within the coding sequence of a gene, it is critical to direct the mutation precisely in the open reading frame of the gene. For technical constraints, a drug-resistance selection cassette needs to be present, usually downstream of the targeted gene (Roebroek et al., 2003). The designed construct is transfected into ES cells and insertion of the mutation at the targeted locus by homologous recombination is selected using an antibiotic compatible with the selection cassette. Subsequently, mutant ES cells can be injected into blastocystes to generate mutant mouse lines.

Generation of knock in models with CRISPR/Cas9 systems

Based on its powerful ability of genomic editing, the clustered regularly interspaced, short palindromic repeats (CRISPR)-associated RNA-guided endonuclease CRISPR associated protein 9 (Cas9) and its variants are more and more used in cell biology research, including generation of animal models (Jinek et al., 2012; Wang and Qi, 2016). The type II CRISPR system is the simplest and most widely used form for genome editing. It contains two necessary components: the Cas9 nuclease and a guide RNA (gRNA). Twenty nucleotides at the 5' end of the gRNA direct Cas9 to a specific target DNA site using standard RNA-DNA complementarity base-pairing rules. And with this system, Cas9 nuclease activity can be directed to any DNA sequence by altering the first 20 nt of the gRNA to correspond to the target DNA sequence (Sander and Joung, 2014).

Compared to the previous gene-editing tools, CRISPR/Cas9 can generate many animal models other than mice, which includes worm, fly, fish, rat, rabbit, goat, sheep, dog, pig, and monkey (Wang and Qi, 2016). Further, CRISPR is an easy, less costly, fast and highly efficient. Nucleic acids encoding the Cas9 protein and target-specific sgRNAs can be conveniently injected into embryos to generate gene-modified mice (Wang and Qi, 2016). Meanwhile, there are some drawbacks of this approach. The 20 nt gRNA may have hundreds to thousands of potential off-target sites that differ at four or five positions (Sander and Joung, 2014). Thus the obtained mutant animals need whole exome/genome sequencing to check for the absence of mis-targeting events, which is also a costly process. Moreover, CRISPR/Cas9 already showed high efficiency in gene knockout (KO) studies, whereas, to insert a large gene fragment into the mammalian genome for KI studies still has a rather lower productivity (Wang and Qi, 2016).

VGLUT1^{mEos2} KI mouse line

Our lab previously generated a VGLUT1^{venus} KI mouse line, which successfully labels VGLUT1 with the fluorescent protein. And the tagged VGLUT1 behaves the same as the endogenous VGLUT1 (Herzog et al., 2011). Due to the dense cortical expression of VGLUT1^{venus} in this KI mouse, although it is possible to identify and follow individual synaptic boutons, it is difficult to monitor a single bouton for a long time scale, especially *in vivo*. To further explore SVs mobility in glutamatergic neurons, I generated a VGLUT1^{mEos2} KI mouse line. mEos2 is a fluorescent protein that can photo-convert from green to red fluorescence upon stimulation with 405nm laser. mEos2 is widely used for

pointillist super-resolution techniques. Moreover, a selective conversion VGLUT1^{mEos2} molecules would allow to get rid of the high dense cortical expression by imaging in the red channel and thus could be easily detected both *in vitro* and *in vivo*.

Generating mutant mouse line by homologous recombination is a time-consuming and expensive process. In general, the success rate of right recombination is relatively low. It is mainly based on the locus of the targeting gene. But it may also be affected by the different genetic backgrounds of ES cells. For instance, I obtained around 70% positive clones when I generated VGLUT1^{mEOS2} KI mouse with SV129/ola ES cells. Later on, I also tried another two constructs, conditional knock out (KO) VGLUT1 and VGLUT1^{mCherryminiSOG} KI construct, with C57BL/6N ES cells to avoid the long backcross procedure. These two constructs target the same locus as VGLUT1^{venus} and VGLUT1^{mEOS2}, but I didn't get the positive recombinant colonies. In addition, the generation of VGLUT2^{venus} KI mouse line seems impossible. We tried both genetic background ES cells, but we didn't get any positive clone after screening around 4000 colonies with 3 different constructs.

However, it is still worth new attempts for generating VGLUT2 KI mouse line, which would be extremely important for us to understand the different molecular mechanisms of VGLUT isoforms in neurotransmission. In that case, CRISPR/Cas9 should be the right approach to obtain the new mouse model.

Results

Article 1: VGLUT1 poly-proline domain controls synaptic vesicle super-pool size in mammals

The absence of VGLUT1 can alter SVs tonicity. Moreover, it can also reduce SVs numbers at the presynapse and increase the SV trafficking in the axon between synapses. Thus the super-pool size is increased in the absence of VGLUT1, and VGLUT1 may be involved in the regulation of SV mobility.

We checked the SVs exchange rate between the presynaptic bouton and the super-pool with FRAP method. We found that SV exchange rate is dependent on VGLUT1 expression. The exchange rate is higher in VGLUT1$^{-/-}$ culture, whereas, there is less SV exchange when VGLUT1 is overexpressed. Therefore, VGLUT1 tends to cluster SVs in the presynaptic boutons.

We dissociated the features of VGLUT1 tonicity and the VGLUT1 interaction with other proteins by abolishing the glutamate uploading ability. With a "silent" VGLUT1 mutant, we identified that the VGLUT1 structure, rather than the glutamate uploading state, is essential for SV mobility regulation.

The N- and C-terminals of VGLUTs are highly divergent. We performed C-terminal structure-function analyses of VGLUT1 to further explore the molecular mechanism of VGLUT1 regulating SVs mobility. The deletion of PP2 and P554A mutant failed to rescue the oversized super-pool, suggesting that the interaction between VGLUT1 and endophilin A1 is essential for SVs mobility regulation.

My contribution to this work includes generating the viral vectors constructs, the primary culture, the virus transduction, in vitro FRAP and stream imaging as well as analysis of the FRAP and stream data. I also participated in the management of VGLUT1 knock-out mouse line and performed the genotyping of the pups. I generated the data for figure 2, 3, and 4 and contributed to figure 5.

In Preparation

VGLUT1 poly-proline domain controls synaptic vesicle super-pool size in mammals.

Running title: VGLUT1 regulation of synaptic vesicle mobility

Xiao-Min Zhang [1,2,3]*, Katlin Silm [4]*†, Maria Florencia Angelo [1,2], Maria Victoria Fernandez-busch [1,2],Clémence Peyrot [1,2], Mona Maged[1,2], Christelle Martin [1,2], Fabrice Cordelière [5], Stéphanie Pons[6], Uwe Maskos[6], Alexis Bemelmans[7], Sonja M. Wojcik[3], Salah El Mestikawy[4], Yann Humeau[1,2], Nils Brose[3], Etienne Herzog[1,2]

[1] Interdisciplinary Institute for Neuroscience, Université de Bordeaux, UMR 5297, 33000 Bordeaux, France.
[2] Team Synapse in Cognition, Interdisciplinary Institute for Neuroscience, CNRS UMR 5297, 33000 Bordeaux, France.
[3] Department of Molecular Neurobiology, Max Planck Institute of Experimental Medicine, D-37075 Göttingen, Germany.
[4] Pathophysiology of Central Nervous System Disorders, Université Pierre et Marie Curie, INSERM U952, CNRS UMR 7224, F-75005, Paris, France.
[5] Bordeaux Imaging Center, Université de Bordeaux, CNRS UMS 3420, INSERM US4, 33000, Bordeaux, France.
[6] Institut Pasteur, CNRS UMR 3571, Unité NISC, Paris, France.
[7] Commissariat à l'Energie Atomique et aux Energies Alternatives (CEA), Département des Sciences du Vivant (DSV), Institut d'Imagerie Biomédicale (I2BM), Molecular Imaging Research Center (MIRCen), Fontenay-aux-Roses, France.
[8] Centre National de la Recherche Scientifique (CNRS), Université Paris-Sud, Université Paris-Saclay, UMR 9199, Neurodegenerative Diseases Laboratory, Fontenay-aux-Roses, France.
†*Present address*: Department of Neurology, UCSF School of Medicine, San Francisco, CA 94143, USA.

Corresponding author: Etienne Herzog; etienne.herzog@u-bordeaux.fr

Acknowledgements:

Abstract:

Excitatory synaptic vesicles (SVs) release glutamate upon presynaptic calcium rise. Yet, release competence is regulated by several molecular interactions and constrained by biophysical parameters. As a result, several functional pools of SVs have been identified and characterized. Recently SVs transiting along the axon forming en passant synapses were imaged and named SV super-pool. Prior to release, glutamate is loaded into SVs through the action of Vesicular GLUtamate Transporters (VGLUT). Among them VGLUT1 fascinatingly seems to specialize in mammals with the gain of a conserved poly-proline domain that was shown to reduce release probability at VGLUT1 synapses. In the present work we identify that the second poly-proline stretch (PP2) of VGLUT1 controls SV super-pool size independently of glutamate loading. The absence of PP2 increases the exchange of clustered SVs with SV super-pool, which may lead to changes in physical constraints over SV mobility within synapses in relation to release probability.

INTRODUCTION

Synaptic vesicles (SVs) engaged in multiple protein interactions at the presynaptic active zone (Südhof and Rizo, 2011), fuse with the presynaptic plasma membrane, upon action calcium influx, to release their neurotransmitter content (Lisman et al., 2007). To avoid "silent" events, each vesicle should be equipped with the vesicular neurotransmitter transporters allowing its loading. Thereby, at glutamatergic excitatory synapses, SVs are thought to contain between 4 and 14 molecules of Vesicular Glutamate Transporters (VGLUTs; Takamori et al., 2006; Mutch et al., 2011). Three isoforms of VGLUTs have been identified, and named VGLUT1-3 (Bellocchio et al., 2000; Takamori et al., 2000; Fremeau et al., 2001; Herzog et al., 2001; Gras et al., 2002; Varoqui et al., 2002). They share a nearly common glutamate transport mechanism that is instrumental for neurotransmission accuracy and efficiency (Schenck et al., 2009; Preobraschenski et al., 2014; Eriksen et al., 2016). While VGLUT3 is atypically expressed in sparse populations of phenotypically identified neurons (Fremeau et al., 2002; Gras et al., 2002; Schäfer et al., 2002), VGLUT1 and 2 unraveled the complementary territories of 2 main populations of *bona fide* glutamatergic neurons (Fremeau et al., 2001; Herzog et al., 2001). VGLUT1 is prominently expressed in olfactory bulb, neo-cortex, hippocampus, cerebellum, while VGLUT2 is strongly expressed in deeper regions of the forebrain such as the thalamus and in the brainstem.

Attractively this RNA and protein distribution has soon been seen matching the release probability variations measured at several afferences by physiologists. VGLUT1 being associated to low-, and VGLUT2 to high release probabilities (Varoqui et al., 2000; Fremeau et al., 2004b). Indeed, VGLUT1 was shown to lower SV release probability through an interaction with endophilin A1 that is not occurring with VGLUT2 (Vinatier et al., 2006; Weston et al., 2011). VGLUT1/endophilin A1 interaction was also shown to mildly promote

SV endocytosis upon long trains of stimulation (Voglmaier et al., 2006). Finally, VGLUT1 was shown to influence the endocytosis kinetics of several other SV proteins (Pan et al., 2015). SV supply at synapses in adult neurons has recently been shown to depend not only on *de novo* synthesis of proteins and lipids but also through the exchange of genuine SVs between *en passant* boutons along the axon (Darcy et al., 2006; "SV super-pool"; Westphal et al., 2008; Herzog et al., 2011). VGLUT1$^{-/-}$ mice display a normal density of synapses but a strong reduction in the number of SVs at hippocampal Schaffer collateral and cerebellar parallel fiber terminals (Fremeau et al., 2004a; Siksou et al., 2013). Furthermore, we could reveal the hypo-osmotic state of VGLUT-less SVs probably as a consequence of the loss of massive ionic exchanges induced by VGLUT function (Siksou et al., 2013; Preobraschenski et al., 2014). In the mean time we have shown that in *VGLUT1*$^{-/-}$ neurons around 40% of SVs are displaced from the cluster to axonal super-pool (Siksou et al., 2013).

In the present work, we embarked in a thorough structure-function study of VGLUT1 relationship to SV super-pool size and determined the minimal domain responsible for this aditional function of mammalian VGLUT1.

MATERIALS & METHODS

Animals

The VGLUT1$^{-/-}$ mouse line is on C57BL/6N background, mice are 2-5 months old, housed in 12/12 LD with ad libitum feeding. Every effort was made to minimize the number of animals used and their suffering. The experimental design and all procedures were in accordance with the European guide for the care and use of laboratory animals and approved by the ethics committee of Bordeaux Universities (CE50) under the APAFIS n°1692.

Hippocampal cell culture

Hippocampal primary dissociated cultures were prepared from P0 *vglut1*$^{-/-}$ mice. The hippocampi were dissected in ice-cold Leibovitz's L-15 medium (11415064; Gibco), and then

incubated in 0.05% trypsin-EDTA (25300054, Gibco) for 15 min at 37°C. The tissues were washed with Dulbecco's Modified Eagle's Medium (DMEM, 61965026, Gibco) containing 10% FBS (CVFSVF0001, Eurobio), 1% Penicillin-streptomycin (15140122, Gibco). Cells were mechanically dissociated by pipetting up and down, and plated onto poly-L-lysine (P2636, Sigma) coated coverslips at a density of 20 000 cells/cm^2. Cells were grown in Neurobasal A medium (12349105, Gibco) containing 2% B27 supplement (17504044, Gibco), 0.5 mM Glutamax(35050038, Gibco), and 0.2% MycoZap plus-PR (VZA2021, Lonza). After 10 days, half of the medium was changed. Imaging of live dissociated neuron cultures was performed at 17-21 days *in vitro* (DIV) in culture medium with added Hepes buffer (40 mM). Neurons were infected with custom-made lentiviral vectors [F(syn)W-RBN] containing either WT/mutant VGLUT1^{venus} or synaptovbrevin 2 (Syb2)^{EGFP} inserts, or AAV 2/9 vectors containing either WT/silent VGLUT1^{mCherryminiSOG} inserts for expression under the control of the synapsin promoter. Viral particles were used to rescue VGLUT1 expression to endogenous VGLUT1 expression level, which was identified by both western-blot and fluorescent intensity checking. Lentiviral particles were added to wells in the 12-well plates at DIV 2 and AAV vectors transductions were performed at DIV 3.

FRAP imaging

FRAP experiments were performed to determine the mobility of Syb2 (for silent VGLUT1 rescue experiments) or VGLUT1 (for VGLUT1 C-terminal mutants rescue experiments) at synapses. The mobile fraction of Syb2/VGLUT1 is defined by the proportion of fluorescent material that can be replenished after photobleaching. FRAP was performed on a spinning-disk confocal microscope: an inverted Leica DMI 6000 microscope (Leica Microsystems, Wetzlar, Germany) equipped with a confocal head Yokogawa CSU-X1 (Yokogawa Electric Corporation, Tokyo, Japan), a sensitive Quantem camera (Photometrics, Tucson, USA), and a scanner FRAP system (Roper Scientific, Evry, France). Surrounding the setup, a thermal

incubator is set to 37°C (Bordeaux Imaging Center). The z stacks were done with a piezo P721.LLQ (Physik Instrumente (PI), Karlsruhe, Germany). The imaging fields were randomly selected from hippocampal cell culture. A 4.8 μm Z-stacks (7 steps per stack) sequences was acquired with a 63×/1.4 numerical aperture oil-immersion objective at each field. For each stack, five fluorescent boutons, distant from each other, were selected for bleaching.

For monitoring of Syb2 mobility, three passes of the 491 nm laser (40 mW) were applied to bleach the synapses (containing both VGLUT1 and Syb2) at the midplane of the stack, which results an average bleaching to 50% of the initial fluorescence of boutons.

For monitoring of VGLUT1 mobility, synapses were bleached by two laser passes focused at the midplane of the stack using the 491 nm laser (30 mW) and the 405 nm laser (10 mW). This bleaching protocol prevents spontaneous recovery of Venus/EYFP fluorescence that has previously been reported (McAnaney et al., 2005) and ensure an average bleaching to 50% of the initial fluorescence of boutons.

Fluorescent recovery was monitored every 30 s during the first 3 min and then every 5 min during the next 70 min. The entire FRAP procedure was controlled by MetaMorph software (Molecular Devices, Sunnyvale, USA). Image processing was automated using Image J macro commands. Sum projections of the individual stacks, assembly and *x-y* realignment were applied, resulting in 32 bits/pixel sequences. Integrated fluorescence intensities of the five bleached, and the cells in the field, as well as one background area were extracted. The background signal was subtracted, and data were normalized to the average baseline before bleaching and corrected for photobleaching against the cells. Experiments were discarded if photobleaching exceeded 60% (risk of phototoxicity) or didn't reach 30% (low signal to noise ratio) of initial fluorescence before the end.

Analysis of FRAP experiments

The intensity of the boutons was normalized that the intensity before the bleaching as 1, and the first frame after the bleaching as 0. A double exponential function was used to fit the average of all normalized traces, and the parameters of the best fitting curve were considered as the parameters of a hypothetical average synapse.

Stream imaging

Stream experiments were performed to quantify the VGLUT1^{venus} material moving in intersynaptic areas. Imaging was performed with the spinning disk confocal microscope. Images were sampled at 5 frames/s for 30 seconds with 200 ms exposure time (151 frames in total). Synaptic boutons were saturated in order to allow better visualization of the dimmer fluorescent material moving along the axons.

Quantification of the speed of moving clusters was performed with the kymograph Toolbox plugin in Image J. In each sequence, 4 axons ranged from 10 – 15 µm were randomly selected for speed analysis.

Material moving in intersynaptic segments was quantified by drawing line regions of ROIs perpendicularly to the axon and measuring the integrated density values in each of the 151 images. Background was subtracted, and all values were divided by the average of 10 lowest values to normalize for the differences in fluorescence intensity between different sets of experiments. All normalized values from each line selection were summed to evaluate the total amount of material going through the given cross-section. The statistical significance of the differences in cumulative traffic between the WT and VGLUT1 mutants (S540A and P554A) were evaluated with unpaired *t*-test.

Antibodies

The detections of wild type VGLUT1 was performed with the BN3L2Bf rabbit polyclonal VGLUT1 antiserum (Herzog et al., 2001) while the detection of VGLUT1^{Venus} was done with a mouse monoclonal anti-GFP antibody (11814460001, Roche). Additionally, anti-VIAAT

guinea pig polyclonal antiserum (131004, SYSY) was used. Secondary HRP-coupled anti-rabbit, anti mouse and anti-guinea pig antibodies IgG (711-035-152, 715-035-150, 706-035-148, respectively, Jackson ImmunoResearch) were used for western blotting.

Biochemistry

All steps were performed at 4°C or on ice. Brains of wild type adult mice were dissected for collection of the forebrain or several regions. The samples were treated with homogenization buffer (0.32 M sucrose, 4 mM HEPES pH 7.4). For the culture with the expression of different VGLUT1 mutants, the cells were collected on DIV 17 with 1× PBS. Both buffers were supplemented with protease inhibitor cocktail (539134, Millipore) and Halt™ phosphatase Inhibitor Cocktail (78420, Thermo Fisher Scientific).

Protein samples were treated with alkaline phosphatase prior to the biochemical analysis. FastAP Thermosensitive Alkaline Phosphatase (1 unit/µl) and FastAP 10× buffer (EF0654, Thermo Scientific) were added to samples and incubated for 1 h at 37°C.

Sodium dodecylsulfate polyacrylamide gel electrophoresis (SDS-PAGE) and phosphate affinity SDS-PAGE (Kinoshita et al., 2006) were conducted according to Laemmli's method. For phosphate affinity SDS-PAGE (Mn^{2+}-Phos-tag SDS-PAGE), 25 µM Phostag (AAL-107, Wako) and 0.1 mM $MnCl_2$ were added to the resolving gel before polymerization. Western blotting was performed according to standard procedures using HRP-coupled secondary antibodies for qualitative detection. Chemiluminiscence signals were visualized with ChemiDoc MP System (Bio-Rad) using SuperSignal™ West Dura Extended Duration Substrate (34075, Thermo Scientific).

RESULTS

A specific and dose dependent regulation of super-pool size by VGLUT1

To explore VGLUT1 effect on SV super-pool size we established viral driven expression of fluorescently tagged SV proteins in neuron cultures under the control of the neuron specific synapsin promoter. This ensures a broad expression of our transgenes in a majority of neurons

and a fine tuning of expression levels. A broad expression is important to reduce biases related to competitions between cells in the network and the fine tuning is instrumental in preventing over-expression related artifacts. We first expressed a tagged synaptobrevin protein ($Syb2^{EGFP}$) to track SV exchange between synaptic clusters and the axonal flow (Fig 1AB). Through fluorescence recovery after photobleaching (FRAP) we could measure higher exchange rates for *VGLUT1*$^{-/-}$ neurons compared to wild-type neurons from littermates (Fig 1C, *VGLUT1*$^{+/+}$: $N = 8$ cultures, $n = 27$ synapses; *VGLUT*$^{-/-}$: $N = 11$ cultures, $n = 31$ synapses. F test, $P < 0.0001$, F ratio = 19.32). Higher exchange with axonal super-pool is in line with our previous findings (Siksou et al., 2013). We then transduced $VGLUT1^{Venus}$ cDNA (Herzog et al., 2011) to rescue *VGLUT1*$^{-/-}$ neurons or over-express VGLUT1 in *VGLUT1*$^{+/+}$ neurons (Fig 1D). FRAP experiments of $VGLUT1^{Venus}$ fluorescence in this configuration identifies that VGLUT1 overexpression reduces SV exchange with axonal pools compared to knock-out rescue (Fig 1E; *VGLUT1*$^{+/+}$: $N = 4$ cultures, $n = 14$ synapses; *VGLUT*$^{-/-}$: $N = 3$ cultures, $n = 15$ synapses. F test, $P < 0.0001$, F ratio = 9.467). Finally we could show that a $VGLUT2^{venus}$ cannot rescue *VGLUT1*$^{-/-}$ super-pool phenotype (Fig S1).

Structure analysis of VGLUT1

To establish the molecular signature supporting VGLUT1 function on SV super-pool size we generated a series of mutants spanning the sequence of the transporter (Fig2A). VGLUT1 presents 12 transmembrane domains with both termini at the cytoplasmic side and N-glycosylation on the first luminal loop (Almqvist et al., 2007). As VGLUT1 mediated transport strongly impacts SV tonicity we first aimed at determining whether SV loading state impacts SV mobility between SV clusters and axonal super-pool. A triple point mutant R80Q, R176K, R314Q was generated to produce a silent transporter (sVGLUT1) as previously reported for VGLUT2 (Juge et al., 2006; Fig 2A blue residues; Almqvist et al., 2007; Herman et al., 2014). We then focused our efforts on several conserved patterns at VGLUT1 C-

terminus. Indeed, in all mammals, VGLUT1 displays a unique double poly-proline (PP) pattern surrounding a SYGAT (540-544) sequence conserved from invertebrates (Vinatier et al., 2006). To that end we used 3 deletions (ΔC-term from S504 included, ΔPP1+2 from P530 included, ΔPP2 from P550; Fig 2A red bars) and 4 specific features where alanine screened (Vinatier et al., 2006; Voglmaier et al., 2006; Santos et al., 2014). All mutants were tagged using our succesful c-terminal strategy and the expression following lentiviral transduction (or AAV for sVGLUT1 see methods) was monitored and tuned using both epi-fluorescent microscopy (Fig 2B) and immunoblot (not shown). All mutants displayed a typical VGLUT1 like punctate expression of venus signals at boutons with low signal at cell soma (see examples on Fig2B). Only the full ΔC-term mutant displayed a significant alteration of expression pattern (diffuse fluorescence along neurites) and was therefore not included in subsequent imaging experiments but only for biochemistry.

Vesicular glutamate uptake is not influencing SV super-pool size.

SV mobility and access to distinct pools may be dependent on biophysical properties such as the tonicity of the organelle. To establish whether VGLUT1 influence on SV super-pool size is dependent on SV loading state and tonicity, we used a silent VGLUT1 mutant (Juge et al., 2006; Fig 2A blue residues; Almqvist et al., 2007; Herman et al., 2014). Indeed, sVGLUT could not rescue VGLUT1 knock-out electrophysiological phenotype and SV tonicity as shown by Herman and colleagues (Herman et al., 2014). We transduced VGLUT1^{mCherry} or sVGLUT1^{mCherry} together with Syb2^{EGFP} in neurons (Fig 3A) and probed SV turn over at synapses using Syb2^{EGFP} FRAP. Both rescue conditions lowered significantly and to the same degree the exchange of SVs compared to *VGLUT1*$^{-/-}$ synapses of the same cultures (Fig 3B, silent VGLUT1: N = 10 cultures, n = 36 synapses; WT VGLUT1: N = 5 cultures, n = 23 synapses; none rescue: N = 7 cultures, n = 16 synapses. F test, silent VGLUT1 *vs.* WT: P =

0.2941, *F* ratio = 1.235; *vs.* none rescue: $P < 0.0001$, *F* ratio = 30.25). Hence SV tonicity is not a biophysical parameter involved in regulating SV super-pool size regulation.

VGLUT1 PP2 domain regulates SV super-pool size.

To identify the molecular determinant supporting SV super-pool size regulation on VGLUT1 sequence, we tested a series of VGLUT1^{venus} mutants (Fig 2) for rescue of the *VGLUT1*$^{-/-}$ SV super-pool phenotype. VGLUT1^{venus} FRAP experiments allowed measuring SV exchange rates (Fig 4). Only mutants disrupting the PP2 sequence were not efficient at rescuing SV super-pool size to WT levels (Fig 4AB; *F* test, WT *vs*. ΔPP1+2, $P < 0.0001$, *F* ratio = 19.54; WT *vs*. ΔPP2, $P < 0.0001$, $F = 10.58$; WT *vs*. P554A, $P < 0.0001$, *F* ratio = 15.32). To further measure SV super-pool size we performed time-lapse imaging at high sampling rates (5 images per seconds) and tracked VGLUT1^{venus} axonal transport between synaptic boutons (Fig 4C-E). This assay confirmed a significantly larger axonal pool of SVs for VGLUT1$^{P554A\text{-}venus}$ but not for VGLUT1$^{S540A\text{-}venus}$ compared to WT rescue (Fig 4D, unpaired *t* test, WT *vs.* P554A: $P = 0.0092$, $t = 3.564$; *vs*. S540A: $P = 0.8963$, $t = 0.1351$. $N = 5$ cultures for WT, and $N = 4$ cultures for both P554A and S540A). Yet, no difference in axonal transport speed could be measured between the 3 constructs (Fig 4E; One-way ANOVA, $P = 0.0634$, *F* ratio = 2.431. Speed for each mutant, WT: 1.564 ± 0.02692 µm/s; P554A: 1.536 ± 0.02860 µm/s; S540A: 1.460 ± 0/02942 µm/s.). We can therefore conclude from this series of experiments that the PP2 C-terminal sequence is the minimal determinant mediating VGLUT1 dependent regulation of SV super-pool size.

VGLUT1 is not phosphorylated at its C-terminus.

To test for the possible regulation of PP2 function by phosphorylation of the conserved 540-SYGAT sequence, we investigated on VGLUT1 phosphorylation. To that end, we probed VGLUT1 by immuno-blot on samples protected with phosphatase inhibitors or exposed to alkaline phosphatase (Fig 5A). Electrophoretic shift upon dephosphorylation brings evidence

for a phosphorylation on VGLUT1 in most brain regions as previously shown for the inhibitory amino-acid transporter VIAAT (Bedet et al., 2000). To identify a possible phosphorylation on VGLUT1 C-terminus we implemented the PhosTag assay that shifts specifically the electrophoretic mobility of phospho-protein (Kinoshita et al., 2006). VGLUT1 constructs tested including ΔC-term displayed a slow band in PhosTag gels migration except when digesting samples with alkaline phosphatase (Fig 5C). VGLUT1 may be phosphorylated but not at the C-terminal tail, and the function of the extremely conserved SYGAT sequence remains unclear.

DISCUSSION

Our present work shows that mammalian VGLUT1 is regulating SV exchange rates between synaptic clusters and axonal super-pool (Fig 1). Through a thorough structure function analysis, we excluded a cross-talk of glutamate transport function and SV super-pool regulation function (Fig 2, 3). Also we show, that regulation is supported by the PP2 motif but not by any other parts of the C-terminus (Fig 2, 4). Finally, we discarded the hypothesis that PP2 function may be regulated by a putative phosphorylation of the nearby 540-SYGAT sequence (Fig 2, 5).

Molecular mechanisms of VGLUT1 trafficking at SV.

VGLUT1 localization largely correlates with neuronal projections prone to low release probability (Varoqui et al., 2002). Among other aspects, speciation of mammals occurred with a prominent development of the neo-cortex and a molecular specialization of VGLUT1 that gained a dual poly-proline domain at the c-terminus (Fig 2A; Herzog et al., 2001; Vinatier et al., 2006). We and others could show that endophilin A1 is a binding partner of VGLUT1 at the second poly-proline stretch PP2 (De Gois et al., 2006; Vinatier et al., 2006; Voglmaier et al., 2006). SV endocytosis seem more efficiently driven to the AP2 clathrin dependent pathway when VGLUT1 interacts with endophilin A1 (Voglmaier et al., 2006). However this

work may be subjected to biases due to overexpression and the cis-link between tested mutations and the pHluorin probe for endocytosis ((Voglmaier et al., 2006)). Finally, VGLUT1 endophilin interaction was shown to lower SV release probability in autaptic cultures of rescued *VGLUT1*$^{-/-}$ neurons (Weston et al., 2011).

Our data now show that VGLUT1 PP2 domain is necessary and sufficient to drive a regulation of SV exchange between clustered pools and the recently characterized SV super-pool. Our VGLUT1^{venus} strategy preserves both endophilin A1 interaction and SV release parameters (Herzog et al., 2011; Rothman et al., 2016), and P554A mutation is sufficient to disrupt interaction with endophilin A1 and most likely any other putative SH3 binding partner(Vinatier et al., 2006). Hence we can speculate that either endophilin A1 drives SVs endocytosis more toward the AP2 than AP3 clathrin dependent endocytic pathways which in turn would confine SVs more efficiently to clustered pools (Voglmaier et al., 2006). Alternatively, SV super-pool size regulation may involve another SH3 domain protein yet to be identified. To date, we tested several possible alternative partners without success (*sorbs2*, *nck1*, *nck2* data not shown). Finally, endophilin A1 may recruit a larger complex to fulfill its influence on SV pools size. For instance, endophilin A1 and intersectin1 were recently shown to interact through an unconventional SH3 to SH3 domains binding that preserves free endophilin A1 poly-prolin binding (Pechstein et al., 2015). Intersectin1 is a multiple SH3 domain, and Rho GEF scaffold protein that may recruit synapsins and promote SV clustering after endocytosis at drosophila neuromuscular junction(Winther et al., 2015), and influence actin cytoskeleton polymerization (Humphries et al., 2014). Though we could bring evidence for the phosphorylation of VGLUT1, but not at C-terminus, our investigation failed to identify additional sites modulating the super-pool function of the PP2 domain, and our work together with previous ones now calls for a thorough investigation of scaffolds surrounding VGLUT1 PP2 domain.

Relationship between SV release probability and SV mobility.

Chiefly, VGLUT1 supports glutamatergic transmission through the loading of SVs with glutamate (Bellocchio et al., 2000; Takamori et al., 2000), and the plasticity of quanta following changes in VGLUT levels is debated (Daniels et al., 2004; Wojcik et al., 2004; Wilson et al., 2005; Daniels et al., 2006; Moechars et al., 2006). Here we identify that VGLUT1 PP2 reduces axonal SV super-pool and as previously shown reduces SV release probability (Weston et al., 2011). In a conventional view of SV pools it may seem odd that increasing SV clustering results in lower release probability as more release competent SVs to fill release sites (Denker and Rizzoli, 2010). Yet, if one considers a more dynamic view of SV supply at active zone, SV release may be promoted by higher SV mobility and lower SV cluster density (Rizzoli and Betz, 2004; Rothman et al., 2016). Future investigations using single particle tracking at SV clusters should establish whether VGLUT1 also modulates mobility states within presynaptic terminals (Joensuu et al., 2016).

Altogether, we contribute to establish an important new function of VGLUT1 in the regulation of glutamtergic transmission through the alteration of synaptic vesicle mobility states in axons. This feature seem to have been positively selected with the emergence of mammals and the massive development of neo-cortex, it will thus be key to understand how mammalian VGLUT1 contributes to specific cognitive features of this taxon.

BIBLIOGRAPHY

Almqvist, Huang, Laaksonen, Wang, Hovmöller (2007) Docking and homology modeling explain inhibition of the human vesicular glutamate transporters. Protein Sci.

Bedet C, Isambert MF, Henry JP, Gasnier B (2000) Constitutive phosphorylation of the vesicular inhibitory amino acid transporter in rat central nervous system. J Neurochem 75:1654–1663.

Bellocchio EE, Reimer RJ, Fremeau RT, Edwards RH (2000) Uptake of glutamate into synaptic vesicles by an inorganic phosphate transporter. Science 289:957–960.

Daniels RW, Collins CA, Chen K, Gelfand MV, Featherstone DE, DiAntonio A (2006) A

single vesicular glutamate transporter is sufficient to fill a synaptic vesicle. Neuron 49:11–16.

Daniels RW, Collins CA, Gelfand MV, Dant J, Brooks ES, Krantz DE, DiAntonio A (2004) Increased expression of the Drosophila vesicular glutamate transporter leads to excess glutamate release and a compensatory decrease in quantal content. J Neurosci 24:10466–10474.

Darcy KJ, Staras K, Collinson LM, Goda Y (2006) Constitutive sharing of recycling synaptic vesicles between presynaptic boutons. Nat Neurosci 9:315–321.

De Gois S, Jeanclos E, Morris M, Grewal S, Varoqui H, Erickson JD (2006) Identification of endophilins 1 and 3 as selective binding partners for VGLUT1 and their co-localization in neocortical glutamatergic synapses: implications for vesicular glutamate transporter trafficking and excitatory vesicle formation. Cell Mol Neurobiol 26:679–693.

Denker A, Rizzoli SO (2010) Synaptic vesicle pools: an update. Front SynNeurosci 2:135.

Eriksen J, Chang R, McGregor M, Silm K, Suzuki T, Edwards RH (2016) Protons Regulate Vesicular Glutamate Transporters through an Allosteric Mechanism. Neuron.

Fremeau RT, Burman J, Qureshi T, Tran CH, Proctor J, Johnson J, Zhang H, Sulzer D, Copenhagen DR, Storm-Mathisen J, Reimer RJ, Chaudhry FA, Edwards RH (2002) The identification of vesicular glutamate transporter 3 suggests novel modes of signaling by glutamate. Proc Natl Acad Sci USA 99:14488–14493.

Fremeau RT, Kam K, Qureshi T, Johnson J, Copenhagen DR, Storm-Mathisen J, Chaudhry FA, Nicoll RA, Edwards RH (2004a) Vesicular glutamate transporters 1 and 2 target to functionally distinct synaptic release sites. Science 304:1815–1819.

Fremeau RT, Troyer MD, Pahner I, Nygaard GO, Tran CH, Reimer RJ, Bellocchio EE, Fortin DL, Storm-Mathisen J, Edwards RH (2001) The expression of vesicular glutamate transporters defines two classes of excitatory synapse. Neuron 31:247–260.

Fremeau RT, Voglmaier S, Seal RP, Edwards RH (2004b) VGLUTs define subsets of excitatory neurons and suggest novel roles for glutamate. Trends Neurosci 27:98–103.

Gras C, Herzog E, Bellenchi GC, Bernard V, Ravassard P, Pohl M, Gasnier B, Giros B, Mestikawy El S (2002) A third vesicular glutamate transporter expressed by cholinergic and serotoninergic neurons. J Neurosci 22:5442–5451.

Herman MA, Ackermann F, Trimbuch T, Rosenmund C (2014) Vesicular glutamate transporter expression level affects synaptic vesicle release probability at hippocampal synapses in culture. J Neurosci 34:11781–11791.

Herzog E, Bellenchi GC, Gras C, Bernard V, Ravassard P, Bedet C, Gasnier B, Giros B, Mestikawy El S (2001) The existence of a second vesicular glutamate transporter specifies subpopulations of glutamatergic neurons. J Neurosci 21:RC181.

Herzog E, Nadrigny F, Silm K, Biesemann C, Helling I, Bersot T, Steffens H, Schwartzmann R, Nägerl UV, Mestikawy El S, Rhee J, Kirchhoff F, Brose N (2011) In vivo imaging of intersynaptic vesicle exchange using VGLUT1 Venus knock-in mice. J Neurosci

31:15544–15559.

Humphries AC, Donnelly SK, Way M (2014) Cdc42 and the Rho GEF intersectin-1 collaborate with Nck to promote N-WASP-dependent actin polymerisation. J Cell Sci 127:673–685.

Joensuu M, Padmanabhan P, Durisic N, Bademosi ATD, Cooper-Williams E, Morrow IC, Harper CB, Jung W, Parton RG, Goodhill GJ, Papadopulos A, Meunier FA (2016) Subdiffractional tracking of internalized molecules reveals heterogeneous motion states of synaptic vesicles. J Cell Biol 215:277–292.

Juge N, Yoshida Y, Yatsushiro S, Omote H, Moriyama Y (2006) Vesicular glutamate transporter contains two independent transport machineries. J Biol Chem 281:39499–39506.

Kinoshita E, Kinoshita-Kikuta E, Takiyama K, Koike T (2006) Phosphate-binding tag, a new tool to visualize phosphorylated proteins. Mol Cell Proteomics 5:749–757.

Lisman JE, Raghavachari S, Tsien RW (2007) The sequence of events that underlie quantal transmission at central glutamatergic synapses. Nat Rev Neurosci 8:597–609.

McAnaney TB, Zeng W, Doe CFE, Bhanji N, Wakelin S, Pearson DS, Abbyad P, Shi X, Boxer SG, Bagshaw CR (2005) Protonation, photobleaching, and photoactivation of yellow fluorescent protein (YFP 10C): a unifying mechanism. Biochemistry 44:5510–5524.

Moechars D, Weston MC, Leo S, Callaerts-Vegh Z, Goris I, Daneels G, Buist A, Cik M, van der Spek P, Kass S, Meert T, D'Hooge R, Rosenmund C, Hampson RM (2006) Vesicular glutamate transporter VGLUT2 expression levels control quantal size and neuropathic pain. J Neurosci 26:12055–12066.

Mutch S, Kensel-Hammes P, Gadd J, Fujimoto B, Allen R, Schiro P, Lorenz R, Kuyper C, Kuo J, Bajjalieh SM, Chiu D (2011) Protein Quantification at the Single Vesicle Level Reveals That a Subset of Synaptic Vesicle Proteins Are Trafficked with High Precision. Journal of Neuroscience 31:1461.

Pan P-Y, Marrs J, Ryan TA (2015) Vesicular Glutamate Transporter 1 orchestrates recruitment of other synaptic vesicle cargo proteins during synaptic vesicle recycling. J Biol Chem.

Pechstein A, Gerth F, Milosevic I, Jäpel M, Eichhorn-Grünig M, Vorontsova O, Bacetic J, Maritzen T, Shupliakov O, Freund C, Haucke V (2015) Vesicle uncoating regulated by SH3-SH3 domain-mediated complex formation between endophilin and intersectin at synapses. EMBO Rep 16:232–239.

Preobraschenski J, Zander J-F, Suzuki T, Ahnert-Hilger G, Jahn R (2014) Vesicular glutamate transporters use flexible anion and cation binding sites for efficient accumulation of neurotransmitter. Neuron 84:1287–1301.

Rizzoli SO, Betz WJ (2004) The structural organization of the readily releasable pool of synaptic vesicles. Science 303:2037–2039.

Rothman JS, Kocsis L, Herzog E, Nusser Z, Silver RA (2016) Physical determinants of vesicle mobility and supply at a central synapse. eLife 5.

Santos MS, Foss SM, Park CK, Voglmaier SM (2014) Protein Interactions of the Vesicular Glutamate Transporter VGLUT1. PLoS ONE 9:e109824.

Schäfer MK-H, Varoqui H, Defamie N, Weihe E, Erickson JD (2002) Molecular cloning and functional identification of mouse vesicular glutamate transporter 3 and its expression in subsets of novel excitatory neurons. J Biol Chem 277:50734–50748.

Schenck S, Wojcik SM, Brose N, Takamori S (2009) A chloride conductance in VGLUT1 underlies maximal glutamate loading into synaptic vesicles. Nat Neurosci 12:156–162.

Siksou L, Silm K, Biesemann C, Nehring RB, Wojcik SM, Triller A, Mestikawy El S, Marty S, Herzog E (2013) A role for vesicular glutamate transporter 1 in synaptic vesicle clustering and mobility. Eur J Neurosci 37:1631–1642.

Südhof TC, Rizo J (2011) Synaptic vesicle exocytosis. Cold Spring Harb Perspect Biol 3.

Takamori S et al. (2006) Molecular anatomy of a trafficking organelle. Cell 127:831–846.

Takamori S, Rhee JS, Rosenmund C, Jahn R (2000) Identification of a vesicular glutamate transporter that defines a glutamatergic phenotype in neurons. Nature 407:189–194.

Varoqui H, Schäfer MKH, Zhu H, Weihe E, Erickson JD (2002) Identification of the differentiation-associated Na+/PI transporter as a novel vesicular glutamate transporter expressed in a distinct set of glutamatergic synapses. J Neurosci 22:142–155.

Varoqui H, Zhu H, Yao D, Ming H, Erickson JD (2000) Cloning and functional identification of a neuronal glutamine transporter. J Biol Chem 275:4049–4054.

Vinatier J, Herzog E, Plamont M-A, Wojcik SM, Schmidt A, Brose N, Daviet L, Mestikawy El S, Giros B (2006) Interaction between the vesicular glutamate transporter type 1 and endophilin A1, a protein essential for endocytosis. J Neurochem 97:1111–1125.

Voglmaier SM, Kam K, Yang H, Fortin DL, Hua Z, Nicoll RA, Edwards RH (2006) Distinct endocytic pathways control the rate and extent of synaptic vesicle protein recycling. Neuron 51:71–84.

Weston MC, Nehring RB, Wojcik SM, Rosenmund C (2011) Interplay between VGLUT isoforms and endophilin A1 regulates neurotransmitter release and short-term plasticity. Neuron 69:1147–1159.

Westphal V, Rizzoli S, Lauterbach M, Kamin D, Jahn R, Hell S (2008) Video-Rate Far-Field Optical Nanoscopy Dissects Synaptic Vesicle Movement. Science.

Wilson NR, Kang J, Hueske EV, Leung T, Varoqui H, Murnick JG, Erickson JD, Liu G (2005) Presynaptic regulation of quantal size by the vesicular glutamate transporter VGLUT1. J Neurosci 25:6221–6234.

Winther ÅME, Vorontsova O, Rees KA, Näreoja T, Sopova E, Jiao W, Shupliakov O (2015) An Endocytic Scaffolding Protein together with Synapsin Regulates Synaptic Vesicle

Clustering in the Drosophila Neuromuscular Junction. J Neurosci 35:14756–14770.

Wojcik SM, Rhee JS, Herzog E, Sigler A, Jahn R, Takamori S, Brose N, Rosenmund C (2004) An essential role for vesicular glutamate transporter 1 (VGLUT1) in postnatal development and control of quantal size. Proc Natl Acad Sci USA 101:7158–7163.

FIGURE LEGENDS

Figure 1: Dose dependent regulation of SV super-pool size by VGLUT1.

A: Expression of Synaptobrevin2 fused to Enhanced Green Fluorescent Protein ($Syb2^{EGFP}$) in hippocampal neurons at 18 days in culture. B: examples of FRAP sequences from both VGLUT1 +/+ and -/- genotypes. Boutons are imaged for 3 min, bleached and recovery is recorded for 73 min. C. Average FRAP kinetics. 27 synapses from +/+ and 31 synapses from -/- were measured by FRAP and the average traces are displayed here (for +/+ N = 11 cultures; for -/- N = 8 cultures). The two traces were fitted using double exponential components equations and the convergence of the traces to a common fit was tested using the extra sum of squares F test. The F test indicates that the traces are best fitted by 2 divergent models (F ratio = 19.32; P<0.0001). Fast FRAP recovery was monitored every 5s in an independent set of experiments (inset). D: Expression of $VGLUT1^{venus}$ in hippocampal neurons. E: Average FRAP recovery of $VGLUT1^{venus}$ at 68 minutes post-bleach in rescue or over-expression. Over-expression reduces the mobility of SVs (Unpaired t test, P = 0.0385, t = 2.176. For overexpression: N = 4 cultures, n = 14 synapses; for rescue: N = 3 cultures, n = 15 synapses.). Scale bar: 2μm in A and D, 1 μm in B.

Figure 2: Structure analysis of VGLUT1 and expression of mutants in neurons.

A: snake scheme of VGLUT1 structure with 560 amino acids, 12 transmembrane domains (Almqvist et al., 2007), N- and C-termini facing the cytoplasmic side, and N-glycosylation at the first luminal loop. In blue the 3 residues mutated to silence VGLUT1 transport

(sVGLUT1 see Fig 3). Red bars display the 3 deletions used (ΔC-term, ΔPP1+2, ΔPP2). Red residues where mutated to alanine in order to test their implication in the super-pool regulation supported by VGLUT1. All mutations carried a venus tag at the C-terminus. B: examples of expression patterns obtained with VGLUT1 WT and mutants upon transduction in hippocampal neurons matching endogenous expression levels. Note the dense expression and low somatic signals. Scale bar 10µm.

Figure 3: SV tonicity is not involved in the regulation of SV super-pool size

A: Expression of VGLUT1^{mCherry}, sVGLUT1^{mCherry} and Syb2^{EGFP} in hippocampal neurons. FRAP was performed on Syb2^{EGFP} at axons colocalized with mCherry signal or not. Scale bar 5µm. B: Average FRAP kinetics from knock out cells rescued by VGLUT1^{mCherry}, sVGLUT1^{mCherry} or not. Synapses from each genotype were measured by FRAP and the average traces are displayed here (N = 7 independent cultures, 16 synapses for -/-; N = 5 cultures, 23 synapses for WT rescue, and N = 10 cultures, 36 synapses for sVGLUT1 rescue). The 3 traces were fitted using double exponential components equations and the convergence of the traces to a common fit was tested using the extra sum of squares F test. The F test indicates that the traces are best fitted by 2 divergent models (one for -/- synapses and the other one for both rescues, F ratio = 30.25; P<0.0001). FRAP kinetics for the 2 types of rescued synapses are best fitted by one convergent model (F ratio = 1.235; P = 0.294).

Figure 4: VGLUT1 PP2 domain mediates SV super-pool size regulation

A: Comparison of VGLUT1^{venus} and VGLUT1$^{P554A\text{-}venus}$ rescues of *vglut1*$^{-/-}$ on SV exchange rates at synapses. 14 (WT) and 23 (P554A) synapses from each rescue were measured by FRAP and the average traces are displayed here (N = 4 cultures for WT and N = 5 cultures for P554A). The two traces were fitted using double exponential components equations and the

convergence of the traces to a common fit was tested using the extra sum of squares F test. The F test indicates that the traces are best fitted by 2 divergent models (*F* ratio = 15.32; *P* < 0.0001). B: Similar experiments where performed for ΔPP1+2, ΔPP2, DQL514AQA, PP534AA, S540A and T544A. The results are displayed here as a comparison of fluorescence recovery to the corresponding WT control 68 min after bleaching. Only mutants affecting the PP2 pattern display a lack of rescue to WT levels and a significantly higher SV exchange rate (*t* test, WT *vs.* ΔPP1+2: *P* = 0.0005, *t* = 3.790; *vs.* ΔPP2: *P* < 0.0001, *t* = 4.369; *vs. P*554A: *P* = 0.0242, *t* = 2.366). C: Time lapse imaging of SV axonal transport. VGLUT1^{venus}, or VGLUT1$^{P554A\text{-}venus}$, or VGLUT1$^{S540A\text{-}venus}$ were expressed in *vglut1*$^{-/-}$ neurons. Example sequence extracted from the boxed fiber (left) sampled every 200ms over 30s (middle). Vertical arrow head points to a venus fluorescent dot traveling along the axon. Kymograph of fluorescence movements within the example fiber (boxed in middle panel). Vertical arrow head points to the same traced event shown in the middle panel. Scale bar: left 5µm, middle 2µm. D: Cumulative axonal fluorescence traffic measured over time lapse sequences. A significant increase in VGLUT1^{venus} traffic is seen when P554A is expressed compared to WT and S540A mutant (unpaired *t* test, WT *vs.* P554A: *P* = 0.0092, *t* = 3.564; *vs*. S540A: *P* = 0.8963, *t* = 0.1351. *N* = 5 cultures for WT, and *N* = 4 cultures for both P554A and S540A.). E: Average speed of VGLUT1^{venus} dots was extracted from kymographs. No significant changes in speed was seen for mutants tested compared to WT (One-way ANOVA, *P* = 0.0634, *F* ratio = 2.431. Speed for each mutant, WT: 1.564 ± 0.02692 µm/s; P554A: 1.536 ± 0.02860 µm/s; S540A: 1.460 ± 0/02942 µm/s).

Figure 5: VGLUT1 is phosphorylated but not at the conservation 540-SYGAT

A: Effect of alkaline phosphatase on the electrophoretic mobility of VGLUT1 from forebrain homogenates (and positive control VIAAT ; Vesicular Inhibitory Amino-Acid Transporter).

B : regional distribution of VGLUT1 phosphorylation state. Homogenates of several brain regions where probed for VGLUT1 signal as in panel A. OB : olfactory bulb, St : Striatum, Hipp : Hippocampus, BS : Brain Stem, Thal : Thalamus, Cb : Cerebellum, Cx : Cortex. C : PhosTag assay on *vglut1*$^{-/-}$ primary neuron cultures rescued with VGLUT1^{venus} WT and C-terminal mutant constructs. Note that PhosTag assays prevent from using a size ladder. All constructs display a phospho-shifted band that disapeared upon desphosphorylation by alkaline phosphatase. PI : phosphatase inhibitors ; AP : alkaline phosphatase. Selected lanes blotted on the same membranes were reorganised for display purpose.

Figure 1.

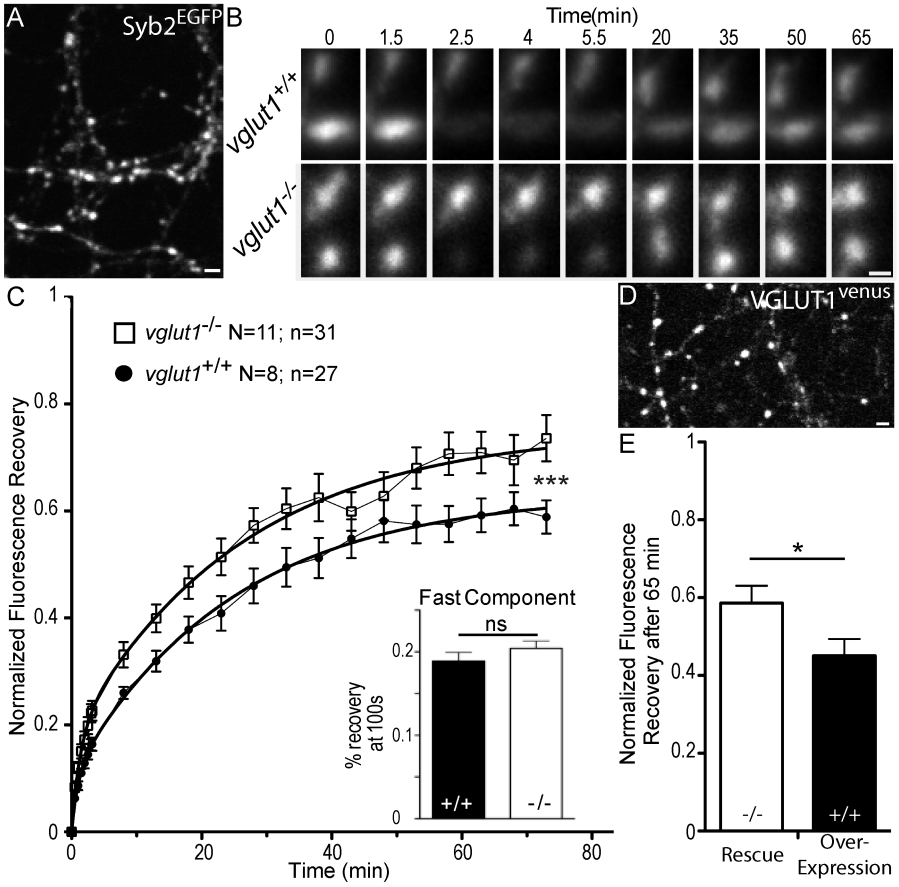
A
Syb2EGFP
B
Time(min)
0
1.5
2.5
4
5.5
20
35
50
65
vglut1+/+
vglut1-/-
C
vglut1-/- N=11; n=31
vglut1+/+ N=8; n=27
Normalized Fluorescence Recovery
Time (min)
***
Fast Component
ns
% recovery at 100s
+/+
-/-
D
VGLUT1venus
E
Normalized Fluorescence Recovery after 65 min
*
-/-
+/+
Rescue
Over-Expression

Figure 2.

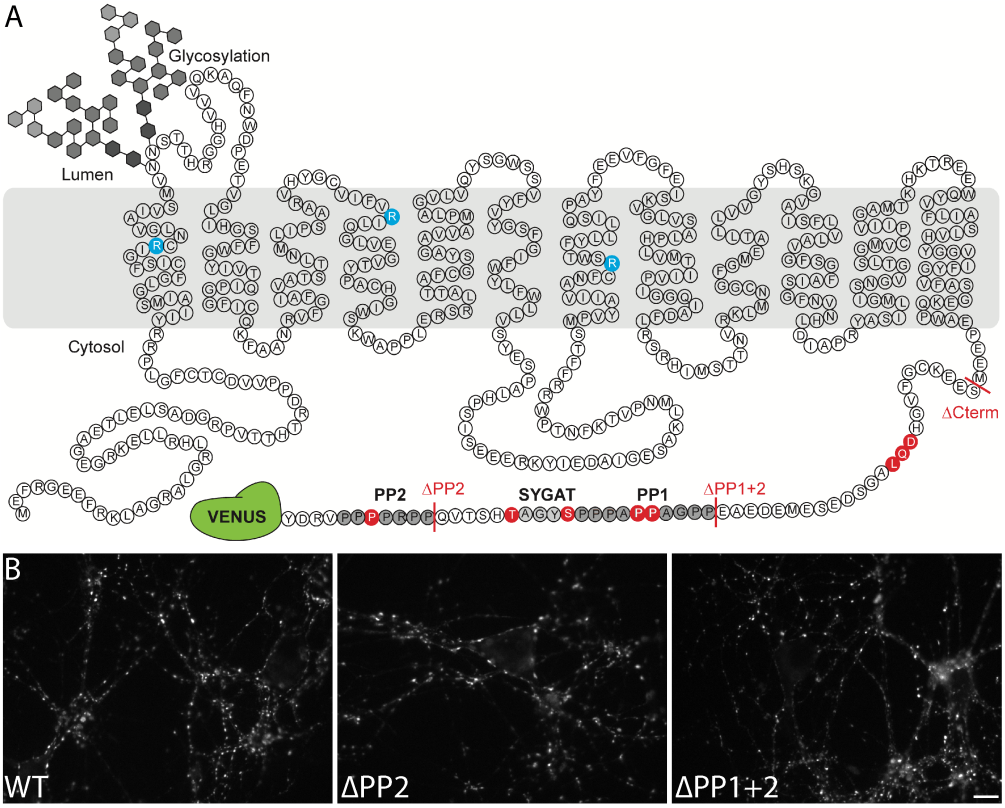
A
Glycosylation
Lumen
Cytosol
ΔCterm
VENUS
PP2
ΔPP2
SYGAT
PP1
ΔPP1+2
B
WT
ΔPP2
ΔPP1+2

Figure 3.

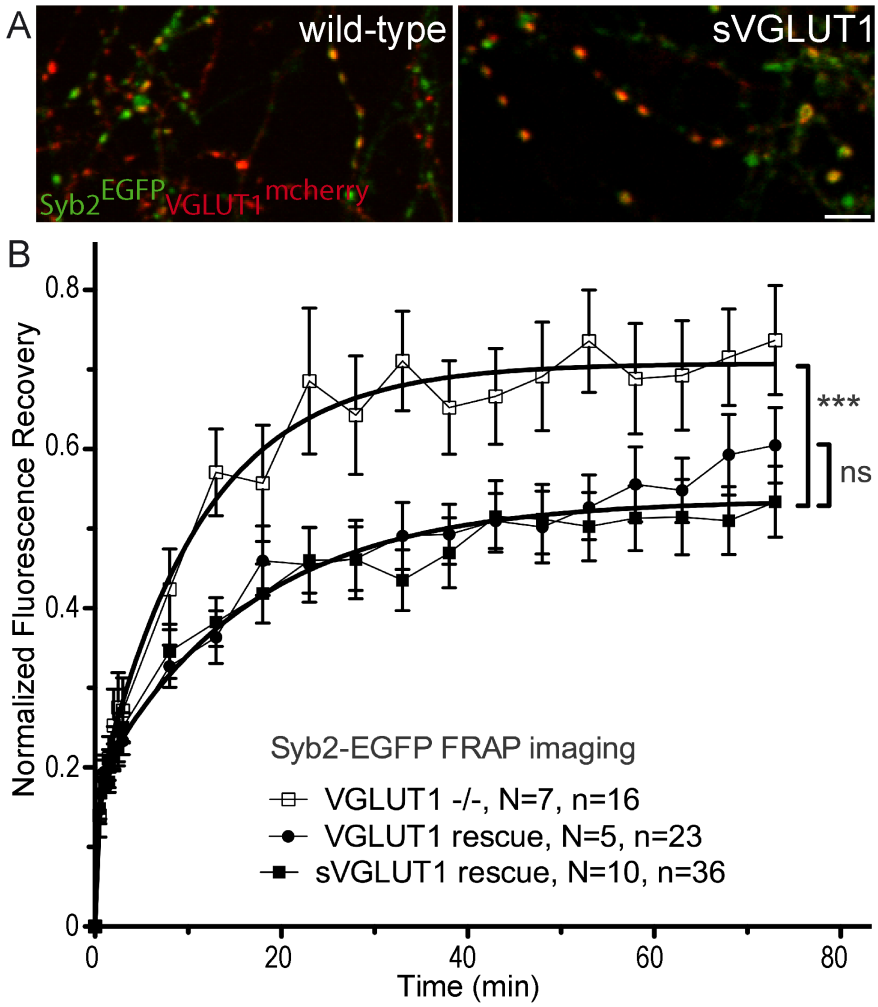
A
wild-type
sVGLUT1
Syb2EGFP
VGLUT1mcherry
B
Normalized Fluorescence Recovery
0.8
0.6
0.4
0.2
0
0
20
40
60
80
Time (min)
***
ns
Syb2-EGFP FRAP imaging
VGLUT1 -/-, N=7, n=16
VGLUT1 rescue, N=5, n=23
sVGLUT1 rescue, N=10, n=36

Figure 4.

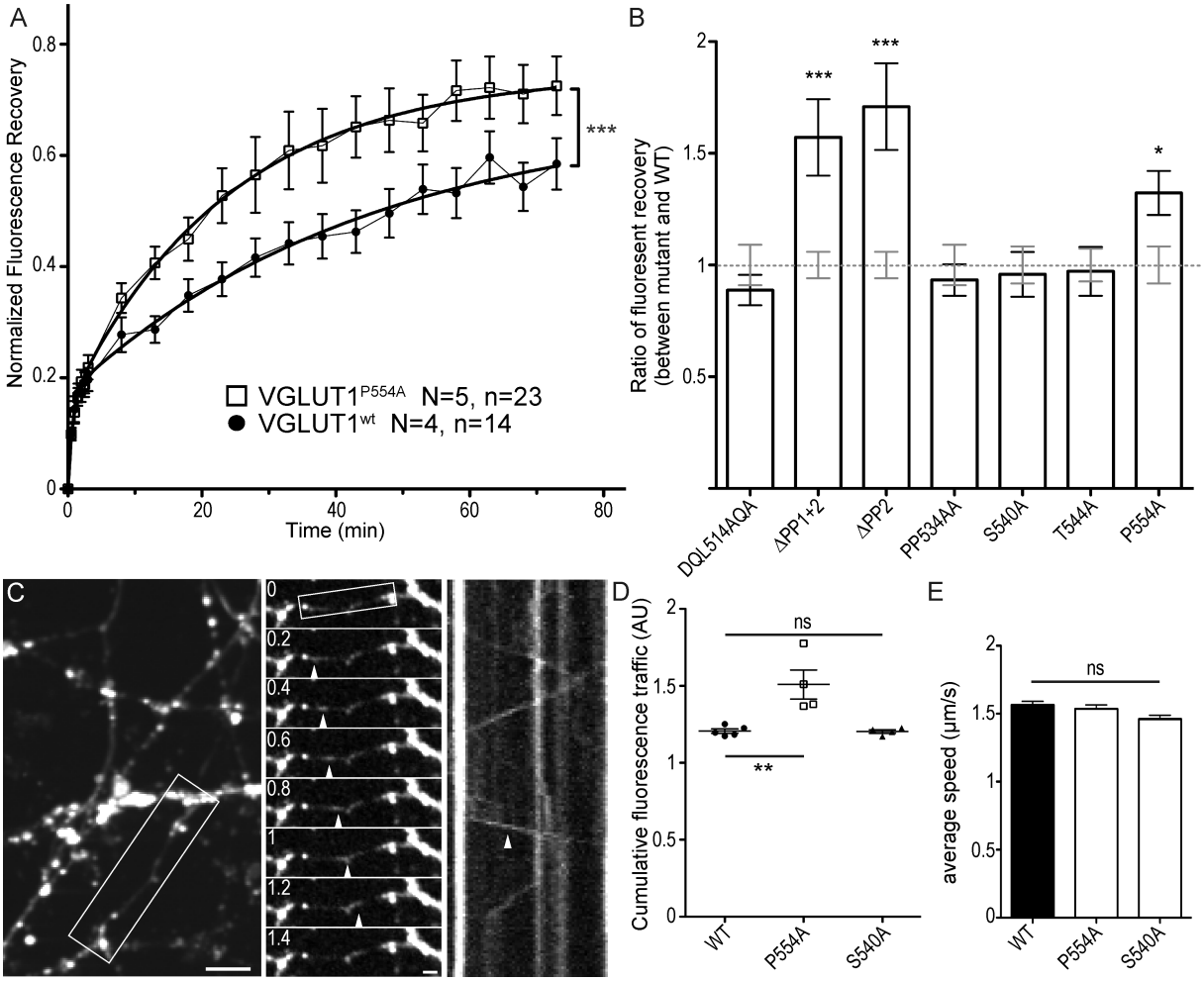
A
Normalized Fluorescence Recovery
Time (min)
VGLUT1P554A N=5, n=23
VGLUT1wt N=4, n=14
***
B
Ratio of fluoresent recovery (between mutant and WT)
DQL514AQA
ΔPP1+2
ΔPP2
PP534AA
S540A
T544A
P554A
C
D
Cumulative fluorescence traffic (AU)
ns
**
WT
P554A
S540A
E
average speed (µm/s)
ns
WT
P554A
S540A

Figure 5.

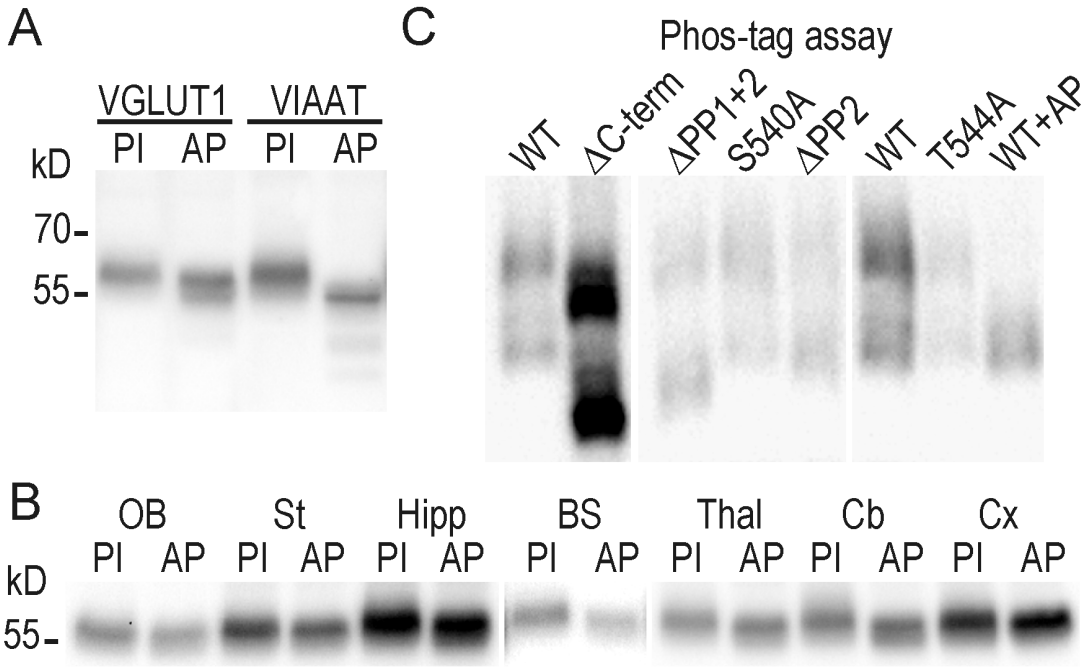

Figure S1.

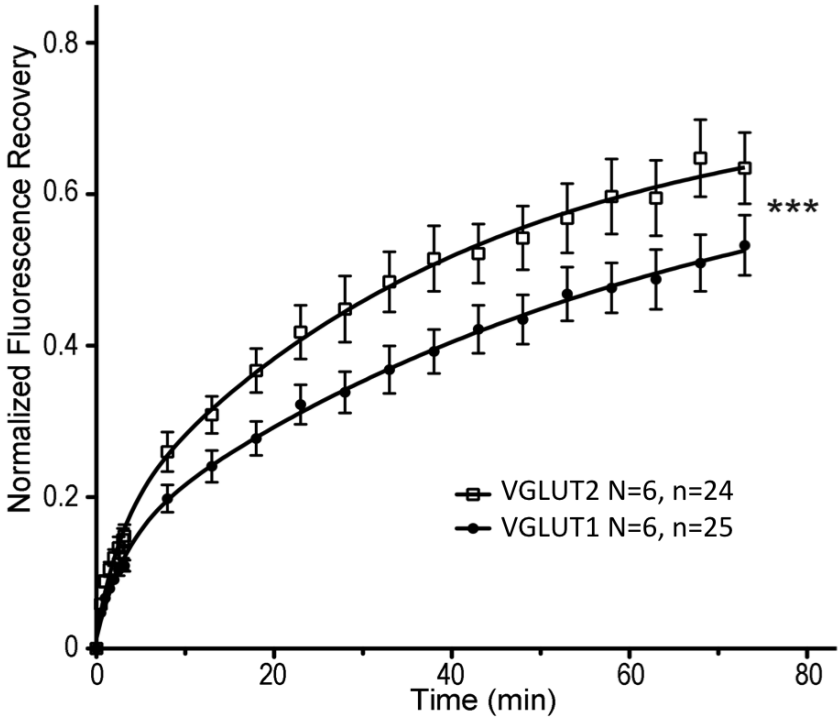

Article 2: Characterization of a VGLUT1^{mEOS2} knock in mouse line for the study synaptic vesicle mobility in excitatory neurons

VGLUT1 uploads glutamate into SVs, thus, it is a specific marker for glutamatergic SVs. By labeling VGLUT1 with fluorescent proteins, we can trace SV mobility with live imaging approaches. With the previous VGLUT1^{Venus} KI mice, our lab identified that SVs share among synapses in the same axon both *in vitro* and *in vivo*. We generated the VGLUT1^{mEos2} KI mouse line with the same strategy of VGLUT1^{Venus} mice. This mouse line would allow us to trace the individual SVs with super-resolution techniques and overcome some limits faced when tracing synaptic vesicles (SVs) or individual synaptic boutons on long timescales with VGLUT1^{Venus} mice.

In the VGLUT1^{mEos2} KI mice, VGLUT1^{mEos2} is temporally, spatially accurately replacing the WT protein. But unlike the VGLUT1^{Venus} mice, VGLUT1^{mEos2} mouse line shows a knock down effect of VGLUT1. Compared to the *vglut1*$^{+/+}$ allele, the *vglut1*$^{Eo/Eo}$ allele results an only 20-25% expression of VGLUT1, which indicates a low efficiency of protein synthesis, or an altered protein degradation.

VGLUT1^{mEos2} is functional in neurotransmission. Unlike VGLUT1 KO pups that die around 3 weeks after birth, the *VGLUT1*$^{Eo/Eo}$ mice do not show obvious deficits compared to the *VGLUT1*$^{Eo/+}$ or *VGLUT1*$^{+/+}$ littermates. It means that a quarter expression of VGLUT1^{mEos2} can maintain the basic glutamatergic activity of VGLUT1 neurons in mice.

VGLUT1^{mEos2} can be photoconverted with UV light illumination. With PALM imaging, we could trace the individual SV trafficking along the axons. Moreover, by following the photoconverted SVs that originated from one presynaptic bouton, we could highlight the potential of our KI line for the further characterization of SV super-pool.

My contribution in this work includes generating the VGLUT1^{mEos2} mouse line, the primary culture and the genotyping of the pups, and the live imaging of photoconversion. I also participated in the western blot and the management of the VGLUT1^{mEos2} mouse line.

In Preparation

Characterization of a VGLUT1^{mEos2} knock-in mouse line for the study synaptic vesicle mobility in excitatory neurons.

Xiao-Min Zhang [1,2,3], Noa Lipstein[3], Maria Florencia Angelo[1,2], Corey Buttler[1,2], Clémence Peyrot [1,2], Christelle Martin [1,2], Jean-Baptiste Sibarita[1,2], Yann Humeau[1,2], Brose Nils[3], and Herzog Etienne[1,2]

[1] Interdisciplinary Institute for Neuroscience, Université de Bordeaux, UMR 5297, 33000 Bordeaux, France.
[2] Interdisciplinary Institute for Neuroscience, CNRS UMR 5297, 33000 Bordeaux, France.
[3] Department of Molecular Neurobiology, Max Planck Institute of Experimental Medicine, D-37075 Göttingen, Germany.

Corresponding author: Etienne Herzog; etienne.herzog@u-bordeaux.fr

Acknowledgements : Fabrice Cordelière

Abstract:

Excitatory synaptic vesicles (SVs) release glutamate upon presynaptic calcium rise. Prior to release, glutamate is loaded into SVs through the action of Vesicular GLUtamate Transporters (VGLUT). The 3 VGLUTs define 3 glutamatergic systems in the brains. Cortical neurons express high levels of VGLUT1, which represents probably the best marker for SVs in these neurons. Following our succesful VGLUT1^{venus} approach, we fused the photoconvertible protein mEos2 with VGLUT1 and generated a VGLUT1^{mEos2} knock-in (KI) mouse line. VGLUT1^{mEos2} replaces accurately VGLUT1, however a reduced expression was detected. Yet, VGLUT1^{mEos2} seem functional and can be successfully photoconverted with UV light illumination. We could show here that this model will allow for the tracking of SV super-pool over long periods of time and wide axonal segments. In the mean time, single molecule tracking in photoactivation localisation microscopy (sptPALM) will provide important insights on SV mobility within boutons.

INTRODUCTION

Synapses have long been thought to represent autonomous units relying on local recycling and delivery of de novo synthetized components delivered from the cell soma through axonal transport (Bonanomi et al., 2006). More and more data suggest that neurite-wide exchange of material is occuring and is necessary for proper network function (Darcy et al., 2006; Kalla et al., 2006; Tsuriel et al., 2006; Fernandez-Alfonso and Ryan, 2008; Westphal et al., 2008; Minerbi et al., 2009; Herzog et al., 2011). The analysis of synaptic vesicle (SV) exchange between en passant boutons has been the most studied and leads to the notion of SV super-pool spanning the axon or a segment of axon. SV super-pool was defined based on morphological observations by contrast to classical SV pools that were defined based on functional properties in electrophysiological paradigms (Denker and Rizzoli, 2010).

Our main contribution to the definition of SV super-pool was to observe SV exchange at cortical synapses of living mice (Herzog et al., 2011), that an experiment was allowed by the establishment of a VGLUT1^{venus} knock-in (KI) mouse line that replaced endogenous VGLUT1 (Vesicular GLUtamate Transporter type 1) by a fluorescently tagged version. VGLUT1^{venus} mice are anatomically and functionally unaltered as established to date (Herzog et al., 2011). VGLUT1^{venus} mice were further used to establish the physical determinants of SV mobility at cerebellar mossy fiber terminals under different regimes of stimulation(Rothman et al., 2016). On a different ground, we used VGLUT1^{venus} to explore VGLUT1 synapses proteome from highly enriched VGLUT1 synaptosome preparation obtained through fluorescence activated synaptosome sorting (Biesemann et al., 2014; Luquet et al., 2016).

To expand SV tracing possibilities and explore further SV mobility parameters in the axonal compartment, we now establish VGLUT1^{mEos2} knock-in line. mEos2 is the second generation photo-convertible fluorescent protein derived from Anthozoans (Nienhaus et al., 2005;

Lippincott-Schwartz and Patterson, 2009). Following the successful knock-in of venus at the *vglut1* locus, we decided to apply the same strategy for mEos2. Here we characterize this mouse model and explore its ability to trace SVs with new paradigms.

MATERIALS AND METHODS

Animals

All mice are housed in 12/12 LD with ad libitum feeding. Every effort was made to minimize the number of animals used and their suffering. The experimental design and all procedures were in accordance with the European guide for the care and use of laboratory animals and approved by the ethics committee of Bordeaux Universities (CE50) under the APAFIS n°1692.

Antibodies

The primary antibodies used were: VGLUT1 rabbit polyclonal antiserum BN3L2Bf (Herzog et al., 2001), Snap 25 mouse monoclonal antibody (111011, SYSY). The secondary antibodies were: Donkey anti-rabbit Alexa 488 (A21206, Invitrogen), goat anti-mouse Alexa 488 (A32723, Invitrogen) and goat anti-rabbit IRDye 800CW (P/N 925-32211, Li-COR).

Generation of VGLUT1^{mEOS2} KI mice

The targeting vector was constructed on the basis of a 14 kb genomic clone of the *VGLUT1* locus in pBluescript, which had been isolated from a λFIXII genomic library of the SV129 mouse strain (Stratagene). In the targeting vector, the STOP codon in the last exon (exon 12) of the *VGLUT1* gene was replaced in-frame by a *mEOS2-loxP-neo-loxP* cassette using recombineering techniques with engineered primers. The *venus-loxP-neo-loxP* cassette was inserted between a 6.7 kb genomic sequence in 5' position and a 7.9 kb genomic sequence in 3' position. Mice carrying the mutant *VGLUT*$^{mEOS2\text{-}neo}$ gene (*VGLUT1*$^{Eon/+}$) were generated by homologous recombination in embryonic stem cells (SV129/ola) and identified by Southern bloting. To eliminate deleterious effects of the neomycin resistance gene, we crossed

heterozygous *VGLUT1*$^{Eon/+}$ mice with Stella-Cre mice that express Cre recombinase in early embryonic stages (Liu et al., 2011). Successfully recombined *VGLUT1*^{mEOS2} alleles (Eo/+) in offspring from these interbreedings were genotyped by PCR. It is located on the mouse chromosome 7 contig NT_039424.7 at position 6081938-6082223. The following oligonucleotides were used for genotyping PCRs: 9420, CTGGCTGGCAGTGACGAAAG; 9421, CGCTCAGGCTAGAGGTGTATGGA; 32896, CTGAAGTCACATCGGTAATG. Oligonucleotides 9420 and 9421 were used to amplify the *VGLUT1*$^{+}$ and *VGLUT1*^{Eo} allele, with expected band size 202 bp and 1033 bp respectively. Oligonucleotides 9420 and 32896 were used to amplify the *VGLUT1*^{Eo} allele with an expected band of 668 bp.

Hippocampal cell culture

Hippocampal primary dissociated cultures were prepared from P0 *vglut1*$^{EO/+}$ and *vglut1*$^{+/+}$ mice. The hippocampi were dissected in ice-cold Leibovitz's L-15 medium (11415064; Gibco), and then incubate in 0.05% trypsin-EDTA (25300054, Gibco) for 15 min at 37°C. The tissues were washed with Dulbecco's Modified Eagle's Medium (DMEM, 61965026, Gibco) containing 10% FBS (CVFSVF0001, Eurobio), 1% Penicillin-streptomycin (15140122, Gibco). Cells were mechanically dissociated by pipetting up and down. To better isolate the fluorescent synapse with VGLUT1^{mEos2}, the VGLUT1$^{Eo/+}$ and VGLUT1$^{+/+}$ cells were plated with a ratio 1:5 onto poly-L-lysine (P2636, Sigma) coated coverslips at a density of 20 000 cells/cm^2. Cells were grown in Neurobasal A medium (12349105, Gibco) containing 2% B27 supplement (17504044, Gibco), 0.5 mM Glutamax(35050038, Gibco), and 0.2% MycoZap plus-PR (VZA2021, Lonza). After 10 days, half of the medium was changed. Imaging of live dissociated neuron cultures was performed at 17-21 days *in vitro* (DIV) in culture medium with added Hepes buffer (60 mM).

Biochemical analyses

Sodium dodecylsulfate polyacrylamide gel electrophoresis (SDS-PAGE) and Western blotting were performed according to standard procedures using Alexa-488 or IRDye 800-coupled secondary antibodies for semiquantitative Western detection. Alexa 488 secondary antibodies were used for the VGLUT1 detection in different VGLUT1^{mEos2} genotypes and fluorescent signals were visualized with ChemiDoc MP system (Bio-Rad). Western blotting for VGLUT2 served as a loading control for VGLUT1 and VGLUT^{mEos2}. The IRDye 800 secondary antibody was used for the developmental pattern of VGLUT1^{mEos2} and signals were visualized with Infrared Odyssey (Li-COR Biosciences). Quantitative data are expressed as mean ± SEM.

Imaging of VGLUT1^{mEos2} brain

Direct VGLUT1^{mEos2} fluorescence was performed on perfusion-fixed (4% paraformaldehyde) brain or 60 μm brain section. Pictures were taken with epi-fluorescent microscope (Nikon, ND2). The local photoconversion was done with the DAPI filter under a 40× objective. The duration of UV light exposure was 10 seconds at full intensity of the intensilight source.

PALM imaging

For PALM imaging, the acquisitions were performed on an inverted motorized microscope (Nikon Ti, Japan) equipped with a 100X1.49 NA PL-APO objective with a perfect focus system for axial stabilization. The fluorescence signal was collected by the objective and focused onto a sensitive EMCCD camera (Evolve512, Photometrics) through the combination of a dichroic and emission filters (D101-R561 and F39–617, respectively, Chroma). The entire setup was packaged in a temperature-controlled chamber setting to 37°C (Life Imaging Services, Switzerland). VGLUT1^{mEos2} was photoactivated using a 405 nm laser (3 W/cm2), and the resulting photoconverted single molecule fluorescence was excited with a 561 nm laser (0.8 kW/cm2). Both lasers illuminated the sample simultaneously. The acquisition was

driven by MetaMorph (Molecular Devices, Sunnyvale, USA) in streaming mode at 20 frames per second (50 ms exposure time) for 3,000 frames, each 256x256 pixels. These image stacks were then processed offline for single molecule localization and tracking using the PALMTracer software, from which super resolution tracking images with a pixel size of 40 nm were reconstructed.

Mass photoconversion at individual boutons

Photoconversion was performed with the neuronal culture to check the SVs trafficking along the axons. The imaging acquisition was done with a spinning-disk confocal microscope that a Leica DMI6000 (Leica Microsystems, Wetzlar, Germany) equipped with a confocal Scanner Unit CSU-X1 (Yokogawa Electric Corporation, Tokyo, Japan), and an Evolve EMCCD camera (Photometrics, Tucson, USA) and autofocus system (Bordeaux Imaging Center). The photoconversion experiments were done with a FRAP scanner system (Roper Scientific, Evry, France). Surrounding the setup, a thermal incubator is set to 37°C.

Several presynaptic boutons with VGLUT1^{mEos2} molecules on isolated axons were randomly selected to photoconvert. The 488 nm laser (15 mW) and 561 nm laser (15 mW) were used to monitor the fluorescence of VGLUT1^{mEos2} emitting green or red light respectively. To obtain enough converted mEos2 molecules, the photoconversion was achieved though 40 passes of 405 nm laser (80 mW).

Image acquisition was monitored every 2 s for 4 s before the photoconversion, and every 5 min after the photoconversion during the next 40 min. Then the photoconversion cycle was repeated 9 times. To photoactivate dark mEos2 molecules, a 300 ms exposure with 405 nm (10 mW) was applied at the beginning of the acquisition. This had no measurable impact on fluorescence levels in the red channel. The entire procedure was controlled by the MetaMorph software (Molecular Devices, Sunnyvale, USA).

RESULTS

Homozygous VGLUT1^{mEos2} KIs carrying a mEos2 cDNA instead of the stop codon in exon 12 of the *VGLUT1* gene, followed by a neomycin resistance cassette in the 3' untranslated region (vn/vn) were generated by homologous recombination in embryonic stem cells as described in Materials & Methods (Fig. 1A). To eliminate deleterious effects of the neomycin resistance cassette on VGLUT1 expression (Herzog et al., 2011), Eon/+ mice were crossed with stella-cre mice, which express Cre recombinase in early embryonic stages (Liu et al., 2011). Mice carrying Cre recombined *VGLUT1*^{mEos2} genes were bred to yield homozygous offspring lacking the neomycin resistance cassette (Eo/Eo; Fig. 1AC). 96 ES cell clones were initially screened yielding around 70% positive clones with the desired homologous recombination as identified by Southern blot analysis with a 3' and a 5' external probes (Fig. 1B). For routine breeding, PCR genotyping was performed (Fig. 1C). *VGLUT1*$^{Eo/Eo}$ animals are born at the expected Mendelian frequency and are indistinguishable from their WT and *VGLUT1*$^{Eo/+}$ littermates. Neither *VGLUT1*$^{Eon/Eon}$ nor *VGLUT1*$^{Eo/Eo}$ mice showed any behavioral or morphological alterations at a first glance. They had a normal life expectancy and were fertile though we only have few breeding with the homozygote *VGLUT1*$^{Eo/Eo}$ animals.

To assess the expression level of VGLUT1^{mEos2} in these mice, WT and tagged transporters were systematically quantified in heterozygous and homozygous mouse brain homogenates by western blotting with Alexa 488 or infrared fluorescence detection. In SDS-PAGE, mEos2-tagged VGLUT1 migrates with the expected 25-30 kDa shift as compared to the WT protein and displays a slightly more compact migration profile. Quantification was performed by comparing normalized integrated intensities of both isoforms in the various genotypes. The SNARE (Soluble N-ethylmaleimide-sensitive-factor Attachment protein REceptor) protein SNAP-25 was used as an internal loading control for normalization (Fig. 1D). Surprisingly a

strong knock down of VGLUT1^{mEos2} expression was observed (+/+: 1.0 ± 0.09 AU, *n* = 3, Eo/+: 0.62 ± 0.03, *n* = 6, Eo/Eo: 0.26 ± 0.01 AU, *n* = 5; Fig. 1E). The gene dosage effect was maintained for both variants. Thereby, VGLUT1^{mEos2} knocks down VGLUT1 expression to a quarter of its wild type level. This unexpected phenotype called for further investigations.

To further establish VGLUT1^{mEos2} phenotype, we analyzed the developmental expression pattern in *VGLUT1*$^{Eo/+}$mice. We thus performed western blot analyses of brain homogenates from mice ranging in age between postnatal days P0 and P90 (Fig. 1F). The ratio between both WT and fusion proteins is identical through post natal development with a mean expression of VGLUT1^{mEos2} that represents roughly a fifth of the expression level of the WT band (P5, 0.2995 ± 0.15 AU, *n* = 2; P10, 0.20 ± 0.02 AU, *n* = 2; P15, 0.17 ± 0.02 AU, *n* = 3; P21, 0.17 ± 0.01 AU, *n* = 3; P30, 0.19 ± 0.01 AU, *n* = 3; P60, 0.15 ± 0.02 AU, *n* = 3; P90, 0.19 ± 0.01 AU, *n* = 3; Fig. 1G). VGLUT1^{mEos2} is therefore a knock down of VGLUT1.

Localization of mEos2 fluorescence in VGLUT1^{mEos2} mouse brain

Paraformaldehyde fixed *VGLUT1*$^{Eo/Eo}$ brains display a bright and well-defined fluorescence signal that was excited optimally at 488 nm and collected in the 505-550 nm range (Fig. 2A). Similar excitation and collection yielded a barely detectable background autofluorescence signal in WT brains (not shown). In sagittal brain sections, VGLUT1^{mEos2} fluorescence is prominent in olfactory bulb, cortex, striatum, hippocampus, thalamus and cerebellar cortex (Fig. 2B), all regions that are known to receive dense VGLUT1 positive innervation. Higher magnifications showed typical VGLUT1 labelling patterns in the neuropil of hippocampus, cortex, and cerebellum (Fig. 2CD). As expected, no mEos2 signal was detected in the cell body layers (Fig. 2CD). Upon exposure of VGLUT1^{mEos2} samples to a strong 405nm ultra violet excitation, we could observe the mass photoconversion of green mEos2 signal into red (Fig2A, D). Though *VGLUT1*$^{Eo/Eo}$ expresses only at most a quarter of the normal VGLUT1 level, mEos2 signal is very bright. Indeed, *VGLUT1*$^{Eo/+}$ and *VGLUT1*$^{v/v}$ displayed similar

fluorescence intensities when observed in parallel (not shown). Taken together, above morphological observations demonstrate that the mEos2 tag does not interfere with the qualitative distribution of VGLUT1 as previously shown for venus.

Imaging synaptic vesicle super-pool using VGLUT1^{mEos2}

As *VGLUT1*$^{Eo/+}$ display a bright signal and a moderate knock down on VGLUT1 expression we chose heterozygotes for imaging experiments. We performed sptPALM (single particle tracking Photo Activation Localization Microscopy) on 17-20 days old hippocampal neuron in cultures (Fig 3A). This allowed to unravel individual tragectories of VGLUT1^{mEos2} molecules with a xy precision of a few tens of nanometers (Fig. 3A3). Among these we could monitor extra-synaptic traces accounting for super-pool SVs and cargos (cyan) and synaptic traces accounting for clustered SVs and endosomes (magenta; Fig. 3A3A4).

Next, we optimized protocols for monitoring SV super-pool dynamics using local mass photoconversion at synaptice boutons. To that end, we implemented sparsely labeled cultures in which *VGLUT1*$^{Eo/+}$ cells were diluted 1/5 with wild type cultures of littermates. Through these experiments we faced several limitations due to mEos2 photophysical properties. Indeed, mEos2 seem to bear a significant long lived reversible dark state in the green channel that limits the rate of photoconversion and prevents from using the green channel for quantification (Berardozzi et al., 2016). Nevertheless, we could implement a photoconversion paradigm during which we applied photoconversion pulses recurrently to the same bouton once every 40 min for 10 cycles (Fig. 3B). Here we show an axon with 7 en passant boutons. Recurent photoconversion of one bouton reveals the coverage of SV super-pool exchange over several hours along the axon (Fig. 3C-F). A kymograph representation of both green and red signals over the experiment allows to see the local appearance of red signal upon photoconversion and gradual dispersion during the next 40 min. Dispersion from the target synapses results in a gradual increase in red signal over surounding boutons (Fig. 3EF). In the

mean time little information is gained through the green channel as interchange with the reversible dark state blurs out quantitative changes. Altogether this experiment shows that over several hours SVs are exchanged between a large number of en passant boutons of the same fiber.

DISCUSSION

In the present work we established the first knock in mouse model aimed at monitoring SV mobility stages at single molecule/organelle level through PALM and over wide spatial and temporal scales through mass photoconversion. We generated a VGLUT1^{mEos2} mouse line with the same strategy applied several years ago for VGLUT1^{venus}. VGLUT1^{mEos2} turns out to preserve VGLUT1 function and localization, but generates a severe knock down of VGLUT1 expression. Yet, heterozygote *VGLUT1*$^{Eo/+}$ mice express enough fluorescence and moderate down regulation of VGLUT1 expression so that they are suitable for use in imaging. We could then establish sptPALM and mass photoconversion imaging to monitor SV super-pool at both single particle and wide spatio-temporal scales.

mEos2 photochemistry

From the first live imaging experiments on our model, we could notice that the photochemistry of mEos2 is more complex than we anticipated. VGLUT1^{mEos2} could indeed be photoconverted from green to red with ultra violet (UV) illumination, but we didn't anticipate that a large fraction of mEos2 molecules transit in a long lived reversible dark state (Berardozzi et al., 2016). This dark state seems reluctant to photoconversion but requires a prior transition to the green state through 405 nm UV light illumination (Nienhaus et al., 2005; Lippincott-Schwartz and Patterson, 2009; Berardozzi et al., 2016). For mass photoconversion at single boutons, the consequence is that a quantitative ratio of green *vs*. red molecules at the site of photoconversion is not reached and conversion is limited to the availability of green molecules. This last property is in favor of the PALM approach that

requires limited conversion of a few molecules per frame at each cycle. Increasing 405nm stimulation to empty the long-lived dark state is not compatible with the preservation of physiology and the strict localization of converted molecules.

mEos2 induced the knock down of VGLUT1

For VGLUT1^{mEos2} KI mouse line, we used the exact same genomic strategy as for VGLUT1^{venus}. Yet, the expression level of mEos2 tagged VGLUT1 is severely reduced in the VGLUT1^{mEos2} mice. This could be due to a reduced protein synthesis or faster degradation. However, the constant ratio between VGLUT1^{mEos2} and WT throughout development favors the hypothesis of a reduced synthesis rate of VGLUT1^{mEos2}. Coincidentally, by tagging PSD-95 with mEos2, the PSD-95^{mEos2} KI mouse line also shows a knock down effect of PSD-95 (Broadhead et al., 2016). In contrast, VGLUT1 and Munc18-1 tagged with venus were unaffected (Herzog et al., 2011; Cijsouw et al., 2014; Rothman et al., 2016).

As both tags have a similar size, differences in codon usage or RNA stability may explain the knock down effect observed recurrently. Investigation, on VGLUT1 mRNA levels across genotypes and ages will eventually help understanding the VGLUT1^{mEos2} knock down phenotype.

VGLUT1^{mEos2} is a suitable knock-in model for imaging of synaptic vesicles.

In contrast to VGLUT1 KO mice that display a severe phenotype in the third postnatal week and die around 18 days after birth (Wojcik et al., 2004), *VGLUT1$^{Eo/Eo}$* do not show any sign of deficits. Indeed, previous attempts to abolish glutamate transport function in VGLUT required to mutate 3 sites in the core region of the transporter, and none of the single mutations silenced glutamate release (Herman et al., 2014). Beyond this, VGLUT1^{mEos2} didn't alter VGLUT1 qualitative expression through out the brain and display a punctate localization at thin neurites like VGLUT1. Thorough investigations will show in the future how VGLUT1^{mEos2} knock down affects neurotransmission, yet many evidence suggest that

VGLUT1^{mEos2} is a functional transporter as previously shown for VGLUT1^{venus}. Furthermore, current characterization of *VGLUT1*$^{+/-}$ mice reveal no or very mild impact on neurotransmission and morphology (Fremeau et al., 2004; Wojcik et al., 2004), while a mild impact is measured on behavior and synaptic plasticity (Tordera et al., 2007; Balschun et al., 2009; Garcia-Garcia et al., 2009). Hence, *VGLUT1*$^{Eo/+}$ with a moderate knock down effect above 60% expression level compared to wild type seem a good compromise to study SV super-pool in near native conditions. Furthermore, the fluorescent signal in *VGLUT1*$^{Eo/+}$ is of sufficient intensity to monitor SV mobility under various paradigms.

VGLUT1^{mEos2} extends our ability to trace axonal synaptic vesicle mobility.

Our first sptPALM and mass photoconversion experiments show that VGLUT1^{mEos2} will be an important instrument for the exploration of SV super-pool. Indeed, sptPALM gives access to single VGLUT and single SV trajectories which will provide the possibility to dissect the different mobility stages in SV life cycle. Namely we shall monitor pure axonal transport trajectories, intrasynaptic trajectories, transitions from axonal transport to synaptic cluster and conversely transitions from SV cluster to axonal transport. In addition, mass photoconversion experiments will provide us with the ability to monitor axon or even neuron wide exchanges over long time frames. Finally, in vivo paradigms may allow to tag single boutons and axons to observe them over time in behaviorally relevant paradigms.

Overall, VGLUT1^{mEos2} mice present an unexpected knock down effect on VGLUT1 expression, but remain a promising tool for the investigation of both synaptic vesicle mobility and the impact of VGLUT1 on neurotransmission.

BIBLIOGRAPHY

Balschun D, Moechars D, Callaerts-Vegh Z, Vermaercke B, Van Acker N, Andries L, D'Hooge R (2009) Vesicular Glutamate Transporter VGLUT1 Has a Role in Hippocampal Long-Term Potentiation and Spatial Reversal Learning. Cerebral Cortex:bhp133v1.

Berardozzi R, Adam V, Martins A, Bourgeois D (2016) Arginine 66 Controls Dark-State Formation in Green-to-Red Photoconvertible Fluorescent Proteins. J Am Chem Soc 138:558–565.

Biesemann C, Grønborg M, Luquet E, Wichert SP, Bernard V, Bungers SR, Cooper B, Varoqueaux F, Li L, Byrne JA, Urlaub H, Jahn O, Brose N, Herzog E (2014) Proteomic screening of glutamatergic mouse brain synaptosomes isolated by fluorescence activated sorting. EMBO J 33:157–170.

Bonanomi D, Benfenati F, Valtorta F (2006) Protein sorting in the synaptic vesicle life cycle. Prog Neurobiol 80:177–217.

Broadhead MJ, Horrocks MH, Zhu F, Muresan L, Benavides-Piccione R, DeFelipe J, Fricker D, Kopanitsa MV, Duncan RR, Klenerman D, Komiyama NH, Lee SF, Grant SGN (2016) PSD95 nanoclusters are postsynaptic building blocks in hippocampus circuits. Sci Rep 6:24626.

Cijsouw T, Weber JP, Broeke JH, Broek JAC, Schut D, Kroon T, Saarloos I, Verhage M, Toonen RF (2014) Munc18-1 redistributes in nerve terminals in an activity- and PKC-dependent manner. J Cell Biol 204:759–775.

Darcy KJ, Staras K, Collinson LM, Goda Y (2006) Constitutive sharing of recycling synaptic vesicles between presynaptic boutons. Nat Neurosci 9:315–321.

Denker A, Rizzoli SO (2010) Synaptic vesicle pools: an update. Front SynNeurosci 2:135.

Fernandez-Alfonso T, Ryan TA (2008) A heterogeneous “resting” pool of synaptic vesicles that is dynamically interchanged across boutons in mammalian CNS synapses. Brain Cell Bio 36:87–100.

Fremeau RT, Kam K, Qureshi T, Johnson J, Copenhagen DR, Storm-Mathisen J, Chaudhry FA, Nicoll RA, Edwards RH (2004) Vesicular glutamate transporters 1 and 2 target to functionally distinct synaptic release sites. Science 304:1815–1819.

Garcia-Garcia AL, Elizalde N, Matrov D, Harro J, Wojcik SM, Venzala E, Ramírez MJ, Del Rio J, Tordera RM (2009) Increased vulnerability to depressive-like behavior of mice with decreased expression of VGLUT1. Biol Psychiatry 66:275–282.

Herman MA, Ackermann F, Trimbuch T, Rosenmund C (2014) Vesicular glutamate transporter expression level affects synaptic vesicle release probability at hippocampal synapses in culture. J Neurosci 34:11781–11791.

Herzog E, Bellenchi GC, Gras C, Bernard V, Ravassard P, Bedet C, Gasnier B, Giros B, Mestikawy El S (2001) The existence of a second vesicular glutamate transporter specifies subpopulations of glutamatergic neurons. J Neurosci 21:RC181.

Herzog E, Nadrigny F, Silm K, Biesemann C, Helling I, Bersot T, Steffens H, Schwartzmann R, Nägerl UV, Mestikawy El S, Rhee J, Kirchhoff F, Brose N (2011) In vivo imaging of intersynaptic vesicle exchange using VGLUT1 Venus knock-in mice. J Neurosci 31:15544–15559.

Kalla S, Stern M, Basu J, Varoqueaux F, Reim K, Rosenmund C, Ziv N, Brose N (2006)

Molecular Dynamics of a Presynaptic Active Zone Protein Studied in Munc13-1-Enhanced Yellow Fluorescent Protein Knock-In Mutant Mice. Journal of Neuroscience 26:13054.

Lippincott-Schwartz J, Patterson GH (2009) Photoactivatable fluorescent proteins for diffraction-limited and super-resolution imaging. Trends Cell Biol 19:555–565.

Liu H, Wang W, Chew S-K, Lee S-C, Li J, Vassiliou GS, Green T, Futreal PA, Bradley A, Zhang S, Liu P (2011) Stella-Cre mice are highly efficient Cre deleters. Genesis 49:689–695.

Luquet E, Biesemann C, Munier A, Herzog E (2016) Purification of Synaptosome Populations Using Fluorescence Activated Synaptosome Sorting. Synapse Development 1538.

Methods Mol Biol (Poulopoulos A, ed). Springer US. Available at: http://www.springer.com/us/book/9781493966868.

Minerbi A, Kahana R, Goldfeld L, Kaufman M, Marom S, Ziv NE (2009) Long-term relationships between synaptic tenacity, synaptic remodeling, and network activity. PLoS Biol 7:e1000136.

Nienhaus K, Nienhaus GU, Wiedenmann J, Nar H (2005) Structural basis for photo-induced protein cleavage and green-to-red conversion of fluorescent protein EosFP. Proc Natl Acad Sci USA 102:9156–9159.

Rothman JS, Kocsis L, Herzog E, Nusser Z, Silver RA (2016) Physical determinants of vesicle mobility and supply at a central synapse. eLife 5.

Tordera RM, Totterdell S, Wojcik SM, Brose N, Elizalde N, Lasheras B, Del Rio J (2007) Enhanced anxiety, depressive-like behaviour and impaired recognition memory in mice with reduced expression of the vesicular glutamate transporter 1 (VGLUT1). Eur J Neurosci 25:281–290.

Tsuriel S, Geva R, Zamorano P, Dresbach T, Boeckers T, Gundelfinger ED, Garner CC, Ziv NE (2006) Local sharing as a predominant determinant of synaptic matrix molecular dynamics. PLoS Biol 4:e271.

Westphal V, Rizzoli S, Lauterbach M, Kamin D, Jahn R, Hell S (2008) Video-Rate Far-Field Optical Nanoscopy Dissects Synaptic Vesicle Movement. Science.

Wojcik SM, Rhee JS, Herzog E, Sigler A, Jahn R, Takamori S, Brose N, Rosenmund C (2004) An essential role for vesicular glutamate transporter 1 (VGLUT1) in postnatal development and control of quantal size. Proc Natl Acad Sci USA 101:7158–7163.

FIGURE LEGENDS

Figure 1. Generation of VGLUT1^{mEos2} KI mice.

A: Strategy for the generation of the VGLUT1^{mEos2} KI mutation in mouse embryonic stem cells. The WT VGLUT1 gene, targeting vector, mutated gene after homologous recombination (mEos2Neo, Eon), and mutated gene after Cre recombination (mEos2, Eo) are shown. Exons are indicated by gray boxes. The black triangles indicate loxP sites. Two groups of black horizontal bars (solid line for DraI restriction, dash line with arrow for SexA1 restriction) indicate the 5' and 3' probes used for Southern analysis. Double arrows, represent the amplicons of PCR genotyping in the various genotypes. NEO, Neomycin resistance gene; mEos2, open reading frame of mEos2 fluorescent protein; UTR, 3' untranslated region. B: Southern blot analysis of ES cell DNA after DraI and SexA1 restriction using the probe indicated in A. Eon, mutated allele with neomycin resistance cassette (12.7 kb for DraI, 13.9 kb for SexA1); +, WT allele (10.8 kb for DraI,12.1 kb for SexA1). C: PCR genotyping of WT, mEos2Neo, and mEos2 mouse tail DNA. D: Comparison of VGLUT1 and VGLUT1^{mEos2} expression in VGLUT1^{mEos2} mouse line. mEos2 tagged VGLUT1 is ~25 kDa larger than the WT transporter. E: Semiquantitative Western blot analyses of brain homogenates from +/+ (1.0 ± 0.09 AU, n = 3), Eo/+ (0.62 ± 0.03, n = 6), Eo/Eo (0.26 ± 0.01 AU, n = 5). VGLUT1 signals were normalized to SNAP-25 signals. F: Native and mEos2 tagged VGLUT1 in homogenates of Eo/+ brains at different developmental stages. The qualitative developmental expression profiles of VGLUT1 and VGLUT1^{mEos2} seem identical. A representative array of blots was reconstructed from lanes of the same membrane. P, Postnatal day. G: Semiquantitative Western blot analyses (near infrared fluorescent detection) of brain homogenates from Eo/+ at different developmental stages. The ratio between the levels of native and tagged transporters was constant throughout the developmental stages (P5, 0.2995 ± 0.15 AU, n = 2; P10, 0.20 ± 0.02 AU, n = 2; P15, 0.17 ± 0.02 AU, n = 3; P21, 0.17 ± 0.01 AU, n = 3; P30, 0.19 ± 0.01 AU, n = 3; P60, 0.15 ± 0.02 AU, n = 3; P90, 0.19 ± 0.01 AU, n = 3).

Figure 2. Regional localization and photocoversion of VGLUT1^{mEos2} in the brain.

A: Overview of direct VGLUT1^{mEos2} fluorescence and regional photoconversion in paraformaldehyde-fixed Eo/Eo mouse brain. Scale bar, 2 mm. B: Sagittal section of Eo/Eo brain. Scale bar, 1 mm. C, D: Higher-resolution images of the Eo/Eo section shown in B depicting cortex (Cx), hippocampus (Hipp) and cerebellum. Fine puncta of fluorescent material are concentrated in neuropil areas. Scale bar in C, 200 μm. And the local photoconversion at cerebellum cortex. Scale bar in D, 300 μm.

Figure 3. Imaging SV super-pool with *VGLUT1*$^{Eo/+}$ culture.

A: Tracing SVs mobility with sptPALM imaging. A_1, Wild field of *VGLUT1*$^{Eo/+}$ culture. Scale bar, 2 μm. A_2, Axons from the yellow box of A_1. Individual presynaptic boutons are circled. A_3, SV trajectories inside boutons (magenta) and outside boutons (cyan). A_4, SV trajectories overlayed to wide field distribution. $A_1 – A_3$, scale bar, 1 μm. B: Protocol used for recurrent mass photoconversion of single synapse over several hours. An isolated bouton was photoconverted with a brief pulse of 405nm excitation and monitored every 5 min for 40 min. The photoconversion cycle was repeated 10 times. C: An axonal fiber with 7 *en passant* boutons was selected. Synapse 0 was selected to be converted with 405 nm laser. Neighboring boutons are labeled -1, 1, 2, 3, 4 from left to right. Scale bar, 5 μm. D: Kymographs of the live imaging acquisition in both green and red channel. The time points of photoconversion are labeled with white arrows. E: Surface plots of the two kymographs, which display the intensity changes of each monitored synapses. F: Intensity plot of the -1, 0, and 1 synapses with 561 nm laser excitation. Bouton 0 shows signal waves matched to photoconversion cycles showing dispersion of the photoconverted SVs. Boutons -1 and 1 show increase in red

signal delayed to photoconversion steps corresponding to the integration of converted SVs through super-pool transit.

Figure. 1

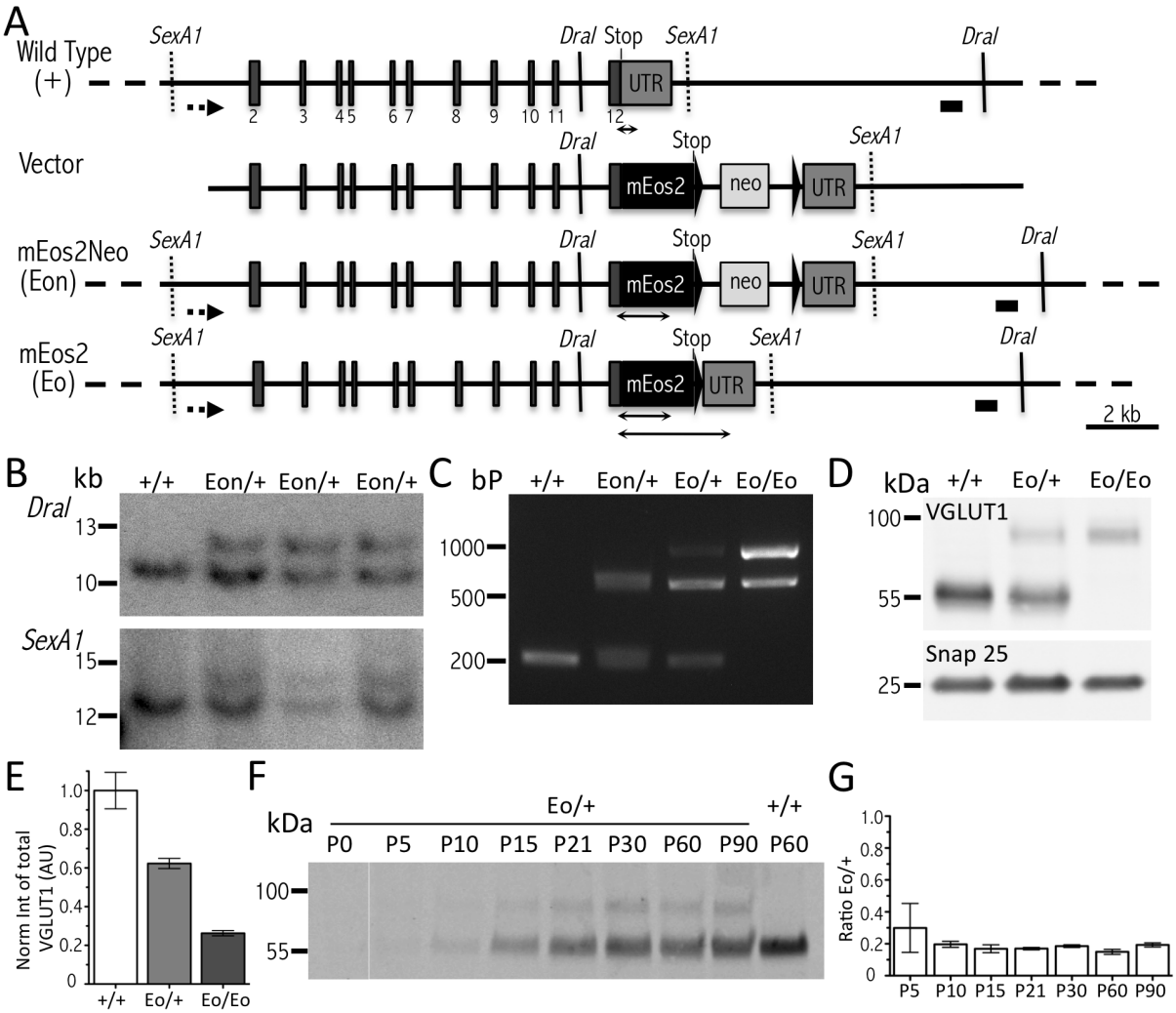
A
Wild Type (+)
SexA1
DraI
Stop
SexA1
DraI
UTR
2 3 4 5 6 7 8 9 10 11 12
Vector
DraI
Stop
SexA1
mEos2
neo
UTR
mEos2Neo (Eon)
SexA1
DraI
Stop
SexA1
DraI
mEos2
neo
UTR
mEos2 (Eo)
SexA1
DraI
Stop
SexA1
DraI
mEos2
UTR
2 kb
B
kb
+/+
Eon/+
Eon/+
Eon/+
DraI
13
10
SexA1
15
12
C
bP
+/+
Eon/+
Eo/+
Eo/Eo
1000
500
200
D
kDa
+/+
Eo/+
Eo/Eo
100
VGLUT1
55
Snap 25
25
E
Norm Int of total VGLUT1 (AU)
1.0
0.8
0.6
0.4
0.2
0
+/+
Eo/+
Eo/Eo
F
kDa
Eo/+
+/+
P0 P5 P10 P15 P21 P30 P60 P90 P60
100
55
G
Ratio Eo/+
1.0
0.8
0.6
0.4
0.2
0
P5 P10 P15 P21 P30 P60 P90

Figure. 2

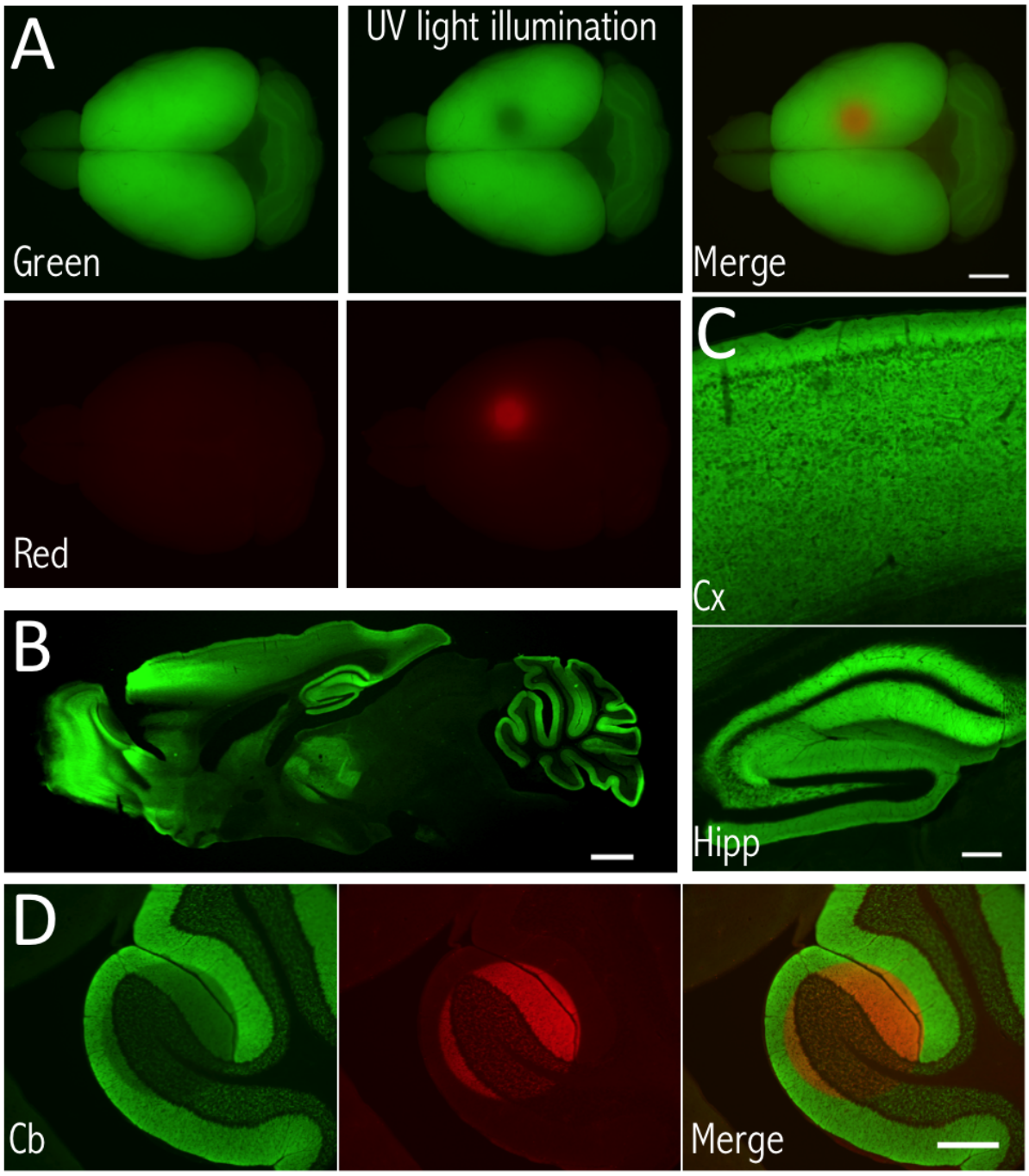

Figure. 3

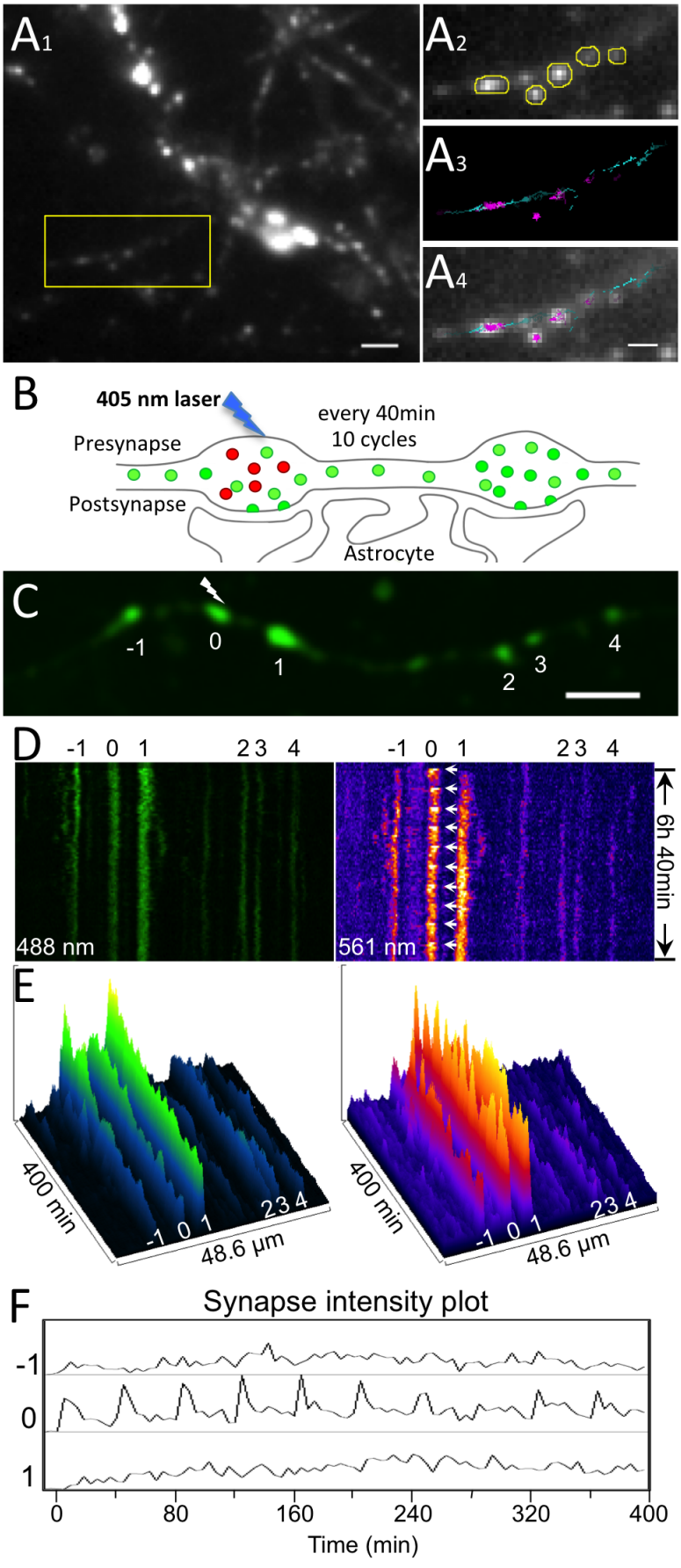
A1
A2
A3
A4
B
405 nm laser
every 40min
10 cycles
Presynapse
Postsynapse
Astrocyte
C
-1
0
1
2
3
4
D
-1 0 1 2 3 4
-1 0 1 2 3 4
6h 40min
488 nm
561 nm
E
400 min
-1 0 1 2 3 4
48.6 μm
400 min
-1 0 1 2 3 4
48.6 μm
F
Synapse intensity plot
-1
0
1
0
80
160
240
320
400
Time (min)

General discussion and perspectives

Through my Ph.D training, I explored several aspects of molecular neurobiology with a focus on synaptic vesicle turn over in the axon. I generated tools to explore SV trafficking (VGLUT1^{mEos2} knock-in mouse line and lenti and AAV vectors for instance). I then used these tools to address issues regarding the homeostasis of SV exchange between synaptic clusters and the axonal super-pool. I will now discuss my results starting with the characterization of VGLUT1^{mEos2} knock-in and following with the new findings regarding VGLUT1 function and SV super-pool regulation.

VGLUT1^{mEos2} knock-in mouse

In the new VGLUT1^{mEos2} knock-in (KI) mouse line, the fluorescent tag mEos2 is fused with VGLUT1 at the C-terminus. The regional, cellular, and subcellular distribution of VGLUT1^{mEos2} is indistinguishable from those of WT VGLUT1 and VGLUT1^{Venus} (Bellocchio et al., 1998; Takamori et al., 2000; Herzog et al., 2001; 2011), but, unlike VGLUT1^{Venus} KI mice (Herzog et al., 2011), we identified a knock down effect of the *vglut1^{mEos2}* allele. Yet, we believe that this model will still be useful as heterozygotes for live imaging of glutamatergic SVs both *in vitro* and *in vivo*. At the same time, the severe knock down effect on VGLUT1 expression in the VGLUT1$^{Eo/Eo}$ mice provides new possibilities to study VGLUT1 function in neurotransmission.

The complex photophysics of mEos2

Photoactivatable fluorescent proteins (PAFPs) are widely used in the super-resolution imaging techniques to trace molecular mobility or localization within live or fixed cells. Photophysical characteristics of PAFPs have great impact on the super-resolution imaging (Lippincott-Schwartz and Patterson, 2009). mEos2, as one of the best green-to-red PAFPs, provides the highest photon output and displays a good photostability (Lippincott-Schwartz and Patterson, 2009; McKinney et al., 2009). It is widely used in live imaging study, especially in photo activated localization microscopy (PALM) (McKinney et al., 2009; Kanchanawong et al., 2010; Rossier et al., 2012). Thus we chose mEos2 to label VGLUT1 and generate a new VGLUT1 KI mouse line. This strategy should allow us to trace synaptic vesicles with super-resolution techniques and to overcome

some limits faced when tracing synaptic vesicles (SVs) or individual synaptic boutons on long timescales with VGLUT1^{Venus} mice (Herzog et al., 2011).

During the first live imaging experiments, we could notice that the photochemistry of mEos2 must be much more complicated than expected. VGLUT1^{mEos2} could indeed be photoconverted from green to red with ultra violet (UV) illumination. But, we didn't anticipate that a large fraction of mEos2 molecules transit in a reversible dark state that seem reluctant to photoconversion before getting back to the green state (Fig. 7). 405 nm light illumination was able to shift mEos2 molecules from the dark state to a green state. Meanwhile, like many other fluorescent proteins, the red form mEos2 could blink repeatedly through a short lived dark states before the bleaching (Dickson et al., 1997; McAnaney et al., 2005; Lippincott-Schwartz and Patterson, 2009; Herzog et al., 2011).

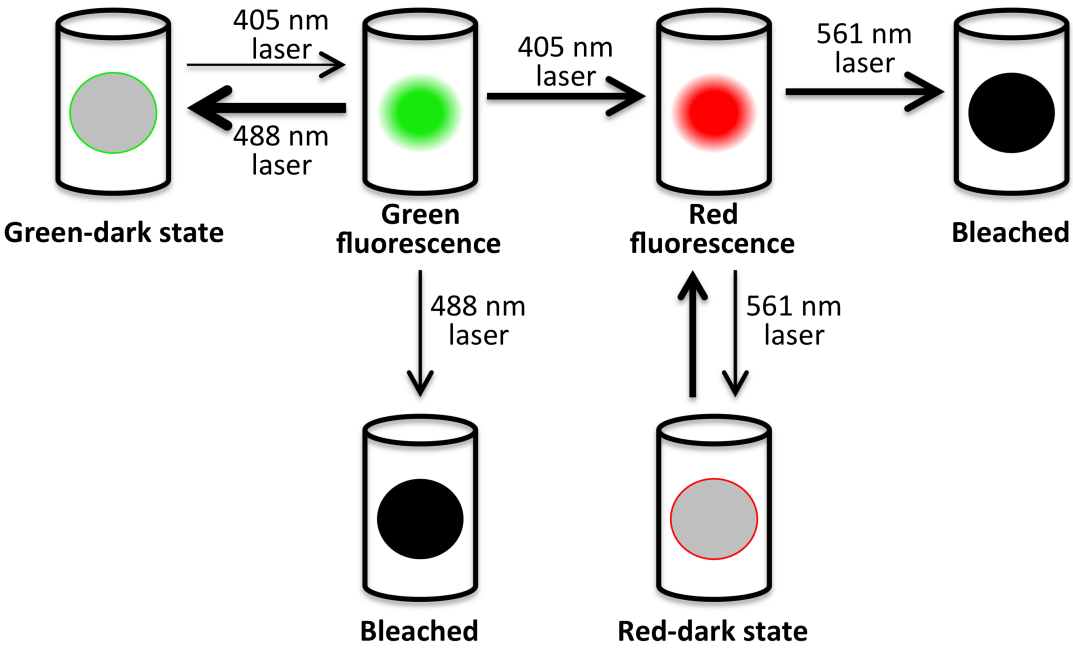

Fig 7. Schematic diagram of mEos2 photophysics. The green state of mEos2 can be easily switched into green-dark state by 488 nm laser. And the green-dark state mEos2 molecules can reversibly be activated to emit green fluorescence with UV light illumination. Only the green state of mEos2 can be photocoverted into red state. The red mEos2 molecules would blink several times before finally being bleached.

However, the dark states before and after the photoactivation are distinct. Because mEos2 is an irreversibly PAFP (Nienhaus et al., 2005; Lippincott-Schwartz and Patterson, 2009), once the molecules are activated into blinking red form, they cannot

be switched into green form anymore. Therefore, the 405 nm light activated green form of mEos2 molecules are not the ones that are already converted into red. Thus, we propose that there is a long lived "green-dark state" of mEos2 molecules before the photoconversion (Fig. 7). Several studies focused on the red-dark state of mEos2 (Lee et al., 2012; Berardozzi et al., 2016). Changing the orientation of arginine 66, which is a highly conserved residue in Anthozoan photoconvertible fluorescent proteins, could affect the fraction of molecules that enter dark states in the photoactivated red form (Berardozzi et al., 2016). So far, there is still no report regarding to the long lived green-dark state of mEos2. Whether the conformation of arginine 66 also affects the dark state in the green form is not known yet.

For our applications requiring mass photoconversion at single boutons, this has a couple of consequences regarding the way imaging can be performed. First, mass photoconversion of VGLUT1^{mEOS2} doesn't results in a quantitative ratio of green *vs.* red molecules at the site of photoconversion. Indeed, the green signal is boosted by the activation of green-dark molecules while the red signal is limited by the availability of green molecules for photoconversion. This last property is in favor of the PALM approach that requires limited conversion of a few molecules per frame at each cycle. One way out could consist in increasing 405 nm stimulation until the long-lived green-dark state is empty, however this is not compatible with the preservation of physiology due to the threat of phototoxicity. Furthermore, local photoconvertion requires tight optimization of the stimulation applied to avoid extra conversion of mEos2 molecules outside of the region of interest (McKinney et al., 2009; Baker et al., 2010; Lee et al., 2012). Second, the green channel turns out to be impossible to quantify because green mEos2 switches massively between bright and dark states. Hence, the green signal of mEos2 is more dependant on the photostimulation history of the experiment than reflecting faithfully the number of molecules present at a given location.

But illuminating the samples with UV light in a longer timescale, from 5-10 seconds to 2 min, could convert most, up to all of the mEos2 to the activated form with red fluorescence (McKinney et al., 2009; Baker et al., 2010; Lee et al., 2012).

mEos2 induced the knock down of VGLUT1

In the VGLUT1^{mEos2} KI mouse line, mEos2 is fused to the C-terminal of VGLUT1 with the exact same strategy as for VGLUT1^{venus}. The VGLUT1^{mEos2} distribution pattern is the

same as wildtype (WT) VGLUT1 and VGLUT1^{Venus} (Herzog et al., 2011), but the expression level of mEos2 tagged VGLUT1 is severely reduced in the VGLUT1^{mEos2} mice. We think that the knock down effect is more likely caused by a reduced protein synthesis. Indeed, when checking VGLUT1^{mEos2} levels in hippocampal neuron cultures and at different post-natal developmental stages, we could see that VGLUT1^{mEos2} expression is constantly lowered to 20-25% of WT VGLUT1 levels. As VGLUT1 synthesis is very strong during post-natal synaptogenesis and SV protein turn-over is estimated to occur over 5 days or more (Cohen et al., 2013), the constant ratio between VGLUT1^{mEos2} and WT favors the hypothesis of a reduced synthesis rate of VGLUT1^{mEos2}. Coincidentally, by tagging PSD-95 with mEos2, the PSD-95^{mEos2} KI mouse line also shows the knock down effect of PSD-95 (Broadhead et al., 2016).

In contrast, VGLUT1 and Munc18-1 tagged with venus were unaffected (Herzog et al., 2011; Cijsouw et al., 2014; Rothman et al., 2016). Although both mEos2 and venus tags were improved for mammalian expression, venus is a 4th generation optimized GFP for fast synthesis, fast folding and low toxicity, while mEos2 is a 1st generation variant of EosFP optimized for reduced acid sensitivity, photostability (Nagai et al., 2002; Miyawaki, 2005; McKinney et al., 2009). As both tags have a similar size, differences in codon usage or RNA stability may explain the knock down effect observed recurrently. Investigation, on VGLUT1 mRNA levels across genotypes and ages will eventually help understanding the VGLUT1^{mEos2} knock down phenotype.

Impact of VGLUT1 expression level on neurotransmission

Although VGLUT1^{mEos2} KI mouse line is not perfect as expected, it is still a good tool for us to answer some specific questions.

VGLUT1 can translocate glutamate into the luminal side of SVs based on the proton electrochemical gradient ($\Delta\mu H^+$), built up by V-ATPase across the vesicle membrane (Maycox et al., 1988; Edwards, 2007). The copy number of VGLUT1 on SVs may influence the quantal size of glutamate release. Overexpression of VGLUT1/DVGLUT results in larger quantal content of glutamate (Daniels et al., 2004; Wojcik et al., 2004; Wilson et al., 2005). However, *Drosophila* DVGLUT knock down mutants, were used to show that one unit of VGLUT transport system may be enough to fill the vesicles and result in normal quantal sizes but decreased mEPSC frequency (Daniels et al., 2006). On average, 4 to 15 copies of VGLUT1 were estimated per SV (Takamori et al., 2006; Mutch

et al., 2011). Possibly, at rest, one copy of VGLUT1 might be sufficient to fill SVs completely, but this would not stand in case of demanding stimulations. Additionaly, it is reported that VGLUT1 is involved in the regulation of SV exocytosis or endocytosis (Voglmaier et al., 2006; Weston et al., 2011).

It is thus necessary to clarify the relationship between VGLUT1 expression and neurotransmission. VGLUT1 is mainly expressed in forebrain and cerebellum cortex and hippocampus (Fremeau et al., 2001; Herzog et al., 2001; Varoqui et al., 2002; Boulland et al., 2004). Unlike the VGLUT1 knock out (KO) pups that die at around three weeks after birth (Fremeau et al., 2004; Wojcik et al., 2004), the *VGLUT1*$^{Eo/Eo}$ mice, with less than a quarter expression of VGLUT1, don't show significant difficulties during breeding and weaning compared to the *VGLUT*$^{Eo/+}$ or *VGLUT*$^{+/+}$ littermates. This indicates that 20% of the VGLUT1 expression is already enough to maintain the normal activity of mice. It is reported that the neurotransmission seems normal with half VGLUT1 expression (Wojcik et al., 2004). Our current investigations suggest that, in the VGLUT1$^{Eo/Eo}$ mice, evoked EPSCs are reduced but not abolished at cortico-lateral amygdala (LA) synapses (typically VGLUT1 expressing; not shown ongoing experiments). Thus, our data confirm that VGLUT1^{mEos2} is a functional transporter, but VGLUT1 knock down results in reduced excitatory synapse function. Further work will explore miniature events to contribute to the characterization of quantal size plasticity. In ultrastructure, *VGLUT1*$^{-/-}$ mice show less synaptic vesicles (SVs) rest in the presynaptic boutons (Fremeau et al., 2004; Siksou et al., 2013). Meanwhile, in the *VGLUT1*$^{+/-}$ mice, SVs in the reserve pool (distance from the active zone >100 µm) are less than the WT mice (Tordera et al., 2007). Thus the investigation of the ultrastructure of SVs and correlated neurotransmission in *VGLUT1*$^{Eo/Eo}$ mice, which have 25% of VGLUT1, may provide more clues to understand the correlation between SVs distribution and neurotransmission.

VGLUT1 and the synaptic vesicle super-pool

VGLUT is short for Vesicular GLUtamate Transporter, which is related to the main function of this protein in loading glutamate into SVs. However, some other properties of the protein might be obscured by its name.

VGLUT1 and synaptic vesicles mobility

For decades, SVs were considered to be confined in the individual boutons and were categorized into three distinct pools based on the different capacities for exocytosis. However, in the past decade, more and more evidences show that SVs are dynamically exchanged between release sites, in a SV super-pool (Darcy et al., 2006; Staras et al., 2010; Herzog et al., 2011; Siksou et al., 2013). Moreover, SVs labeled with FM dye, followed the FRAP (fluorescence recovery after photobleaching) and correlative transmission EM experiments show that recycled SVs could enter into the boutons along the same axon and highly intermix with local SVs (Darcy et al., 2006; Staras et al., 2010).

The previous study from our lab shows that there are more SVs trafficking along the axons when VGLUT1 is absent (Siksou et al., 2013), thus, SV super-pool is oversized. The fluorescence recovery after photobleaching (FRAP) applied to whole presynaptic boutons monitors SV exchange between clustered pools and the super-pool. To test the possibility of a VGLUT1 influence over SV super-pool, we performed FRAP experiments with different VGLUT1 expression levels. Consistent with the previous time lapse study with *VGLUT1*$^{-/-}$ culture (Siksou et al., 2013), when VGLUT1 is absent, presynapses display a higher SVs exchange rate between the presynaptic boutons and the super-pool. In contrast, overexpression of VGLUT1 reduced the SVs exchange rates. Thus it suggests that the super-pool size is regulated by VGLUT1 in a dose dependent manner (Fig. 8). VGLUT1 expression tends to cluster SVs in the presynaptic boutons and reduced the mobility of SVs towards the super-pool.

It should be noted that, VGLUT1 function also impacts SV biophysical stiffness by changing the organelle tonicity (Siksou et al., 2013). Thus SVs mobility regulation may depend on both SV tonicity and/or VGLUT1 interaction with other synaptic proteins. The silent VGLUT1 mutant I generated allowed to dissociate these 2 features (Juge et al., 2006; Almqvist et al., 2007; Herman et al., 2014). By rescuing the VGLUT expression but not glutamate loading, I showed that the structure of VGLUT1 is sufficient to mediate the down regulation of SV super-pool size. In the mean time, glutamate loading doesn't interfere with SV mobility parameters in our hands. More importantly, I could bring a strong evidence that VGLUT1 bears 2 independent mechanisms prone to influence glutamate release. While variation in the stoichiometry of VGLUT1 on each SV, is possibly altering quantal size (Daniels et al., 2004; Wojcik et al., 2004; Wilson et al., 2005; Daniels et al., 2006), it will also alter SVs distribution and possibly dynamics.

Hence, single VGLUT1 tracking within synaptic boutons is our next goal, using the VGLUT1^{mEos2} mouse line I generated. Taking advantage of the knock down of VGLUT1 expression in this mouse line we will play with VGLUT1 levels and monitor SV dynamics using PALM.

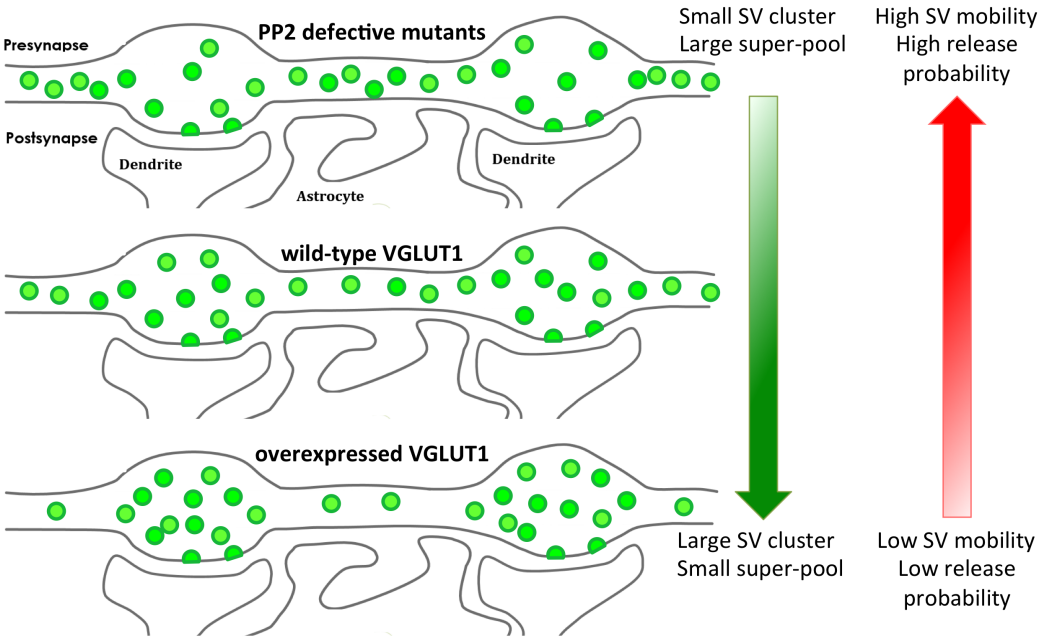

Fig 8. VGLUT1 and SV mobility. VGLUT1 tends to cluster SVs in the presynaptic boutons through the interaction with endophilin A1 at PP2 domain. The PP2 defective mutants result in smaller SV clusters at presynaptic terminals and larger super-pool. In contrast, overexpression of VGLUT1 leads to lager SV clusters and a smaller super-pool. According to the literature (Weston, 2011), crowded cluster conditions correlate with low SV release probability, while low cluster density conditions correlates with high release probability.

VGLUT1 and SVs cycle

To explore how VGLUT1 regulates SVs mobility, we followed our structure-function analysis and focused on the C-terminal. By screening the amino acid sequence of the 3 VGLUTs, it is obvious that the three isoforms are highly homologous at the membrane spanning segments, but quite divergent in the N- and C-termini. These sequence differences may contribute to the diverse distribution patterns and properties of the three isoforms (Takamori, 2006). In the C-terminus, VGLUT1 shares a dileucine-like internalization motif, a type 3 PDZ binding domain, and a highly conserved SYGAT motif with the other two VGLUTs. As a specific feature, mammalian VGLUT1 contains two polyproline domains (PP1 and PP2). The two PP domains contain the consensus for Src homology (SH3) protein interaction domains (PXXP). It has been shown that VGLUT1

can interact with endophilinA1 through PP2 (De Gois et al., 2006; Vinatier et al., 2006; Voglmaier et al., 2006). According to our FRAP results, only the PP2 deletions and the P554A mutants failed to rescue the abnormal SVs exchange rate between the presynaptic boutons and the super-pool in the *VGLUT1*$^{-/-}$ culture. Moreover, the P554A mutant increased the amount but not the speed of trafficking material compared to the WT VGLUT1. The results imply that the PP2 is essential for VGLUT1 to control the SV exchange with the axonal traffic without interference with the cytosqueletal molecular motor machinery (Fig. 8). Thus, the oversized SV super-pool of *vglut1*$^{-/-}$ may result from the altered SV clustering or SV recycling in the presynaptic bouton.

It has been shown that VGLUT1 can recruit endophilinA1 (De Gois et al., 2006; Vinatier et al., 2006; Voglmaier et al., 2006). In turn, recent data show that endophilinA1 can directly bind with the SH3B domain of intersectin to form a complex, which could facilitate vesicle uncoating (Pechstein et al., 2015). Importantly, the SH3-SH3 interaction of endophilinA1 and intersectin is not preventing the PP2 endophilinA1 interaction (Pechstein et al., 2015). Additionally, intersectin is a scaffolding protein and it can interact with synapsin to re-cluster SVs after the stimulation in the *Drosophila* neuromuscular junction (NMJ) (Winther et al., 2015). As a RhoGEF, Intersectin can also influence actin cytoskeleton polymerization (Humphries et al., 2014). The stabilization of actin would strand the recycled SVs at the rear boundary of the cluster after the stimulation (Rey et al., 2015). In this scenario, disrupting the interaction between VGLUT1 and endophilin A1 may alter the tendency of SVs to join the cluster following endocytosis (Fig. 9). Other more complex scenarios are possible and likely, but we believe that investigating on the relationship between VGLUT1 and intersectin is a priority.

Whether other binding partners of the two PP domains may take part to this process is still unknown yet. An *in vitro* study screened a series of SH3 domain-containing proteins, including multiple Src family tyrosine kinases and scaffolding/adaptor proteins, and showed several potential binding partners (e.g. Nck1, Nck2, ArgBP2, sorting nexin 9) (Santos et al., 2009).

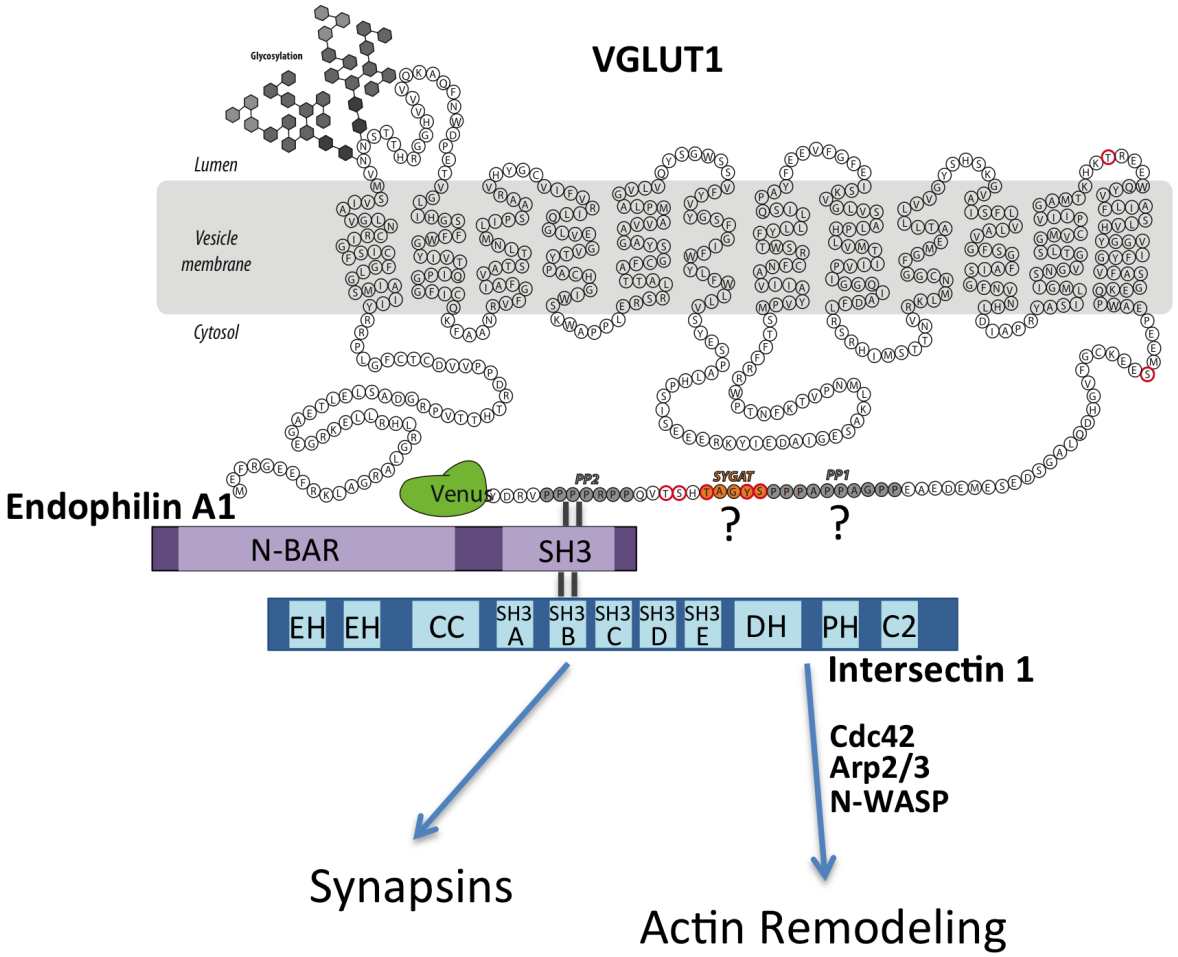

Fig 9. Proposed molecular mechanism of PP2 domain action on SV super-pool size. VGLUT1 interacts endophilin A1 at PP2 domain. Meanwhile, a SH3-SH3 interaction, endophilin A1 and intersectin 1, which can facilitate vesicles uncoating was shown. Additionaly endophilin A1 may interact both with PP domains and Intersectin 1 simultaneously (Pechstein 2015). Intersectin may interact with synapsins and/or participate in actin remodeling. Thus, disrupting the interaction between VGLUT1 and endophilin A1, may prevent SVs to eficiently join clusters.

In addition, it is proposed that VGLUT1 synapses exhibit low release probability, meanwhile, VGLUT2 synapses show high release probability (Fremeau et al., 2001; Varoqui et al., 2002). Some evidences show that endophilinA1 favors high release probability based through its membrane binding and dimerization domains. The binding of VGLUT1 to endophilinA1 could reduce the pool of membrane bound endophilin and lower SV release probability (Weston et al., 2011). However, the consequence of the interaction between endophilin SH3 domain and other presynaptic proteins, such as dynamins and synaptojanin, are not considered in this model. A recent study using VGLUT1^{venus} mice show that, in the mossy fiber terminals, SVs are highly mobile and that

access to the active zone through rapid diffusion may be a limiting step to glutamate release during sustained high-frequency stimulation. Parameters important for this mobility are related to the density of SVs (Rothman et al., 2016). Hence, we propose that VGLUT1 may shift SV dynamics in SV clusters by changing the local density of SVs and/or the interaction with cytoskeletal scaffolds (Fig. 8).

VGLUT1 and phosphorylation

The 540-SYGAT motif of VGLUT1 is highly conserved in most species (Vinatier et al., 2006), our in silico investigations suggested a putative phosphorylation at S540 by GSK-3. Other vesicular neurotransmitter transporters (VNT), such as the vesicular acetylcholine transporter (VAChT), the vesicular inhibitory amino acid transporter (VIAAT), have also been shown to be phosphorylated (Bedet et al., 2000; Krantz et al., 2000). Upon phosphorylation in the C-terminal, VAChT may selectively target large dense core vesicles (LDCVs), while dephosphorylation would favor its location at synaptic vesicles (Krantz et al., 2000). Accordingly, we hypothesized that the phosphorylation of S540 might influence the molecular interaction at both PP domains and possibly impact SVs mobility.

Using classical biochemical approaches like SDS-PAGE and western blotting, together with the novel phosphate-affinity SDS-PAGE technique, we were able to bring evidence in favor of the phosphorylation of VGLUT1 but not at the C-terminal tail. Even though, SYGAT may still be an important motif for VGLUT1 and it probably participates in other aspects, more efforts will be required to unveil the function of this conserved motif that was preserved through the evolutionary selection of both surrounding PP motifs. The chance of having a complex regulation of VGLUT1 PP2 function is still a tempting idea as it would open the possibility to actively finetune SV cluster/super-pool size through VGLUT1.

The exploration of super-pool

In the super-pool, SVs move in both anterograde and retrograde directions and the movement is severely impaired by actin inhibitor treatment (Darcy et al., 2006). Moreover, super-pool SVs labeled with FM dye were shown to enter into target boutons, be the release competent and intermix with local SVs (Darcy et al., 2006; Staras et al.,

2010). However, the precise contribution of the super-pool to neurotransmission and network activity is still barely understood.

The constitutive trafficking and sharing of SVs in the super-pool results in the dynamic scaling of SV content at presynaptic boutons over time. More broadly, the size of synapses was shown to keep remodeling over time even at the rest or under inhibition of activity (Fisher-Lavie et al., 2011; Herzog et al., 2011). Under the stimulation, SVs are temporary dispersed into axons (Fisher-Lavie et al., 2011), and a decreased in SVs motion is observed by inhibiting the synaptic activity (Kamin et al., 2010). It is now considered that super-pool works as an extra source for SVs recruit that can support dynamic changes (Fowler and Staras, 2015).

Whether the super-pool and the SV exchange rate indeed have impacts on the network activity or even the behavior is still far from being understood. Via *in vivo* imaging approaches using the VGLUT1^{mEos2}, VGLUT1^{venus}, and other tools developped during my thesis we shall build paradigms in which we will test and challenge the contribution of SV super-pool to behavior relevant neuronal activity.

Almqvist J, Huang Y, Laaksonen A, Wang D-N, Hovmöller S (2007) Docking and homology modeling explain inhibition of the human vesicular glutamate transporters. Protein Sci 16:1819–1829.

Amilhon B, Lepicard E, Renoir T, Mongeau R, Popa D, Poirel O, Miot S, Gras C, Gardier AM, Gallego J, Hamon M, Lanfumey L, Gasnier B, Giros B, Mestikawy El S (2010) VGLUT3 (vesicular glutamate transporter type 3) contribution to the regulation of serotonergic transmission and anxiety. J Neurosci 30:2198–2210.

Amilhon B, Mestikawy El S (2008) [VGLUT3, an unsuspected agent of striatal cholinergic transmission]. Med Sci (Paris) 24:1009–1011.

Anne C, Gasnier B (2014) Vesicular neurotransmitter transporters: mechanistic aspects. Curr Top Membr 73:149–174.

Aschenbrenner L, Lee T, Hasson T (2003) Myo6 facilitates the translocation of endocytic vesicles from cell peripheries. Mol Biol Cell 14:2728–2743.

Augustin I, Rosenmund C, Südhof TC, Brose N (1999) Munc13-1 is essential for fusion competence of glutamatergic synaptic vesicles. Nature 400:457–461.

Auld DS, Robitaille R (2003) Glial cells and neurotransmission: an inclusive view of synaptic function. Neuron 40:389–400.

Axelrod D, Koppel DE, Schlessinger J, Elson E, Webb WW (1976) Mobility measurement by analysis of fluorescence photobleaching recovery kinetics. Biophys J 16:1055–1069.

Baas PW, Deitch JS, Black MM, Banker GA (1988) Polarity orientation of microtubules in hippocampal neurons: uniformity in the axon and nonuniformity in the dendrite. Proc Natl Acad Sci USA 85:8335–8339.

Bai J, Hu Z, Dittman JS, Pym ECG, Kaplan JM (2010) Endophilin functions as a membrane-bending molecule and is delivered to endocytic zones by exocytosis. Cell 143:430–441.

Baker SM, Buckheit RW, Falk MM (2010) Green-to-red photoconvertible fluorescent proteins: tracking cell and protein dynamics on standard wide-field mercury arc-based microscopes. BMC Cell Biol 11:15.

Balschun D, Moechars D, Callaerts-Vegh Z, Vermaercke B, Van Acker N, Andries L, D'Hooge R (2010) Vesicular glutamate transporter VGLUT1 has a role in hippocampal long-term potentiation and spatial reversal learning. Cereb Cortex 20:684–693.

Bedet C, Isambert MF, Henry JP, Gasnier B (2000) Constitutive phosphorylation of the vesicular inhibitory amino acid transporter in rat central nervous system. Journal of Neurochemistry 75:1654–1663.

Bellocchio EE, Hu H, Pohorille A, Chan J, Pickel VM, Edwards RH (1998) The localization

of the brain-specific inorganic phosphate transporter suggests a specific presynaptic role in glutamatergic transmission. J Neurosci 18:8648–8659.

Bellocchio EE, Reimer RJ, Fremeau RT, Edwards RH (2000) Uptake of glutamate into synaptic vesicles by an inorganic phosphate transporter. Science 289:957–960.

Berardozzi R, Adam V, Martins A, Bourgeois D (2016) Arginine 66 Controls Dark-State Formation in Green-to-Red Photoconvertible Fluorescent Proteins. J Am Chem Soc 138:558–565.

Boulland J-L, Qureshi T, Seal RP, Rafiki A, Gundersen V, Bergersen LH, Fremeau RT, Edwards RH, Storm-Mathisen J, Chaudhry FA (2004) Expression of the vesicular glutamate transporters during development indicates the widespread corelease of multiple neurotransmitters. J Comp Neurol 480:264–280.

Brady ST (1991) Molecular motors in the nervous system. Neuron 7:521–533.

Bridgman PC (1999) Myosin Va movements in normal and dilute-lethal axons provide support for a dual filament motor complex. J Cell Biol 146:1045–1060.

Broadhead MJ, Horrocks MH, Zhu F, Muresan L, Benavides-Piccione R, DeFelipe J, Fricker D, Kopanitsa MV, Duncan RR, Klenerman D, Komiyama NH, Lee SF, Grant SGN (2016) PSD95 nanoclusters are postsynaptic building blocks in hippocampus circuits. Sci Rep 6:24626.

Brodsky FM, Chen CY, Knuehl C, Towler MC, Wakeham DE (2001) Biological basket weaving: formation and function of clathrin-coated vesicles. Annu Rev Cell Dev Biol 17:517–568.

Brose N (2009) Synaptogenic proteins and synaptic organizers: "many hands make light work". Neuron 61:650–652.

Brose N, Hofmann K, Hata Y, Südhof TC (1995) Mammalian homologues of Caenorhabditis elegans unc-13 gene define novel family of C2-domain proteins. J Biol Chem 270:25273–25280.

Brose N, Petrenko AG, Südhof TC, Jahn R (1992) Synaptotagmin: a calcium sensor on the synaptic vesicle surface. Science 256:1021–1025.

Bruckner JJ, Zhan H, O'Connor-Giles KM (2015) Advances in imaging ultrastructure yield new insights into presynaptic biology. Front Cell Neurosci 9:196.

Burré J, Sharma M, Tsetsenis T, Buchman V, Etherton MR, Südhof TC (2010) Alpha-synuclein promotes SNARE-complex assembly in vivo and in vitro. Science 329:1663–1667.

Cai Q, Pan P-Y, Sheng Z-H (2007) Syntabulin-kinesin-1 family member 5B-mediated axonal transport contributes to activity-dependent presynaptic assembly. J Neurosci 27:7284–7296.

Ceccarelli B, Hurlbut WP, Mauro A (1973) Turnover of transmitter and synaptic vesicles

at the frog neuromuscular junction. J Cell Biol 57:499–524.

Cijsouw T, Weber JP, Broeke JH, Broek JAC, Schut D, Kroon T, Saarloos I, Verhage M, Toonen RF (2014) Munc18-1 redistributes in nerve terminals in an activity- and PKC-dependent manner. J Cell Biol 204:759–775.

Cohen LD, Zuchman R, Sorokina O, Müller A, Dieterich DC, Armstrong JD, Ziv T, Ziv NE (2013) Metabolic turnover of synaptic proteins: kinetics, interdependencies and implications for synaptic maintenance. PLoS ONE 8:e63191.

Colonnier M (1968) Synaptic patterns on different cell types in the different laminae of the cat visual cortex. An electron microscope study. Brain Res 9:268–287.

Dal Bo G, Bérubé-Carrière N, Mendez JA, Leo D, Riad M, Descarries L, Levesque D, Trudeau LE (2008) Enhanced glutamatergic phenotype of mesencephalic dopamine neurons after neonatal 6-hydroxydopamine lesion. NSC 156:59–70.

Daniels RW, Collins CA, Chen K, Gelfand MV, Featherstone DE, DiAntonio A (2006) A single vesicular glutamate transporter is sufficient to fill a synaptic vesicle. Neuron 49:11–16.

Daniels RW, Collins CA, Gelfand MV, Dant J, Brooks ES, Krantz DE, DiAntonio A (2004) Increased expression of the Drosophila vesicular glutamate transporter leads to excess glutamate release and a compensatory decrease in quantal content. J Neurosci 24:10466–10474.

Darcy KJ, Staras K, Collinson LM, Goda Y (2006) Constitutive sharing of recycling synaptic vesicles between presynaptic boutons. Nat Neurosci 9:315–321.

De Belleroche JS, Bradford HF (1977) On the site of origin of transmitter amino acids released by depolarization of nerve terminals in vitro. Journal of Neurochemistry 29:335–343.

De Gois S, Jeanclos E, Morris M, Grewal S, Varoqui H, Erickson JD (2006) Identification of endophilins 1 and 3 as selective binding partners for VGLUT1 and their co-localization in neocortical glutamatergic synapses: implications for vesicular glutamate transporter trafficking and excitatory vesicle formation. Cell Mol Neurobiol 26:679–693.

Dehmelt L, Halpain S (2004) Actin and microtubules in neurite initiation: are MAPs the missing link? J Neurobiol 58:18–33.

Deng L, Kaeser PS, Xu W, Südhof TC (2011) RIM proteins activate vesicle priming by reversing autoinhibitory homodimerization of Munc13. Neuron 69:317–331.

Denker A, Rizzoli SO (2010) Synaptic vesicle pools: an update. Front Syna Neurosci 2:135.

Di Paolo G, Sankaranarayanan S, Wenk MR, Daniell L, Perucco E, Caldarone BJ, Flavell R, Picciotto MR, Ryan TA, Cremona O, De Camilli P (2002) Decreased synaptic vesicle recycling efficiency and cognitive deficits in amphiphysin 1 knockout mice. Neuron

33:789–804.

Dickson RM, Cubitt AB, Tsien RY, Moerner WE (1997) On/off blinking and switching behaviour of single molecules of green fluorescent protein. Nature 388:355–358.

Dotti CG, Banker GA (1987) Experimentally induced alteration in the polarity of developing neurons. Nature 330:254–256.

Dulubova I, Khvotchev M, Liu S, Huryeva I, Südhof TC, Rizo J (2007) Munc18-1 binds directly to the neuronal SNARE complex. Proc Natl Acad Sci USA 104:2697–2702.

Edwards RH (2007) The neurotransmitter cycle and quantal size. Neuron 55:835–858.

EIDEN LE, Schäfer MK-H, Weihe E, Schütz B (2004) The vesicular amine transporter family (SLC18): amine/proton antiporters required for vesicular accumulation and regulated exocytotic secretion of monoamines and acetylcholine. Pflugers Arch 447:636–640.

Eriksen J, Chang R, McGregor M, Silm K, Suzuki T, Edwards RH (2016) Protons Regulate Vesicular Glutamate Transporters through an Allosteric Mechanism-supplementary. Neuron 90:768–780 Available at: http://eutils.ncbi.nlm.nih.gov/entrez/eutils/elink.fcgi?dbfrom=pubmed&id=27133463&retmode=ref&cmd=prlinks.

Ettinger A, Wittmann T (2014) Fluorescence live cell imaging. Methods Cell Biol 123:77–94.

Farsi Z, Preobraschenski J, van den Bogaart G, Riedel D, Jahn R, Woehler A (2016) Single-vesicle imaging reveals different transport mechanisms between glutamatergic and GABAergic vesicles. Science 351:981–984.

Fattorini G, Antonucci F, Menna E, Matteoli M, Conti F (2015) Co-expression of VGLUT1 and VGAT sustains glutamate and GABA co-release and is regulated by activity in cortical neurons. J Cell Sci 128:1669–1673.

Fisher-Lavie A, Zeidan A, Stern M, Garner CC, Ziv NE (2011) Use dependence of presynaptic tenacity. J Neurosci 31:16770–16780.

Forgac M (1999) Structure and properties of the vacuolar (H+)-ATPases. J Biol Chem 274:12951–12954.

Foss SM, Li H, Santos MS, Edwards RH, Voglmaier SM (2013) Multiple dileucine-like motifs direct VGLUT1 trafficking. J Neurosci 33:10647–10660.

Fowler MW, Staras K (2015) Synaptic vesicle pools: Principles, properties and limitations. Experimental Cell Research 335:150–156.

Fremeau RT, Kam K, Qureshi T, Johnson J, Copenhagen DR, Storm-Mathisen J, Chaudhry FA, Nicoll RA, Edwards RH (2004) Vesicular glutamate transporters 1 and 2 target to functionally distinct synaptic release sites. Science 304:1815–1819.

Fremeau RT, Troyer MD, Pahner I, Nygaard GO, Tran CH, Reimer RJ, Bellocchio EE, Fortin D, Storm-Mathisen J, Edwards RH (2001) The expression of vesicular glutamate transporters defines two classes of excitatory synapse. Neuron 31:247–260.

Ganguly A, Tang Y, Wang L, Ladt K, Loi J, Dargent B, Leterrier C, Roy S (2015) A dynamic formin-dependent deep F-actin network in axons. J Cell Biol 210:401–417.

Garcia-Garcia AL, Elizalde N, Matrov D, Harro J, Wojcik SM, Venzala E, Ramírez MJ, Del Rio J, Tordera RM (2009) Increased vulnerability to depressive-like behavior of mice with decreased expression of VGLUT1. Biol Psychiatry 66:275–282.

Gasnier B (2004) The SLC32 transporter, a key protein for the synaptic release of inhibitory amino acids. Pflugers Arch 447:756–759.

Gauthier-Kemper A, Kahms M, Klingauf J (2015) Restoring synaptic vesicles during compensatory endocytosis. Essays Biochem 57:121–134.

Gillespie DC, Kim G, Kandler K (2005) Inhibitory synapses in the developing auditory system are glutamatergic. Nat Neurosci 8:332–338.

Glyvuk N, Tsytsyura Y, Geumann C, D'Hooge R, Hüve J, Kratzke M, Baltes J, Boening D, Böning D, Klingauf J, Schu P (2010) AP-1/sigma1B-adaptin mediates endosomal synaptic vesicle recycling, learning and memory. EMBO J 29:1318–1330.

Goh GY, Huang H, Ullman J, Borre L, Hnasko TS, Trussell LO, Edwards RH (2011) Presynaptic regulation of quantal size: K+/H+ exchange stimulates vesicular glutamate transport. Nat Neurosci 14:1285–1292.

Goldstein AYN, Wang X, Schwarz TL (2008) Axonal transport and the delivery of pre-synaptic components. Current Opinion in Neurobiology 18:495–503.

Gracheva EO, Hadwiger G, Nonet ML, Richmond JE (2008) Direct interactions between C. elegans RAB-3 and Rim provide a mechanism to target vesicles to the presynaptic density. Neurosci Lett 444:137–142.

Granger AJ, Mulder N, Saunders A, Sabatini BL (2016) Cotransmission of acetylcholine and GABA. Neuropharmacology 100:40–46.

Granseth B, Andersson FK, Lindström SH (2015) The initial stage of reversal learning is impaired in mice hemizygous for the vesicular glutamate transporter (VGluT1). Genes Brain Behav 14:477–485.

Gras C, Amilhon B, Lepicard ÈM, Poirel O, Vinatier J, Herbin M, Dumas S, Tzavara ET, Wade MR, Nomikos GG, Hanoun N, Saurini F, Kemel M-L, Gasnier B, Giros B, Mestikawy El S (2008) The vesicular glutamate transporter VGLUT3 synergizes striatal acetylcholine tone. Nat Neurosci 11:292–300.

Gras C, Herzog E, Bellenchi GC, Bernard V, Ravassard P, Pohl M, Gasnier B, Giros B, Mestikawy El S (2002) A third vesicular glutamate transporter expressed by cholinergic and serotoninergic neurons. J Neurosci 22:5442–5451.

Gras C, Vinatier J, Amilhon B, Guerci A, Christov C, Ravassard P, Giros B, Mestikawy El S (2005) Developmentally regulated expression of VGLUT3 during early post-natal life. Neuropharmacology 49:901–911.

GRAY EG (1959) Electron microscopy of synaptic contacts on dendrite spines of the cerebral cortex. Nature 183:1592–1593.

Harris KM, Weinberg RJ (2012) Ultrastructure of synapses in the mammalian brain. Cold Spring Harb Perspect Biol 4.

Hartinger J, Jahn R (1993) An anion binding site that regulates the glutamate transporter of synaptic vesicles. J Biol Chem 268:23122–23127.

Hata Y, Slaughter CA, Südhof TC (1993) Synaptic vesicle fusion complex contains unc-18 homologue bound to syntaxin. Nature 366:347–351.

Hatten ME (1999) Central nervous system neuronal migration. Annu Rev Neurosci 22:511–539.

Haucke V, Neher E, Sigrist SJ (2011) Protein scaffolds in the coupling of synaptic exocytosis and endocytosis. Nat Rev Neurosci 12:127–138.

Heise C, Schroeder JC, Schoen M, Halbedl S, Reim D, Woelfle S, Kreutz MR, Schmeisser MJ, Boeckers TM (2016) Selective Localization of Shanks to VGLUT1-Positive Excitatory Synapses in the Mouse Hippocampus. Front Cell Neurosci 10:106.

Herculano-Houzel S (2009) The human brain in numbers: a linearly scaled-up primate brain. Front Hum Neurosci 3:31.

Herman MA, Ackermann F, Trimbuch T, Rosenmund C (2014) Vesicular glutamate transporter expression level affects synaptic vesicle release probability at hippocampal synapses in culture. J Neurosci 34:11781–11791.

Herzog E, Bellenchi GC, Gras C, Bernard V, Ravassard P, Bedet C, Gasnier B, Giros B, Mestikawy El S (2001) The existence of a second vesicular glutamate transporter specifies subpopulations of glutamatergic neurons. J Neurosci 21:RC181.

Herzog E, Gilchrist J, Gras C, Muzerelle A, Ravassard P, Giros B, Gaspar P, Mestikawy El S (2004a) Localization of VGLUT3, the vesicular glutamate transporter type 3, in the rat brain. NSC 123:983–1002.

Herzog E, Landry M, Buhler E, Bouali-Benazzouz R, Legay C, Henderson CE, Nagy F, Dreyfus P, Giros B, Mestikawy El S (2004b) Expression of vesicular glutamate transporters, VGLUT1 and VGLUT2, in cholinergic spinal motoneurons. Eur J Neurosci 20:1752–1760.

Herzog E, Nadrigny F, Silm K, Biesemann C, Helling I, Bersot T, Steffens H, Schwartzmann R, Nägerl UV, Mestikawy El S, Rhee J, Kirchhoff F, Brose N (2011) In vivo imaging of intersynaptic vesicle exchange using VGLUT1 Venus knock-in mice. J Neurosci 31:15544–15559.

Heuser JE, Reese TS (1973) Evidence for recycling of synaptic vesicle membrane during transmitter release at the frog neuromuscular junction. J Cell Biol 57:315–344.

Heuser JE, Reese TS, Landis DM (1974) Functional changes in frog neuromuscular junctions studied with freeze-fracture. J Neurocytol 3:109–131.

Hirokawa N, Niwa S, Tanaka Y (2010) Molecular motors in neurons: transport mechanisms and roles in brain function, development, and disease. Neuron 68:610–638.

Hnasko TS, Hjelmstad GO, Fields HL, Edwards RH (2012) Ventral tegmental area glutamate neurons: electrophysiological properties and projections. J Neurosci 32:15076–15085.

Humphries AC, Donnelly SK, Way M (2014) Cdc42 and the Rho GEF intersectin-1 collaborate with Nck to promote N-WASP-dependent actin polymerisation. J Cell Sci 127:673–685.

Imig C, Min S-W, Krinner S, Arancillo M, Rosenmund C, Südhof TC, Rhee J, Brose N, Cooper BH (2014) The morphological and molecular nature of synaptic vesicle priming at presynaptic active zones. Neuron 84:416–431.

Inta D, Vogt MA, Perreau-Lenz S, Schneider M, Pfeiffer N, Wojcik SM, Spanagel R, Gass P (2012) Sensorimotor gating, working and social memory deficits in mice with reduced expression of the vesicular glutamate transporter VGLUT1. Behav Brain Res 228:328–332.

Jahn R, Fasshauer D (2012) Molecular machines governing exocytosis of synaptic vesicles. Nature 490:201–207.

Jinek M, Chylinski K, Fonfara I, Hauer M, Doudna JA, Charpentier E (2012) A programmable dual-RNA-guided DNA endonuclease in adaptive bacterial immunity. Science 337:816–821.

Juge N, Yoshida Y, Yatsushiro S, Omote H, Moriyama Y (2006) Vesicular glutamate transporter contains two independent transport machineries. J Biol Chem 281:39499–39506.

Kaeser PS, Deng L, Wang Y, Dulubova I, Liu X, Rizo J, Südhof TC (2011) RIM proteins tether Ca2+ channels to presynaptic active zones via a direct PDZ-domain interaction. Cell 144:282–295.

Kamin D, Lauterbach MA, Westphal V, Keller J, Schönle A, Hell SW, Rizzoli SO (2010) High- and low-mobility stages in the synaptic vesicle cycle. Biophys J 99:675–684.

Kanchanawong P, Shtengel G, Pasapera AM, Ramko EB, Davidson MW, Hess HF, Waterman CM (2010) Nanoscale architecture of integrin-based cell adhesions. Nature 468:580–584.

Kaneko T, Fujiyama F (2002) Complementary distribution of vesicular glutamate transporters in the central nervous system. Neurosci Res 42:243–250.

Kapitein LC, Hoogenraad CC (2011) Which way to go? Cytoskeletal organization and polarized transport in neurons. Mol Cell Neurosci 46:9–20.

Karra D, Dahm R (2010) Transfection techniques for neuronal cells. J Neurosci 30:6171–6177.

Katz B (1971) Quantal mechanism of neural transmitter release. Science 173:123–126.

Kawano M, Kawasaki A, Sakata-Haga H, Fukui Y, Kawano H, Nogami H, Hisano S (2006) Particular subpopulations of midbrain and hypothalamic dopamine neurons express vesicular glutamate transporter 2 in the rat brain. J Comp Neurol 498:581–592.

Kevenaar JT, Hoogenraad CC (2015) The axonal cytoskeleton: from organization to function. Front Mol Neurosci 8:44.

Klopfenstein DR, Vale RD (2004) The lipid binding pleckstrin homology domain in UNC-104 kinesin is necessary for synaptic vesicle transport in Caenorhabditis elegans. Mol Biol Cell 15:3729–3739.

Kneussel M, Wagner W (2013) Myosin motors at neuronal synapses: drivers of membrane transport and actin dynamics. Nat Rev Neurosci 14:233–247.

Kononenko NL, Haucke V (2015) Molecular mechanisms of presynaptic membrane retrieval and synaptic vesicle reformation. Neuron 85:484–496.

Kononenko NL, Puchkov D, Classen GA, Walter AM, Pechstein A, Sawade L, Kaempf N, Trimbuch T, Lorenz D, Rosenmund C, Maritzen T, Haucke V (2014) Clathrin/AP-2 mediate synaptic vesicle reformation from endosome-like vacuoles but are not essential for membrane retrieval at central synapses. Neuron 82:981–988.

Koo SJ, Markovic S, Puchkov D, Mahrenholz CC, Beceren-Braun F, Maritzen T, Dernedde J, Volkmer R, Oschkinat H, Haucke V (2011) SNARE motif-mediated sorting of synaptobrevin by the endocytic adaptors clathrin assembly lymphoid myeloid leukemia (CALM) and AP180 at synapses. Proc Natl Acad Sci USA 108:13540–13545.

Korogod N, Petersen CCH, Knott GW (2015) Ultrastructural analysis of adult mouse neocortex comparing aldehyde perfusion with cryo fixation. Elife 4.

Krantz DE, Waites C, Oorschot V, Liu Y, Wilson RI, Tan PK, Klumperman J, Edwards RH (2000) A phosphorylation site regulates sorting of the vesicular acetylcholine transporter to dense core vesicles. J Cell Biol 149:379–396.

Landis DM, Hall AK, Weinstein LA, Reese TS (1988) The organization of cytoplasm at the presynaptic active zone of a central nervous system synapse. Neuron 1:201–209.

Lee S-H, Shin JY, Lee A, Bustamante C (2012) Counting single photoactivatable fluorescent molecules by photoactivated localization microscopy (PALM). Proc Natl Acad Sci USA 109:17436–17441.

Li C, Ullrich B, Zhang JZ, Anderson RG, Brose N, Südhof TC (1995) Ca(2+)-dependent and -independent activities of neural and non-neural synaptotagmins. Nature 375:594–

599.

Lippincott-Schwartz J, Patterson GH (2003) Development and use of fluorescent protein markers in living cells. Science 300:87–91.

Lippincott-Schwartz J, Patterson GH (2009) Photoactivatable fluorescent proteins for diffraction-limited and super-resolution imaging. Trends Cell Biol 19:555–565.

López-Muñoz F, Alamo C (2009) Historical evolution of the neurotransmission concept. J Neural Transm (Vienna) 116:515–533.

Lukinavičius G, Reymond L, D'Este E, Masharina A, Göttfert F, Ta H, Güther A, Fournier M, Rizzo S, Waldmann H, Blaukopf C, Sommer C, Gerlich DW, Arndt H-D, Hell SW, Johnsson K (2014) Fluorogenic probes for live-cell imaging of the cytoskeleton. Nat Meth 11:731–733.

Maday S, Twelvetrees AE, Moughamian AJ, Holzbaur ELF (2014) Axonal transport: cargo-specific mechanisms of motility and regulation. Neuron 84:292–309.

Maeder CI, Shen K, Hoogenraad CC (2014) Axon and dendritic trafficking. Current Opinion in Neurobiology 27:165–170.

Margiotta JF, Walcott B (1983) Conductance and dye permeability of a rectifying electrical synapse. Nature 305:52–55.

Maycox PR, Deckwerth T, Hell JW, Jahn R (1988) Glutamate uptake by brain synaptic vesicles. Energy dependence of transport and functional reconstitution in proteoliposomes. J Biol Chem 263:15423–15428.

McAnaney TB, Zeng W, Doe CFE, Bhanji N, Wakelin S, Pearson DS, Abbyad P, Shi X, Boxer SG, Bagshaw CR (2005) Protonation, photobleaching, and photoactivation of yellow fluorescent protein (YFP 10C): a unifying mechanism. Biochemistry 44:5510–5524.

McKinney SA, Murphy CS, Hazelwood KL, Davidson MW, Looger LL (2009) A bright and photostable photoconvertible fluorescent protein. Nat Meth 6:131–133.

Meinecke M, Boucrot E, Camdere G, Hon W-C, Mittal R, McMahon HT (2013) Cooperative recruitment of dynamin and BIN/amphiphysin/Rvs (BAR) domain-containing proteins leads to GTP-dependent membrane scission. J Biol Chem 288:6651–6661.

Merrifield CJ, Perrais D, Zenisek D (2005) Coupling between clathrin-coated-pit invagination, cortactin recruitment, and membrane scission observed in live cells. Cell 121:593–606.

Mestikawy El S, Wallén-Mackenzie Å, Fortin GM, Descarries L, Trudeau L-E (2011) From glutamate co-release to vesicular synergy: vesicular glutamate transporters. Nat Rev Neurosci 12:204–216.

Miller KE, DeProto J, Kaufmann N, Patel BN, Duckworth A, Van Vactor D (2005) Direct observation demonstrates that Liprin-alpha is required for trafficking of synaptic vesicles. Curr Biol 15:684–689.

Milosevic I, Giovedí S, Lou X, Raimondi A, Collesi C, Shen H, Paradise S, O'Toole E, Ferguson S, Cremona O, De Camilli P (2011) Recruitment of endophilin to clathrin-coated pit necks is required for efficient vesicle uncoating after fission. Neuron 72:587–601.

Miyawaki A (2005) Innovations in the imaging of brain functions using fluorescent proteins. Neuron 48:189–199.

Miyazaki T, Fukaya M, Shimizu H, Watanabe M (2003) Subtype switching of vesicular glutamate transporters at parallel fibre-Purkinje cell synapses in developing mouse cerebellum. Eur J Neurosci 17:2563–2572.

Moechars D, Weston MC, Leo S, Callaerts-Vegh Z, Goris I, Daneels G, Buist A, Cik M, van der Spek P, Kass S, Meert T, D'Hooge R, Rosenmund C, Hampson RM (2006) Vesicular glutamate transporter VGLUT2 expression levels control quantal size and neuropathic pain. J Neurosci 26:12055–12066.

Moriyama Y, Maeda M, Futai M (1992) The role of V-ATPase in neuronal and endocrine systems. J Exp Biol 172:171–178.

Morris SM, Arden SD, Roberts RC, Kendrick-Jones J, Cooper JA, Luzio JP, Buss F (2002) Myosin VI binds to and localises with Dab2, potentially linking receptor-mediated endocytosis and the actin cytoskeleton. Traffic 3:331–341.

Muresan Z, Muresan V (2005) Coordinated transport of phosphorylated amyloid-beta precursor protein and c-Jun NH2-terminal kinase-interacting protein-1. J Cell Biol 171:615–625.

Mutch SA, Kensel-Hammes P, Gadd JC, Fujimoto BS, Allen RW, Schiro PG, Lorenz RM, Kuyper CL, Kuo JS, Bajjalieh SM, Chiu DT (2011) Protein quantification at the single vesicle level reveals that a subset of synaptic vesicle proteins are trafficked with high precision. J Neurosci 31:1461–1470.

Naccache SN, Hasson T, Horowitz A (2006) Binding of internalized receptors to the PDZ domain of GIPC/synectin recruits myosin VI to endocytic vesicles. Proc Natl Acad Sci USA 103:12735–12740.

Nagai T, Ibata K, Park ES, Kubota M, Mikoshiba K, Miyawaki A (2002) A variant of yellow fluorescent protein with fast and efficient maturation for cell-biological applications. Nat Biotechnol 20:87–90.

Naito S, Ueda T (1983) Adenosine triphosphate-dependent uptake of glutamate into protein I-associated synaptic vesicles. J Biol Chem 258:696–699.

Naito S, Ueda T (1985) Characterization of glutamate uptake into synaptic vesicles. Journal of Neurochemistry 44:99–109.

Nakatsu F, Okada M, Mori F, Kumazawa N, Iwasa H, Zhu G, Kasagi Y, Kamiya H, Harada A, Nishimura K, Takeuchi A, Miyazaki T, Watanabe M, Yuasa S, Manabe T, Wakabayashi K, Kaneko S, Saito T, Ohno H (2004) Defective function of GABA-containing synaptic vesicles in mice lacking the AP-3B clathrin adaptor. J Cell Biol 167:293–302.

Neher E (2015) Merits and Limitations of Vesicle Pool Models in View of Heterogeneous Populations of Synaptic Vesicles. Neuron 87:1131–1142.

Ni B, Rosteck PR, Nadi NS, Paul SM (1994) Cloning and expression of a cDNA encoding a brain-specific Na(+)-dependent inorganic phosphate cotransporter. Proc Natl Acad Sci USA 91:5607–5611.

Nienhaus K, Nienhaus GU, Wiedenmann J, Nar H (2005) Structural basis for photo-induced protein cleavage and green-to-red conversion of fluorescent protein EosFP. Proc Natl Acad Sci USA 102:9156–9159.

Pack-Chung E, Kurshan PT, Dickman DK, Schwarz TL (2007) A Drosophila kinesin required for synaptic bouton formation and synaptic vesicle transport. Nat Neurosci 10:980–989.

PALAY SL (1956) Synapses in the central nervous system. J Biophys Biochem Cytol 2:193–202.

Pechstein A, Gerth F, Milosevic I, Jäpel M, Eichhorn-Grünig M, Vorontsova O, Bacetic J, Maritzen T, Shupliakov O, Freund C, Haucke V (2015) Vesicle uncoating regulated by SH3-SH3 domain-mediated complex formation between endophilin and intersectin at synapses. EMBO Rep 16:232–239.

Perkins GA, Jackson DR, Spirou GA (2015) Resolving presynaptic structure by electron tomography. Synapse 69:268–282.

Preobraschenski J, Zander J-F, Suzuki T, Ahnert-Hilger G, Jahn R (2014) Vesicular glutamate transporters use flexible anion and cation binding sites for efficient accumulation of neurotransmitter. Neuron 84:1287–1301.

Raimondi A, Ferguson SM, Lou X, Armbruster M, Paradise S, Giovedí S, Messa M, Kono N, Takasaki J, Cappello V, O'Toole E, Ryan TA, De Camilli P (2011) Overlapping role of dynamin isoforms in synaptic vesicle endocytosis. Neuron 70:1100–1114.

Reimer RJ, Edwards RH (2004) Organic anion transport is the primary function of the SLC17/type I phosphate transporter family. Pflugers Arch 447:629–635.

Rey SA, Smith CA, Fowler MW, Crawford F, Burden JJ, Staras K (2015) Ultrastructural and functional fate of recycled vesicles in hippocampal synapses. Nat Commun 6:8043.

Rizzoli SO, Betz WJ (2005) Synaptic vesicle pools. Nat Rev Neurosci 6:57–69.

Roebroek AJM, Wu X, Bram RJ (2003) Knockin approaches. Methods Mol Biol 209:187–200.

Rossier O, Octeau V, Sibarita J-B, Leduc C, Tessier B, Nair D, Gatterdam V, Destaing O, Albigès-Rizo C, Tampé R, Cognet L, Choquet D, Lounis B, Giannone G (2012) Integrins β1 and β3 exhibit distinct dynamic nanoscale organizations inside focal adhesions. Nat Cell Biol 14:1057–1067.

Rothman JS, Kocsis L, Herzog E, Nusser Z, Silver RA (2016) Physical determinants of vesicle mobility and supply at a central synapse. Elife 5.

Ruel J, Emery S, Nouvian R, Bersot T, Amilhon B, Van Rybroek JM, Rebillard G, Lenoir M, Eybalin M, Delprat B, Sivakumaran TA, Giros B, Mestikawy El S, Moser T, Smith RJH, Lesperance MM, Puel J-L (2008) Impairment of SLC17A8 encoding vesicular glutamate transporter-3, VGLUT3, underlies nonsyndromic deafness DFNA25 and inner hair cell dysfunction in null mice. Am J Hum Genet 83:278–292.

Saheki Y, De Camilli P (2012) Synaptic vesicle endocytosis. Cold Spring Harb Perspect Biol 4:a005645.

Sander JD, Joung JK (2014) CRISPR-Cas systems for editing, regulating and targeting genomes. Nat Biotechnol 32:347–355.

Santos MS, Foss SM, Park CK, Voglmaier SM (2014) Protein interactions of the vesicular glutamate transporter VGLUT1. PLoS ONE 9:e109824.

Santos MS, Li H, Voglmaier SM (2009) Synaptic vesicle protein trafficking at the glutamate synapse. NSC 158:189–203.

Schenck S, Wojcik SM, Brose N, Takamori S (2009) A chloride conductance in VGLUT1 underlies maximal glutamate loading into synaptic vesicles. Nat Neurosci 12:156–162.

Schnell E, Nicoll RA (2001) Hippocampal synaptic transmission and plasticity are preserved in myosin Va mutant mice. Journal of Neurophysiology 85:1498–1501.

Seal RP, Akil O, Yi E, Weber CM, Grant L, Yoo J, Clause A, Kandler K, Noebels JL, Glowatzki E, Lustig LR, Edwards RH (2008) Sensorineural deafness and seizures in mice lacking vesicular glutamate transporter 3. Neuron 57:263–275.

Seal RP, Wang X, Guan Y, Raja SN, Woodbury CJ, Basbaum AI, Edwards RH (2009) Injury-induced mechanical hypersensitivity requires C-low threshold mechanoreceptors. Nature 462:651–655.

Sheng M, Hoogenraad CC (2007) The postsynaptic architecture of excitatory synapses: a more quantitative view. Annu Rev Biochem 76:823–847.

Siksou L, Rostaing P, Lechaire J-P, Boudier T, Ohtsuka T, Fejtová A, Kao H-T, Greengard P, Gundelfinger ED, Triller A, Marty S (2007) Three-dimensional architecture of presynaptic terminal cytomatrix. J Neurosci 27:6868–6877.

Siksou L, Silm K, Biesemann C, Nehring RB, Wojcik SM, Triller A, Mestikawy El S, Marty S, Herzog E (2013) A role for vesicular glutamate transporter 1 in synaptic vesicle clustering and mobility. Eur J Neurosci 37:1631–1642.

Siksou L, Varoqueaux F, Pascual O, Triller A, Brose N, Marty S (2009) A common molecular basis for membrane docking and functional priming of synaptic vesicles. Eur J Neurosci 30:49–56.

Song Y, Brady ST (2014) Stabilization of neuronal connections and the axonal cytoskeleton. Bioarchitecture 4:22–24.

Soykan T, Maritzen T, Haucke V (2016) Modes and mechanisms of synaptic vesicle recycling. Current Opinion in Neurobiology 39:17–23.

Söllner T, Bennett MK, Whiteheart SW, Scheller RH, Rothman JE (1993) A protein assembly-disassembly pathway in vitro that may correspond to sequential steps of synaptic vesicle docking, activation, and fusion. Cell 75:409–418.

Spudich G, Chibalina MV, Au JS-Y, Arden SD, Buss F, Kendrick-Jones J (2007) Myosin VI targeting to clathrin-coated structures and dimerization is mediated by binding to Disabled-2 and PtdIns(4,5)P2. Nat Cell Biol 9:176–183.

Staras K, Branco T, Burden JJ, Pozo K, Darcy K, Marra V, Ratnayaka A, Goda Y (2010) A vesicle superpool spans multiple presynaptic terminals in hippocampal neurons. Neuron 66:37–44.

Stehbens S, Pemble H, Murrow L, Wittmann T (2012) Imaging intracellular protein dynamics by spinning disk confocal microscopy. Meth Enzymol 504:293–313.

Stobrawa SM, Breiderhoff T, Takamori S, Engel D, Schweizer M, Zdebik AA, Bösl MR, Ruether K, Jahn H, Draguhn A, Jahn R, Jentsch TJ (2001) Disruption of ClC-3, a chloride channel expressed on synaptic vesicles, leads to a loss of the hippocampus. Neuron 29:185–196.

Stone MC, Roegiers F, Rolls MM (2008) Microtubules have opposite orientation in axons and dendrites of Drosophila neurons. Mol Biol Cell 19:4122–4129.

Stornetta RL, Sevigny CP, Schreihofer AM, Rosin DL, Guyenet PG (2002) Vesicular glutamate transporter DNPI/VGLUT2 is expressed by both C1 adrenergic and nonaminergic presympathetic vasomotor neurons of the rat medulla. J Comp Neurol 444:207–220.

Südhof TC (2004) The synaptic vesicle cycle. Annu Rev Neurosci 27:509–547.

Südhof TC (2012) The presynaptic active zone. Neuron 75:11–25.

Südhof TC (2013) Neurotransmitter release: the last millisecond in the life of a synaptic vesicle. Neuron 80:675–690.

Takagishi Y, Futaki S, Itoh K, Espreafico EM, Murakami N, Murata Y, Mochida S (2005) Localization of myosin II and V isoforms in cultured rat sympathetic neurones and their potential involvement in presynaptic function. J Physiol (Lond) 569:195–208.

Takamori S (2006) VGLUTs: “exciting” times for glutamatergic research? Neurosci Res 55:343–351.

Takamori S (2016) Vesicular glutamate transporters as anion channels? Pflugers Arch 468:513–518.

Takamori S et al. (2006) Molecular anatomy of a trafficking organelle. Cell 127:831–846.

Takamori S, Rhee JS, Rosenmund C, Jahn R (2000) Identification of a vesicular glutamate transporter that defines a glutamatergic phenotype in neurons. Nature 407:189–194.

Takamori S, Rhee JS, Rosenmund C, Jahn R (2001) Identification of differentiation-associated brain-specific phosphate transporter as a second vesicular glutamate transporter (VGLUT2). J Neurosci 21:RC182.

Tanaka M, Kirito K, Kashii Y, Uchida M, Watanabe T, Endo H, Endoh T, Sawada K, Ozawa K, Komatsu N (2001) Forkhead family transcription factor FKHRL1 is expressed in human megakaryocytes. Regulation of cell cycling as a downstream molecule of thrombopoietin signaling. J Biol Chem 276:15082–15089.

Taylor MJ, Perrais D, Merrifield CJ (2011) A high precision survey of the molecular dynamics of mammalian clathrin-mediated endocytosis. PLoS Biol 9:e1000604.

Thomas KR, Folger KR, Capecchi MR (1986) High frequency targeting of genes to specific sites in the mammalian genome. Cell 44:419–428.

Tordera RM, Totterdell S, Wojcik SM, Brose N, Elizalde N, Lasheras B, Del Rio J (2007) Enhanced anxiety, depressive-like behaviour and impaired recognition memory in mice with reduced expression of the vesicular glutamate transporter 1 (VGLUT1). Eur J Neurosci 25:281–290.

Trimbuch T, Rosenmund C (2016) Should I stop or should I go? The role of complexin in neurotransmitter release. Nat Rev Neurosci 17:118–125.

Uchizono K (1965) Characteristics of excitatory and inhibitory synapses in the central nervous system of the cat. Nature 207:642–643.

Varoqui H, Schäfer MK-H, Zhu H, Weihe E, Erickson JD (2002) Identification of the differentiation-associated Na+/PI transporter as a novel vesicular glutamate transporter expressed in a distinct set of glutamatergic synapses. J Neurosci 22:142–155.

Vasileva M, Horstmann H, Geumann C, Gitler D, Kuner T (2012) Synapsin-dependent reserve pool of synaptic vesicles supports replenishment of the readily releasable pool under intense synaptic transmission. Eur J Neurosci 36:3005–3020.

Verhage M, Maia AS, Plomp JJ, Brussaard AB, Heeroma JH, Vermeer H, Toonen RF, Hammer RE, van den Berg TK, Missler M, Geuze HJ, Südhof TC (2000) Synaptic assembly of the brain in the absence of neurotransmitter secretion. Science 287:864–869.

Verstegen AMJ, Tagliatti E, Lignani G, Marte A, Stolero T, Atias M, Corradi A, Valtorta F, Gitler D, Onofri F, Fassio A, Benfenati F (2014) Phosphorylation of synapsin I by cyclin-dependent kinase-5 sets the ratio between the resting and recycling pools of synaptic vesicles at hippocampal synapses. J Neurosci 34:7266–7280.

Vinatier J, Herzog E, Plamont M-A, Wojcik SM, Schmidt A, Brose N, Daviet L, Mestikawy El S, Giros B (2006) Interaction between the vesicular glutamate transporter type 1 and endophilin A1, a protein essential for endocytosis. Journal of Neurochemistry 97:1111–1125.

Voglmaier SM, Kam K, Yang H, Fortin DL, Hua Z, Nicoll RA, Edwards RH (2006) Distinct endocytic pathways control the rate and extent of synaptic vesicle protein recycling. Neuron 51:71–84.

Wallén-Mackenzie Å et al. (2009) Restricted cortical and amygdaloid removal of vesicular glutamate transporter 2 in preadolescent mice impacts dopaminergic activity and neuronal circuitry of higher brain function. J Neurosci 29:2238–2251.

Wallén-Mackenzie Å, Gezelius H, Thoby-Brisson M, Nygård A, Enjin A, Fujiyama F, Fortin G, Kullander K (2006) Vesicular glutamate transporter 2 is required for central respiratory rhythm generation but not for locomotor central pattern generation. J Neurosci 26:12294–12307.

Wang F, Qi LS (2016) Applications of CRISPR Genome Engineering in Cell Biology. Trends Cell Biol 26:875–888.

Washbourne P, McAllister AK (2002) Techniques for gene transfer into neurons. Current Opinion in Neurobiology 12:566–573.

Watanabe S, Rost BR, Camacho-Pérez M, Davis MW, Söhl-Kielczynski B, Rosenmund C, Jorgensen EM (2013) Ultrafast endocytosis at mouse hippocampal synapses. Nature 504:242–247.

Watanabe S, Trimbuch T, Camacho-Pérez M, Rost BR, Brokowski B, Söhl-Kielczynski B, Felies A, Davis MW, Rosenmund C, Jorgensen EM (2014) Clathrin regenerates synaptic vesicles from endosomes. Nature 515:228–233.

Weston MC, Nehring RB, Wojcik SM, Rosenmund C (2011) Interplay between VGLUT isoforms and endophilin A1 regulates neurotransmitter release and short-term plasticity. Neuron 69:1147–1159.

Wilson NR, Kang J, Hueske EV, Leung T, Varoqui H, Murnick JG, Erickson JD, Liu G (2005) Presynaptic regulation of quantal size by the vesicular glutamate transporter VGLUT1. J Neurosci 25:6221–6234.

Winther ÅME, Vorontsova O, Rees KA, Näreoja T, Sopova E, Jiao W, Shupliakov O (2015) An Endocytic Scaffolding Protein together with Synapsin Regulates Synaptic Vesicle Clustering in the Drosophila Neuromuscular Junction. J Neurosci 35:14756–14770.

Wojcik SM, Rhee JS, Herzog E, Sigler A, Jahn R, Takamori S, Brose N, Rosenmund C (2004) An essential role for vesicular glutamate transporter 1 (VGLUT1) in postnatal development and control of quantal size. Proc Natl Acad Sci USA 101:7158–7163.

Wong MY, Zhou C, Shakiryanova D, Lloyd TE, Deitcher DL, Levitan ES (2012) Neuropeptide delivery to synapses by long-range vesicle circulation and sporadic

capture. Cell 148:1029–1038.

Wu YE, Huo L, Maeder CI, Feng W, Shen K (2013) The balance between capture and dissociation of presynaptic proteins controls the spatial distribution of synapses. Neuron 78:994–1011.

Xu K, Zhong G, Zhuang X (2013) Actin, spectrin, and associated proteins form a periodic cytoskeletal structure in axons. Science 339:452–456.

Xue M, Craig TK, Xu J, Chao H-T, Rizo J, Rosenmund C (2010) Binding of the complexin N terminus to the SNARE complex potentiates synaptic-vesicle fusogenicity. Nat Struct Mol Biol 17:568–575.

Yang X, Kaeser-Woo YJ, Pang ZP, Xu W, Südhof TC (2010) Complexin clamps asynchronous release by blocking a secondary Ca(2+) sensor via its accessory α helix. Neuron 68:907–920.

Yuan A, Rao MV, Veeranna, Nixon RA (2012) Neurofilaments at a glance. J Cell Sci 125:3257–3263.

Zahs KR (1998) Heterotypic coupling between glial cells of the mammalian central nervous system. Glia 24:85–96.

Zala D, Hinckelmann M-V, Yu H, Lyra da Cunha MM, Liot G, Cordelières FP, Marco S, Saudou F (2013) Vesicular glycolysis provides on-board energy for fast axonal transport. Cell 152:479–491.

Zander J-F, Münster-Wandowski A, Brunk I, Pahner I, Gómez-Lira G, Heinemann U, Gutiérrez R, Laube G, Ahnert-Hilger G (2010) Synaptic and vesicular coexistence of VGLUT and VGAT in selected excitatory and inhibitory synapses. J Neurosci 30:7634–7645.

Zeitelhofer M, Vessey JP, Xie Y, Tübing F, Thomas S, Kiebler M, Dahm R (2007) High-efficiency transfection of mammalian neurons via nucleofection. Nat Protoc 2:1692–1704.

Zuber B, Nikonenko I, Klauser P, Muller D, Dubochet J (2005) The mammalian central nervous synaptic cleft contains a high density of periodically organized complexes. Proc Natl Acad Sci USA 102:19192–19197.